



Calhoun: The NPS Institutional Archive
DSpace Repository

Theses and Dissertations

1. Thesis and Dissertation Collection, all items

2012-09

Artifacts in Radar Imaging of Moving Targets

Tng, Yan Siong

Monterey, California. Naval Postgraduate School

<https://hdl.handle.net/10945/17470>

Downloaded from NPS Archive: Calhoun



Calhoun is the Naval Postgraduate School's public access digital repository for research materials and institutional publications created by the NPS community. Calhoun is named for Professor of Mathematics Guy K. Calhoun, NPS's first appointed -- and published -- scholarly author.

Dudley Knox Library / Naval Postgraduate School
411 Dyer Road / 1 University Circle
Monterey, California USA 93943

<http://www.nps.edu/library>



**NAVAL
POSTGRADUATE
SCHOOL**

MONTEREY, CALIFORNIA

THESIS

**ARTIFACTS IN RADAR IMAGING OF MOVING
TARGETS**

by

Yan Siong Tng

September 2012

Thesis Advisor:
Second Reader:

Brett H. Borden
Roberto Cristi

Approved for public release; distributed is unlimited

THIS PAGE INTENTIONALLY LEFT BLANK

REPORT DOCUMENTATION PAGE			<i>Form Approved OMB No. 0704-0188</i>
Public reporting burden for this collection of information is estimated to average 1 hour per response, including the time for reviewing instruction, searching existing data sources, gathering and maintaining the data needed, and completing and reviewing the collection of information. Send comments regarding this burden estimate or any other aspect of this collection of information, including suggestions for reducing this burden, to Washington headquarters Services, Directorate for Information Operations and Reports, 1215 Jefferson Davis Highway, Suite 1204, Arlington, VA 22202-4302, and to the Office of Management and Budget, Paperwork Reduction Project (0704-0188) Washington DC 20503.			
1. AGENCY USE ONLY (Leave blank)	2. REPORT DATE 21 September 2012	3. REPORT TYPE AND DATES COVERED Master's Thesis	
4. TITLE AND SUBTITLE Artifacts in Radar Imaging of Moving Targets		5. FUNDING NUMBERS	
6. AUTHOR(S) Yan Siong Tng		8. PERFORMING ORGANIZATION REPORT NUMBER	
7. PERFORMING ORGANIZATION NAME(S) AND ADDRESS(ES) Naval Postgraduate School Monterey, CA 93943-5000		10. SPONSORING/MONITORING AGENCY REPORT NUMBER	
9. SPONSORING /MONITORING AGENCY NAME(S) AND ADDRESS(ES) N/A		11. SUPPLEMENTARY NOTES The views expressed in this thesis are those of the author and do not reflect the official policy or position of the Department of Defense or the U.S. Government. IRB Protocol number: N/A.	
12a. DISTRIBUTION / AVAILABILITY STATEMENT Approved for public release; distribution is unlimited		12b. DISTRIBUTION CODE	
13. ABSTRACT (maximum 200 words) In this thesis, we study the artifacts that occur when a scene being imaged by radar contains moving targets. The physics of interaction between radar waves and moving targets were studied to develop a model using MATLAB for the received signal which does not make use of the start-stop approximation. The effects of target motion in the image formation process were studied for different radar configurations, including multistatic radars and Synthetic Aperture Radar. The key limitation of this model is its high computational resource requirements when simulating high bandwidth or long pulses. It was observed that range profiles may experience distortion due to the received waveform's differences from the matched filter. The exact outcome is waveform dependent; generally, both main lobe broadening and range errors were introduced by target motion. This leads to the wrong object localization and defocusing on the image. For SAR, a moving target's physical location varies throughout the imaging process. This means that standard backprojection fails to yield a focused image even if the range error due to the Doppler shift has been corrected, resulting in smearing. This is similar to "motion blur" experienced in optical cameras with a fast object.			
14. SUBJECT TERMS Radar Imaging, Synthetic Aperture Radar, Bistatic Radar, Multistatic Radar, Moving Targets, Backprojection		15. NUMBER OF PAGES 133	
		16. PRICE CODE	
17. SECURITY CLASSIFICATION OF REPORT Unclassified	18. SECURITY CLASSIFICATION OF THIS PAGE Unclassified	19. SECURITY CLASSIFICATION OF ABSTRACT Unclassified	20. LIMITATION OF ABSTRACT UU

THIS PAGE INTENTIONALLY LEFT BLANK

Approved for public release; distributed is unlimited

ARTIFACTS IN RADAR IMAGES OF MOVING TARGETS

Yan Siong Tng
Civilian, Defence Science & Technology Agency, Singapore
B.Eng (Electrical), National University of Singapore, 2000

Submitted in partial fulfillment of the
requirements for the degree of

MASTER OF SCIENCE IN COMBAT SYSTEMS TECHNOLOGY

from the

NAVAL POSTGRADUATE SCHOOL
September 2012

Author: Yan Siong Tng

Approved by: Brett H. Borden
Thesis Advisor

Roberto Cristi
Second Reader

Andres Larraza
Chair, Department of Physics

THIS PAGE INTENTIONALLY LEFT BLANK

ABSTRACT

In this thesis, we study the artifacts that occur when a scene being imaged by radar contains moving targets. The physics of interaction between radar waves and moving targets were studied to develop a model using MATLAB for the received signal, which does not make use of the start-stop approximation. The effects of target motion on the image formation process were studied for different radar configurations, including multistatic radars and Synthetic Aperture Radars. The key limitation of this model is its high computational resource requirements when simulating high bandwidth or long pulses.

It was observed that range profiles may experience distortion due to the received waveform's differences from the matched filter. The exact outcome is waveform dependent; generally, both main lobe broadening and range errors were introduced by target motion. This leads to incorrect object localization and defocusing on the image. For SAR, a moving target's physical location varies throughout the imaging process. This means that standard backprojection fails to yield a focused image even if the range error due to the Doppler shift has been corrected, resulting in smearing. This is similar to the "motion blur" experienced in optical cameras with a fast object.

THIS PAGE INTENTIONALLY LEFT BLANK

TABLE OF CONTENTS

I.	INTRODUCTION.....	1
A.	HISTORY AND PRINCIPLES OF RADAR	1
B.	RADAR IMAGING	2
1.	Radar Resolution	3
2.	One-Dimensional Imaging	7
3.	Two-Dimensional Imaging	8
C.	MOTIVATION AND FOCUS OF THESIS	11
D.	THESIS ORGANISATION	12
II.	MOTION IN RADAR IMAGING.....	13
A.	SCENARIO AND ASSUMPTIONS.....	13
B.	TRANSMISSION AND PROPAGATION	13
C.	INTERACTION AND RECEPTION	15
D.	LINEAR TRAJECTORY	16
E.	WAVEFORM DISTORTION	18
F.	DOPPLER MODULATION EFFECT	19
G.	ROLE OF START-STOP APPROXIMATION	20
H.	ARTIFACTS FROM MOVING TARGETS.....	21
I.	METHODS TO ADDRESS DE-FOCUSING.....	22
1.	Velocity Estimation Techniques in Single Channel SARs	22
2.	Multichannel SAR (MSAR)	23
3.	Compressive Sensing	23
4.	Linearized Theory by Cheney and Borden	24
III.	DESCRIPTION OF MODEL	27
A.	OVERVIEW OF SINGLE PULSE MODEL	27
B.	DEFINITION OF TARGET AND SENSOR TRAJECTORY.....	28
C.	WAVEFORM GENERATION CONCEPT	29
D.	MATCHED FILTERBANK AND RANGE PROFILE	36
E.	IMAGE RECONSTRUCTION	37
1.	Range Alignment.....	38
2.	Image Reconstruction Using Backprojection.....	39
IV.	RESULTS	43
A.	SIMULATION PARAMETER SELECTION	43
1.	Waveform Definition	43
2.	Imaged Scene Definition.....	44
B.	ONE-DIMENSION MODEL VERIFICATION.....	44
1.	Doppler Shift for Approaching and Receding Target	45
2.	Non-linear Relationship Between Transmission and Reception Times	48
3.	Ambiguity Functions for Known Waveforms	50

C.	TWO-DIMENSION IMAGING MODEL VERIFICATION.....	51
1.	Time Map Implementation for 2-D Imaging.....	51
2.	Single Pulse Image Map	53
D.	EFFECT OF TARGET SPEED ON RANGE PROFILE	55
E.	MULTI-STATIC RADAR CASE STUDY	58
1.	Multiple Monostatic Radars	59
2.	Multistatic Radars	62
F.	MONO-STATIC SINGLE CHANNEL SAR CASE STUDY	65
1.	SAR Cross Range Resolution.....	65
2.	Point Spread Function for a Moving Target	67
V.	CONCLUSIONS	73
	APPENDIX A. DERIVATION OF EQUATIONS	75
A.	PROPAGATION TIME FROM TRANSMITTER TO TARGET	75
B.	PROPAGATION TIME FROM TARGET TO RECEIVER.....	76
C.	DOPPLER-SHIFT FOR INCOMING TARGET	78
	APPENDIX B. MATLAB CODES	81
A.	FUNCTIONS	81
1.	Generation of Linear Trajectory Path	81
2.	Computation of Wave Interception Time	81
3.	Generation of Rectangular Pulse.....	82
4.	Generation of Barker-Coded Binary Phase Modulated Pulse.....	84
5.	Generation of Linear-Frequency-Modulated Pulse.....	85
6.	Correlation Receiver	87
7.	Create the Time Map for Given Target-Sensor Geometry	89
8.	Update the Image Map based on Current Range Samples	90
9.	Check Time Vector for Required Length Constraints before Processing	90
B.	SCRIPTS.....	91
1.	Example of Multistatic Radar.....	91
a.	Scenario Definition	91
b.	Main Script.....	94
2.	Example of SAR	98
a.	Scenario Definition	98
b.	Main Script.....	101
3.	Script for Re-imaging the Scene After Generation.....	105
	APPENDIX C. STUDY ON FLOATING POINT PRECISION	107
	LIST OF REFERENCES	111
	INITIAL DISTRIBUTION LIST	113

LIST OF FIGURES

Figure 1.	Key principles and phenomena for operation of typical pulse radar (After [2]).....	2
Figure 2.	Radar imagery (Top) and a photo of the corresponding object (Bottom). (From [4]).....	3
Figure 3.	A two-dimensional monostatic range cell (From [7]).....	4
Figure 4.	Stripmap modes for SAR imaging (from [9]).....	5
Figure 5.	Spotlight mode for SAR imaging (from [9])	6
Figure 6.	Example of a range profile generated by a high resolution radar	7
Figure 7.	Example of backprojected image for a single monostatic radar pulse for multiple point targets. The grey lines are contours lines of equal reception times passing through the targets' locations. (From [14])	10
Figure 8.	Composite backprojection image for monostatic radar pulses taken at three different aspects for multiple point targets. All three sets of lines intersect at the true target locations. (From [14])	10
Figure 9.	Example of an imaging point spread function (From [5])	11
Figure 10.	Illustration of geometry at interaction between wave and target.	16
Figure 11.	Effects of target motion on SAR imaging (From [17])	22
Figure 12.	Block diagram for range profile generation.....	27
Figure 13.	Illustration of relationship between transmitted and received waveforms	31
Figure 14.	Illustration of received waveform generation process	35
Figure 15.	Block diagram illustrating concept of image reconstruction	38
Figure 16.	Illustration of the backprojection method	42
Figure 17.	Geometry of the approaching target (Top) and receding target (Bottom) scenarios.....	45
Figure 18.	Change in propagation time as a function of transmission time for various approaching and receding radial velocities.	46
Figure 19.	Difference between the simulated change in propagation time versus theoretically predicted linear line as a function of transmission time	47
Figure 20.	Geometry for scenario with crossing target. This is for the case of a target with crossing speed of 7.8 km/s.....	48
Figure 21.	Change in propagation time (referenced to first transmitted sample) for crossing targets at 100 m/s (Left) and 1000 m/s (Right).	49
Figure 22.	Change in propagation time (referenced to start of transmission sample) for a 500 μ sec pulse on a 100m/s crossing target at 100km away.....	49
Figure 23.	Change in propagation time (referenced to start of transmission sample) for a 50 millisec pulse on a 250m/s crossing target at 50km away.....	50
Figure 24.	Ambiguity function and associated zero Doppler cut for a rectangular pulse from model. The delay and frequency axes have been normalized using the simulated pulse width and pulse bandwidth (= reciprocal of pulse width in this case), respectively.....	50

Figure 25.	Ambiguity function and associated zero Doppler cut for a Barker 13 binary phased coded pulse from model. The delay and frequency axes have been normalized using the subpulse width and pulse bandwidth, respectively.	51
Figure 26.	Ambiguity function and associated zero Doppler cut generated for a LFM pulse (Bandwidth=15MHz) from model. The delay and frequency axes have been normalized using the pulse width and pulse bandwidth, respectively.	51
Figure 27.	Contour plot of time map for a monostatic radar located at [20km,20km].	52
Figure 28.	Contour plot of time map for bistatic radar with transmitter at [50km,-50km] and receiver at [10km,-10km].	52
Figure 29.	Detailed time map for 400m x 400m area around scene center based on the geometry shown in Figure 28. Contours are set at 5 μ s intervals for display only. Samples are generated at 10cm intervals.	53
Figure 30.	Single LFM pulse (15 MHz bandwidth) image map using monostatic configuration, with target at [-50m,50m] using the backprojection algorithm.	54
Figure 31.	Single LFM pulse (15 MHz bandwidth) image map using bistatic configuration, with target at [-50m,50m] using the backprojection algorithm.	54
Figure 32.	Combined image map formed from the outputs of the monostatic and bistatic radars. The target is clearly localized at its true location, [-50m, 50m].	55
Figure 33.	Effect of target speed (inbound target) from 1 km/s to 100 km/s on the range profile output for LFM pulse with $T_w = 1\mu$ s, bandwidth = 15 MHz. The delay axis is normalized by the pulse width, the amplitude is normalized using the peak of the auto-correlation function.	56
Figure 34.	Effect on the range profile output for LFM pulse with $T_w = 1\mu$ s, bandwidth = 15 MHz when a 100km/s target is at 45 degree aspect angle (Left) and when velocity is at 90 deg to the down-range direction (Right). The delay axis is normalized by the pulse width, the amplitude is normalized using the peak of the auto-correlation function.	57
Figure 35.	Effect on the range profile output for LFM pulse with longer pulse, $T_w = 10\mu$ s (Left) and higher bandwidth = 150 MHz (Right) with an 100km/s inbound target. The delay axis is normalized by the pulse width, the amplitude is normalized using the peak of the auto-correlation function.	57
Figure 36.	Effect on the range profile output for Barker-13 binary phase coded pulse with subpulse width, $T_w = 0.667\mu$ s for a 50 km/s and 100 km/s inbound target. The delay axis is normalized by the <i>subpulse</i> width, the amplitude is normalized using the peak of the auto-correlation function.	58
Figure 37.	Layout of radars for multiple monostatic imaging case study	59
Figure 38.	Point Spread Function for stationary target at [-50,50] meters. Radars are at [-100,100,0]km, [0,100,0]km, [50,0,0]km and [50,86.6,0]km. Amplitudes are normalized by the number of pulses processed.	60

Figure 39.	Point Spread Function for target with initial position [-50,50,0] meters moving at 7.5 km/s, (a) parallel to +Y-axis (Top Left), (b) parallel to +X-axis (Top Right). The PSF for the stationary target (Bottom) is shown for reference.....	61
Figure 40.	Point Spread Function for target with initial position [-50,50,0] meters moving at 50 km/s.....	61
Figure 41.	Point Spread Function for configuration using Barker-13 binary phase coded signal for target towards +Y direction at, (a) 7.5 km/s (Top Left), (b) 50 km/s. The point spread function for a stationary target (Bottom) is shown for reference.....	63
Figure 42.	Layout of target, transmitter and receivers (Left) and Point Spread Function (Right) for the multistatic radar scenario.....	63
Figure 43.	Multistatic configuration Point Spread Function for target with initial position [-50,50,0] meters moving at 7.5 km/s, (a) parallel to +Y-axis (Top Left), (b) parallel to +X-axis (Top Right). The PSF for the stationary target (Bottom) is shown for reference.	64
Figure 44.	Geometry of reference SAR scenario. The SAR's speed is chosen to be 50m/s. The X and Y axes are the down-range and cross-range directions, respectively.	66
Figure 45.	Point Spread Function for reference SAR scenario.	66
Figure 46.	Point Spread Function for SAR scenario with observation widths of 1.5km (Left) and 6km (Right).....	66
Figure 47.	Point Spread Function for SAR scenario with carrier frequencies of 50 MHz (Left) and 150 MHz (Right)	67
Figure 48.	Point Spread Function for SAR scenario with target, initially located at [0,0,0] meters, moving at 0.1 m/s in the down-range direction. The PSF for a stationary target is shown (Bottom) for reference.....	68
Figure 49.	Point Spread Function for SAR scenario with target, initially located at [0,0,0] meters, moving at 0.1 m/s in the cross-range direction.....	68
Figure 50.	Point Spread Function for SAR scenario with target, initially located at [0,0,0] meters, moving at 10 m/s in the down-range direction.	69
Figure 51.	Point Spread Function for SAR scenario with target, initially located at [0,0,0] meters, moving at 10 m/s in the cross-range direction.....	69
Figure 52.	Point Spread Function for SAR scenario with target, initially located at [0,0,0] meters, moving at 10 m/s in the down-range direction and with SAR moving at 250 m/s.....	70
Figure 53.	Point Spread Function for SAR scenario with target, initially located at [0,0,0] meters, moving at 10 m/s in the cross-range direction and with SAR moving at 250 m/s.....	70

THIS PAGE INTENTIONALLY LEFT BLANK

LIST OF TABLES

Table 1.	Required pulse bandwidths versus desired range resolution for monostatic radars.....	8
Table 2.	Examples of possible sensor configuration that can be studied.....	28
Table 3.	Examples of waveform functions	29

THIS PAGE INTENTIONALLY LEFT BLANK

LIST OF ACRONYMS AND ABBREVIATIONS

ADC	Analog to Digital Convertor
CS	Compressive Sensing
CW	Continuous Wave
DAC	Digital to Analog Convertor
DFT	Discrete Fourier Transform
FBP	Filtered Back Projection
FFT	Fast Fourier Transform
GPS	Global Positioning System
HRR	High Resolution Radar
IDFT	Inverse Discrete Fourier Transform
INS	Inertial Navigation System
ISAR	Inverse Synthetic Aperture Radar
LFM	Linear Frequency Modulated
MSAR	Multi-channel Synthetic Aperture Radar
MTI	Moving Target Indicator
PRF	Pulse Repetition Frequency
PSF	Point Spread Function
SAR	Synthetic Aperture Radar
SNR	Signal to Noise Ratio
STAP	Space-Time Adaptive Processing
VPA	Variable Precision Arithmetic
VSAR	Velocity Synthetic Aperture Radar

THIS PAGE INTENTIONALLY LEFT BLANK

ACKNOWLEDGMENTS

First and foremost, this thesis was very much made possible largely by the efforts of my spouse, Khai Pin, for without her constant support and toil in taking care of the family, this journey would have been so much more difficult.

I am also thankful to Professor Brett Borden for his guidance and encouragement. His patient and insightful advice inspired and helped me greatly during the preparation of this thesis.

I would also like to thank Professor Andres Larraza and Professor Roberto Cristi for kindly reviewing my thesis and their encouraging remarks from doing so.

My two children, Rae Lynn and Ray Kye, have been a constant source of joy in my life throughout this endeavor (despite their incessant attempts to pry me away from working on the thesis).

Lastly, I am grateful to the many authors whose works I have read and gained from along the way. It is only by standing on the shoulders of those who have learned and shared that I have managed to achieve the work that I had.

THIS PAGE INTENTIONALLY LEFT BLANK

I. INTRODUCTION

A. HISTORY AND PRINCIPLES OF RADAR

The physical principles behind radar operations are often said to have been first demonstrated by Heinrich Hertz in his series of experiments on the properties of electromagnetic waves in the late 1880–1890s. In April 1904, a German Engineer Christian Hülsmeyer patented a device in Germany for ship collision avoidance called a “Telemobiloskop,” which had the complete functionality of radar [1]. Thus, the idea behind radar—which is an acronym for “RADio Detection And Ranging”—has been around for more than a hundred years. The basic working principles of radars can be simply summarized as follows:

- A radio transmitter sends out a known electromagnetic wave that travels through the surrounding transmission media (e.g., the atmosphere)
- This wave reaches and interacts with some objects. Part of the wave may be reflected/deflected in different directions.
- A radio receiver senses the portion of the wave that emanates back from the objects and compares the characteristics (reception time, frequency, phase, etc.) of the received wave versus the transmitted wave to extract information (position, speed, etc.) about the object through processing of the received signal.

The prime advantage of radar over other forms of detection utilizing the visible light and infra-red portions of electromagnetic spectrum lies in the fact that the microwaves that radars utilize are relatively unaffected by weather or atmospheric absorption.

Even amongst radars, there are many different types. The electromagnetic wave sent out by a radar may either be pulses of energy, leading to what is called “pulsed radar,” or they may be a continuous transmission of energy, leading to what are called “continuous wave” or “CW radars.” Radars where the transmitters and receivers are at different locations are termed “multi-static;” and they are termed “mono-static” if these are co-located. The work done here addresses pulsed radars in both mono-static and multi-static configurations.

Figure 1 illustrates the key principles and phenomena that govern the operation of a typical radar.

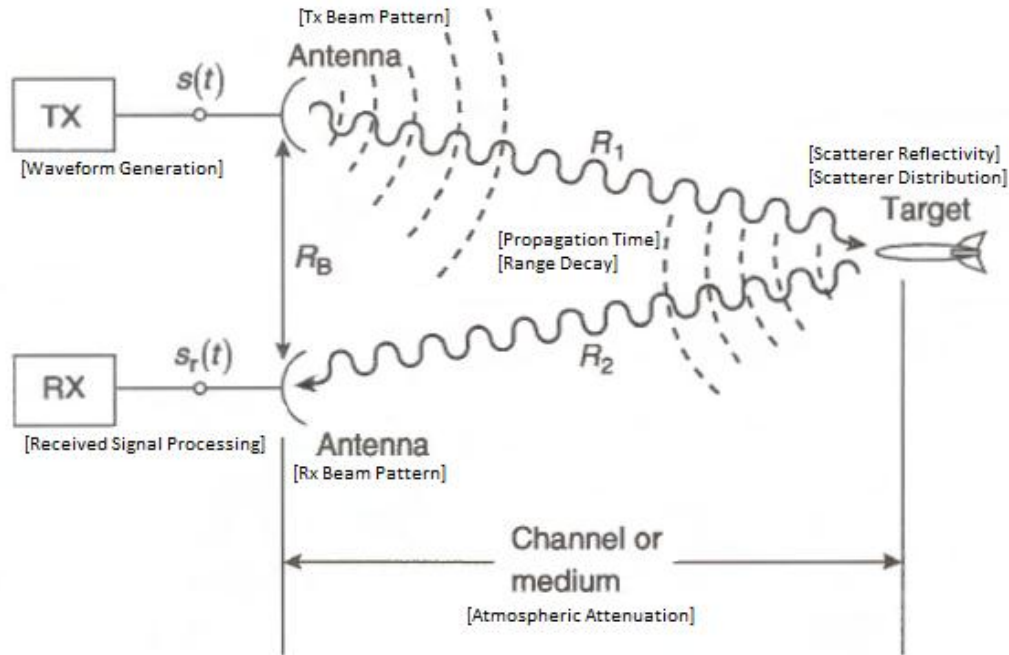


Figure 1. Key principles and phenomena for operation of typical pulse radar (After [2])

B. RADAR IMAGING

The concept of radar imaging represents an extension of the conventional use of radar and was an idea developed from the 1950's onwards following the realization of its possibilities by Carl Wiley of Goodyear Aircraft Corporation. Radar imaging basically seeks to form a spatial image of the radar reflectivity of an observed scene or target using an analysis of scattered wave returns. While the intent, like optical images, is to draw information from the imaged scene, radar imagery typically looks different from the optical equivalent. Figure 2 shows an example of a radar image versus an optical image. At radar wavelengths, the backscattering of waves depends on different factors than those of optical wavelengths. In radar imagery, the surface roughness determines how much of the wave is backscattered to the receiver; in general, a rougher surface backscatters more of the wave to the receiver. As the backscattered waves are coherently processed in

radars, objects where the waves coherently sum up (e.g., corner reflectors) in the backscattered waves appear to be bright points. These bright points can be clearly seen in Figure 2. In a general radar image, the coherent summing of random scatterers contributes to bright points on the imagery, which is known as speckle noise [3].

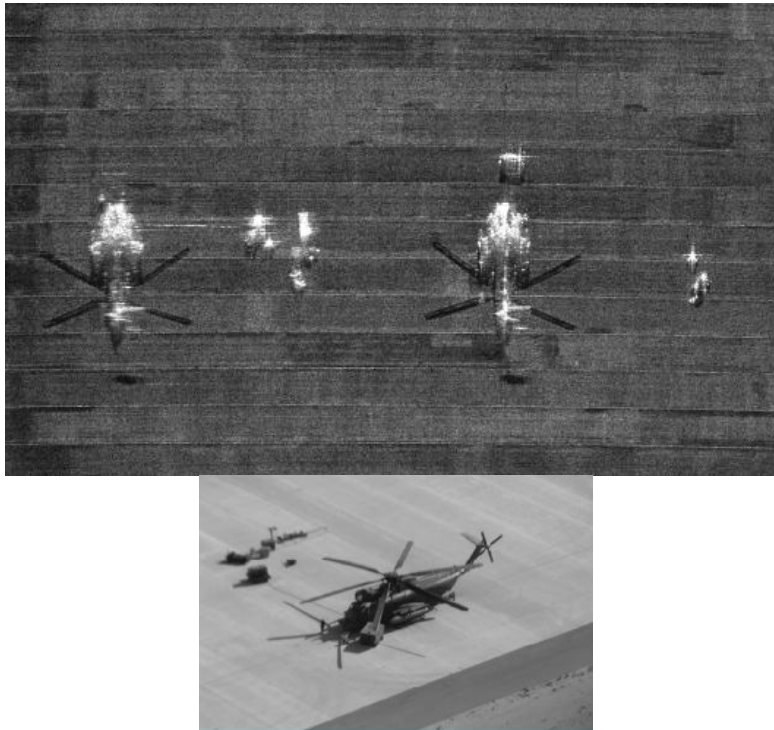


Figure 2. Radar imagery (Top) and a photo of the corresponding object (Bottom).
(From [4])

Despite their differences, the resolution is usually an important measure of performance in both optical and radar imagery as it determines the ability to discriminate distinct objects within the scene. The factors that affect radar resolution are discussed next.

1. Radar Resolution

Radar resolution provides a measure of how close together two distinct point targets can be in order to discriminate them as separate. Imaging resolution for radars is typically defined in terms of the down-range (i.e., along the radial direction from radar)

and cross-range dimensions. This is illustrated in Figure 3. For a monostatic radar, the down-range resolution is dependent on the pulse bandwidth as ([5], p. 13)

$$\Delta DR = \frac{c}{2\beta} \quad (1)$$

where β is bandwidth of the transmitted pulse and c is the speed of light. In radars, where detection performances are important, longer pulse widths are desired as these improve detection performances (assuming the same peak power). Equation (1) implies that the resolution of a long pulse can be made arbitrarily small, provided the pulse is modulated with a sufficiently large bandwidth β . The Linear Frequency Modulated (LFM) waveform is a common example of such modulated waveforms used in imaging.

The cross-range resolution, ΔCR , for a stationary monostatic radar depends on the angular beamwidth, θ , of the radar, which in turn depends on the physical dimensions of the radar antenna effective aperture as follows ([6], p. 155):

$$\theta_{3dB} \text{ (in radians)} = \frac{K_A \lambda}{D} \quad (2)$$

where K_A equals to 1.25 for uniform illumination pattern of a square antenna aperture, λ is the carrier wavelength and D is the antenna's physical dimension in the azimuth plane.

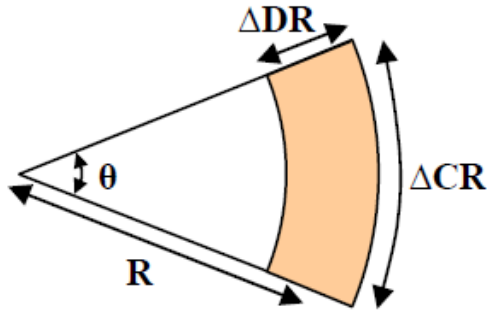


Figure 3. A two-dimensional monostatic range cell (From [7])

Synthetic Aperture Radar (SAR) processing allows the improvement of cross-range resolution of monostatic radars beyond the bounds of its physical antenna aperture. This is done by creating a large synthetic aperture by taking multiple snapshots from a

moving platform. This approach is much akin to creating a large physical planar array, except that the elements are transmitted at different times. This scheme also implies that, in order to achieve similar “antenna element spacing,” a sufficiently high sampling rate (along the synthetic aperture) should be needed to avoid the presence of artifacts such as grating lobes ([8], pp. 28–29). The signals obtained along this “array” are coherently summed to achieve the equivalent narrow beamwidth. Thus, the achievable cross-range resolution depends on the length of the synthetic aperture that can be created. This resolution therefore varies with the different types of imaging data collection schemes. Figure 4 and Figure 5 illustrate two commonly described schemes.

A strip-map or scan mode of SAR imaging continually sweeps along a track and produces a strip of imagery. Here, the size of the synthesis aperture, with respect to a single point target, is limited by the antenna’s actual beamwidth as it sweeps across the track. Hence, the resolution for a broadside target is given by ([5], p. 22)

$$\Delta CR_{Stripmap} \approx \frac{\lambda}{2\Delta\theta} = \frac{\lambda}{2(\lambda/D)} = \frac{D}{2} \quad (3)$$

where λ is the carrier wavelength and D is the physical dimension of the antenna. This seems to be a counter-intuitive result as it suggests that the smaller the antenna dimension, the better the cross-range resolution. This is because a smaller antenna tends to have a wider beamwidth, which results in a longer observation time for a given target.

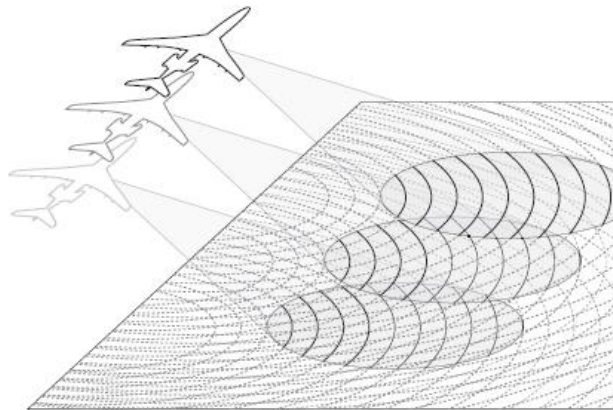


Figure 4. Stripmap modes for SAR imaging (from [9])

In the spotlight mode of SAR imaging, the antenna beam is placed on a fixed scene of interest and the beam is continually steered to remain on this fixed scene as the platform moves. Here, the size of the synthetic aperture is typically limited by the observation time and the radar velocity. Hence, the resolution for a broadside target is given by [5], p. 23.

$$\Delta CR_{Spotlight} \simeq \frac{\lambda}{2\Delta\theta} = \frac{\lambda}{2(vT/R)} = \frac{\lambda R}{2vT} \quad (4)$$

where λ is the carrier wavelength, R is the range to the target in down-range direction, v is the speed of the SAR platform and T is the observation time.

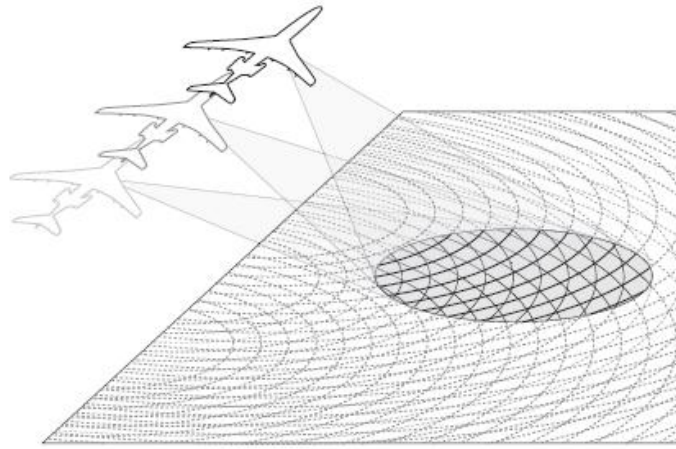


Figure 5. Spotlight mode for SAR imaging (from [9])

For the studies done in this thesis, the transmitters and receivers are assumed to be omnidirectional and range decay is neglected. Hence, the aperture is only limited by the observation baseline (i.e., radar velocity times observation time) simulated. Thus, the cross-range resolution can also be given by Equation (4).

For multi-static radar imaging, the point spread function that defines resolution will depend on the multi-static geometry as well as the effectiveness of the coherent sum (e.g., due to time synchronization). The down-range and cross-range resolutions are best worked out through simulations [7], [10].

2. One-Dimensional Imaging

In the simplest case of a stationary mono-static pulsed radar with directional antenna, a single pulse generates a series of returns corresponding to reflections along the transmit-receive path direction, with the strength of the echo proportional to the radar reflectivity of the object after adjusting for range decay. This series of returns are known as a range profile, and it provides a one-dimensional image of the reflectors along the down-range axis of the radar. In order for such an image to be useful, the image must allow the distinctly separately objects of interest to be resolved clearly. Figure 6 shows an example of a range profile generated by a High-Resolution Radar (HRR).

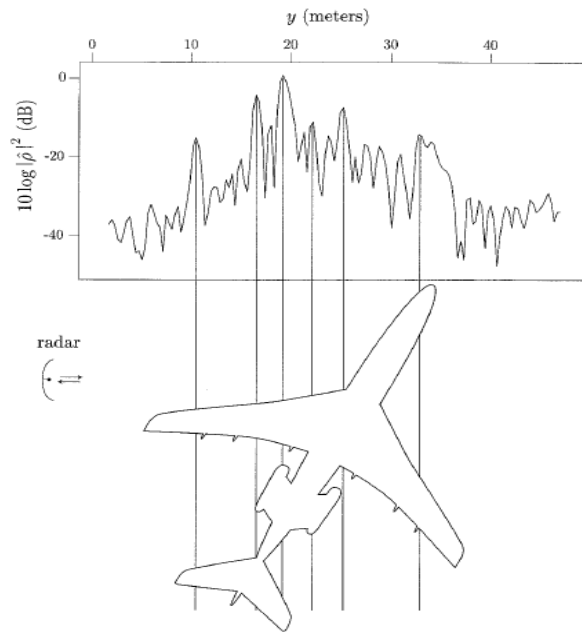


Figure 6. Example of a range profile generated by a high resolution radar (From [11])

Table 1 provides a feel of the necessary transmitted pulse bandwidth versus desired down-range resolution. It is quite clearly seen that higher resolutions either require higher transmission frequencies (and have higher hardware requirements in order to accommodate the larger bandwidths required), or require the complex processing of waveforms in ultra-wideband radar systems, since narrowband assumptions may no longer be valid.

Table 1. Required pulse bandwidths versus desired range resolution for monostatic radars

Desired Range Resolution	Required Pulse Bandwidth
10 meters	15 MHz
1 meter	150 MHz
0.1 meter	1.5 GHz

Before proceeding, a brief note can be made about the domain of validity of one-dimensional (1-D) imaging. A common approximation used in the SAR image processing is the start-stop, or stop-and-go, approximation [12], [13], where the radar and target are assumed to be momentarily stationary during their respective times of interaction with the wave. While literature commonly mentions this approximation in conjunction with two-dimensional (2-D) imaging, we note that the assumption basically simplifies the 1-D imaging processing (or fast-time domain processing as it is commonly known in SAR literature). This approximation is generally valid when the radar and target do not move significantly during their interaction times with the wave. For typical radar applications, the speeds of the radar and target are small relative to the speed of electromagnetic wave propagation and pulse widths are sufficiently short to ensure this validity. The consequence is that the received signal is expected to just be a time-shifted scaled replica of the transmitted signal. Hence, in the typical radar, a replica of the transmitted signal is used in the correlation receiver for matched filtering to generate the range profile.

3. Two-Dimensional Imaging

Two-dimensional radar imaging seeks to create a 2-D spatial image in terms of the radar reflectivity of an observed scene or target. There is much available literature, such as [13], that provide descriptions of methods or algorithms to form a 2-D radar image. These methods all seek the same outcome, which is to take advantage of the underlying information contained within observations of the target from multiple aspects

angles to create an image. This procedure requires the observation of a scene or target from multiple aspect angles, which is typically achieved using the following methods:

- The most commonly discussed method is Synthetic Aperture Radar (SAR) imaging. This involves a radar taking snapshots of the desired scene at different positions while it moves.
- A second method known as the Inverse SAR or ISAR method observes a moving target with multiple looks as the target moves and turns.
- Multi-static imaging involves having multiple receivers that receive scattered waves at different directions with respect to the scene or target. The transmitters are not co-located with the receivers.

The concept of “backprojection” provides a simple way of understanding the physical method behind radar image reconstruction. Backprojection essentially involves taking the received signal and mapping it to the set of possible physical locations using a known physical relationship. In the case of radar, this is the relationship between a spatial location and the propagation time required for the signal to travel from the transmitter to that location and then back to the receiver. Since the transmission and reception times for a radar signal are typically known, the set of possible spatial locations from which the associated signal was backscattered can be determined¹. The received signal is proportional to the radar reflectivity of target, weighted by the beam patterns of the transmitter and receiver, propagation effects and range-decay. Hence, the associated radar reflectivity to be allocated to each location is the signal strength, adjusted by the inverse of the two-way antenna beam pattern and range-decay. In this thesis, the antennas are all assumed to be omni-directional. Propagation effects and range-decay are neglected as only the relative amplitudes within a small far-away scene are examined, and hence the differences within each scene are small. Hence, the radar reflectivity in this case is directly proportional to the signal received. Figure 7 illustrates an example of the backprojected image for a single monostatic radar pulse corresponding to multiple point targets.

¹ We assume that the radar is operating within its unambiguous range and thus all signal returns are from the pulse that was transmitted immediately before. In the case of a radar operating with range ambiguity, the received signal may contain a mixture of returns from multiple pulses and hence additional ambiguity is introduced into the mapping between the spatial domain and reception time.

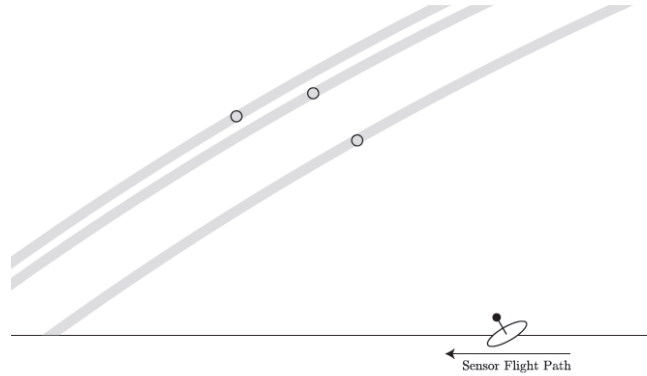


Figure 7. Example of backprojected image for a single monostatic radar pulse for multiple point targets. The grey lines are contours lines of equal reception times passing through the targets' locations. (From [14])

To localize the scatterers, an observation can be made from another aspect angle and the backprojected images are overlaid. Figure 8 shows the composite image formed. It can clearly be seen that the intersections of the backprojections correspond to the true locations of the scatterers. This is somewhat akin to position triangulation. In this case, the backprojected images are coherently summed to obtain the final image.

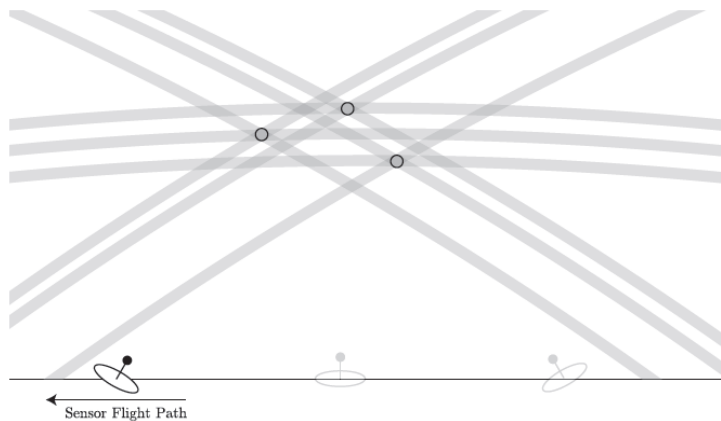


Figure 8. Composite backprojection image for monostatic radar pulses taken at three different aspects for multiple point targets. All three sets of lines intersect at the true target locations. (From [14])

In the case of a practical radar pulse, the response to each point scatterer is not a delta-function, but rather, spreads over period of time around the target location. This is

because signals which are bandlimited in the frequency domain must have a finite duration in the time domain. The consequence of this in 2-D imaging is that the imaging outcome to an ideal target is a response that is centered on the target location, but is spread around its spatial vicinity. This is known as the imaging Point Spread Function (PSF). Figure 9 shows an example of an imaging PSF. The PSF is of interest in imaging studies as it defines the imaging characteristics of the system, including the imaging resolution attainable. Assuming that the objects are non-interacting, the imaging response to multiple point targets is the superposition of the point spread functions, each shifted by the spatial coordinates and weighted by the radar reflectivity of each object.

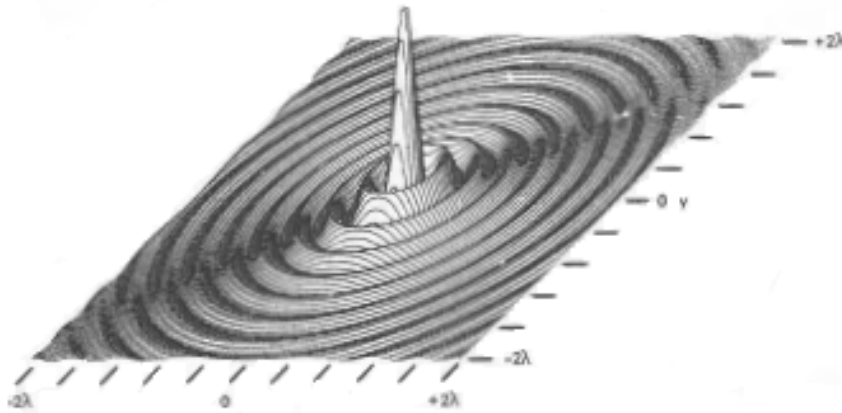


Figure 9. Example of an imaging point spread function (From [5])

C. MOTIVATION AND FOCUS OF THESIS

Radar imaging is of great interest in both civil and military applications, especially due to its day/night all-weather capabilities. The objective of this thesis is to study the imaging degradations that occur when a scene to be imaged by radar contains moving targets. This work began as a study of the linearized theory by Cheney and Borden [12], [15] for the imaging of moving targets. During the course of investigation, it was realized that there was a need to develop an independent model capable of modeling the non-linear effects on the received signal resulting from target and sensor motion, in order to put the linearized theory to test. Hence, the focus of this thesis is the development and verification of such a simulation model, in order to observe the imaging degradations that occur with sensor and target motion.

D. THESIS ORGANISATION

This thesis is organized in the following manner:

Chapter II provides a theoretical overview of the physics of wave interaction with a moving target. This is used to derive the signal propagation time, as a function of the transmission time, for sensors and targets that are moving linearly with constant speed. The effects of motion are briefly explored. This section concludes with a short literature survey providing an overview of current research on the topic of radar imaging with respect to moving targets.

Chapter III provides a description of the implemented simulation model. The rationale and design of the model to generate the received signal at uniformly spaced time intervals is explained in detail. The implementation of the backprojection algorithm is also described.

Chapter IV consists of two main portions. First, the results of model verification for the 1-D and 2-D imaging outputs are presented. Then, two case studies on the imaging of moving targets are presented, one for a multi-static configuration and another with a moving SAR.

Chapter V concludes the thesis by summarizing the results and provides suggestions for future research areas.

II. MOTION IN RADAR IMAGING

In this chapter, we outline a mathematical model that illustrates the scattering of electromagnetic waves and one-dimensional (1-D) imaging of scenes containing moving targets. The investigation here focuses on the 1-D point spread function (PSF)—i.e., the received response to a single perfect point target resulting from a transmitted signal. A general discussion of the various methods found in literature to address moving targets rounds out the chapter.

A. SCENARIO AND ASSUMPTIONS

We consider a mono-static radar system (in which the transmitter and receiver are co-located) mounted on a moving platform with trajectory path, $\vec{\Gamma}_{tx}(t)$, which in this general case need not be restricted to a linear profile. We also have a moving target whose general trajectory path is $\vec{\Gamma}_{tgt}(t)$. To study complex, extended targets, one approach could be to take on the first-order Born approximation which basically assumes targets are made up of non-interacting scatterers (i.e., no multiple reflection terms, etc). When such an approximation is valid, linear superimposition can be used to determine the returns from a more complex target scenario. Beyond this assumption, more complicated models that consider multiple-order interactions between scatters will be needed to accurately model returns, but such modeling will greatly increase complexity and computation requirements. As we are only studying a point-spread function, we assume a single perfect point reflector as our target in the scene of interest.

B. TRANSMISSION AND PROPAGATION

Since we envision that the 1-D image is to be used as an input to a 2-D image formation process in SAR processing, we consider the origin as the center of the observed scene, within which the target exists. At time $t = 0$, we assume the target and a monostatic sensor to be at position $\vec{\Gamma}_{tgt}(t) = \vec{u}_{tgt}(t)$ and $\vec{\Gamma}_{tx}(t) = \vec{u}_{tx}(t)$, respectively.

We assume that the radar transmits, at time $t = t_{tx}$, an arbitrary single narrowband radar waveform, $w_r(t)$, with pulse width T_w . A non-dispersive transmission medium is

taken here as it simplifies the analysis greatly by allowing us to assume that the waveform shape does not naturally change with time. Without loss of generality, this assumption is equivalent to propagation through uniform free space, hence the wave's propagation speed is equal to the speed of light, c . From here on, we proceed by neglecting the scaling effects of range decay found in the 3-D Green's function for point sources in free-space. This approximation is valid when we are only looking at a small scene of interest that is far away from the radar, such that the scaling effects due to range remains relatively constant within the scene and across time during the imaging process ([13], p. 13). Thus, the incident EM wave, at scalar range ρ from the radar and at time t , is given as:

$$E_{in}(\rho, t; t_{tx}) = \begin{cases} w_R(t - t_{tx} - \frac{\rho}{c}) & \text{for } 0 \leq t - t_{tx} - \frac{\rho}{c} \leq T_w \\ 0 & \text{otherwise} \end{cases} \quad (5)$$

For simplicity of expression, we henceforth drop the limits in time and just note that the wave goes to zero outside the corresponding time arguments defined for the waveform.

We note that, when assuming a perfect omni-directional antenna, the strength of the propagating incident wave is determined by its range from the radar and is independent of direction. However, a scalar range can no longer be considered when viewing the wave from the chosen origin, since the radial symmetry of propagation is no longer valid when viewed from a point other than the source. As the radar is assumed to be at $\vec{\Gamma}_{tx}(t_{tx})$ at transmission time, we can rewrite the incident wave (i.e., Equation (5)) with respect to a position from origin, \vec{p} , as:

$$E_{in}(\vec{p}, t; t_{tx}) = w_R \left(t - t_{tx} - \frac{|\vec{p} - \vec{\Gamma}_{tx}(t)|}{c} \right) \quad (6)$$

This incident wave is valid for any fixed position \vec{p} until the wave reaches an object with which it interacts.

C. INTERACTION AND RECEPTION

As already indicated, for this study, the target is only one perfect point located at $\vec{\Gamma}_{tgt}(t)$. This target is also assumed to be idealized in such a way that it supports an infinite bandwidth in its response and hence does not distort the frequency response of the incident wave. It will thus perfectly and instantly reradiate the incident wave omnidirectionally. Thus, the reflectivity is simply a scaling factor at the location at the target. For simplicity, we neglect the negative sign (i.e., phase shift of π radians) as this is a constant phase shift that will not affect our results.

Clearly, the target will interact with the wave when the positions of the wave and the target coincide in space. For the sake of analysis, we denote the time when this happens as t_{ix} , where $t_{ix} > t_{tx}$. We will proceed to derive the relationship between this time and the transmission and reception times for some specific cases later in this chapter. Following wave-target interaction, the scattered wave that is re-radiated omnidirectionally from $\vec{\Gamma}_T(t_{ix})$ can be observed at any given position \vec{q} as:

$$E_{sc}(\vec{q}, t; t_{ix}) = w_R \left(t - t_{ix} - \frac{|\vec{\Gamma}_{tgt}(t_{ix}) - \vec{\Gamma}_{tx}(t_{ix})|}{c} - \frac{|\vec{q} - \vec{\Gamma}_{tx}(t_{ix})|}{c} \right) \quad (7)$$

The total field present in the environment is a combination of the incident and scattered waves. However, for the purpose of reception, we consider only the scattered field. This is valid because practical systems always have some means of isolating the received signal from the transmitted. In pulsed systems, the transmit and listening time periods are designed to be mutually exclusive, and for CW systems, an isolator is normally used. Thus, the received wave is just the scattered wave which propagates back to the receiver, interacting with the receiver when their positions coincide.

$$E_{rx}(\vec{\Gamma}_R(t_{rx}), t; t_{ix}) = w_R \left(t - t_{ix} - \frac{|\vec{\Gamma}_{tgt}(t_{ix}) - \vec{\Gamma}_{tx}(t_{ix})|}{c} - \frac{|\vec{\Gamma}_{tx}(t_{rx}) - \vec{\Gamma}_{tgt}(t_{ix})|}{c} \right) \quad (8)$$

D. LINEAR TRAJECTORY

We note that in general, the positions $\Gamma_{tx}(t_{ix})$, $\Gamma_{rx}(t_{ix})$ and $\Gamma_{rx}(t_{rx})$ are time dependent. Hence, the relationship given in Equation (8) between the received wave and transmitted wave is a very general one and does not particularly offer insights into the behavior affecting the waveform. However, we can deduce from the previous discussion that the various timing within the argument depends on the interception points between the wave and the target/radar and thus is geometry dependent.

To put things into clearer perspective, we select a case where both a monostatic radar and the target are traveling on linear paths with constant velocities:

$$\begin{aligned}\vec{\Gamma}_{ix}(t) &= \vec{u}_{ix} + \vec{v}_{ix}t \\ \vec{\Gamma}_{tgt}(t) &= \vec{u}_{tgt} + \vec{v}_{tgt}t\end{aligned}\quad (9)$$

Figure 10 illustrates the geometry from transmission to target interaction. As defined, t_{ix} is the time when the positions of the wave and the target are equal.

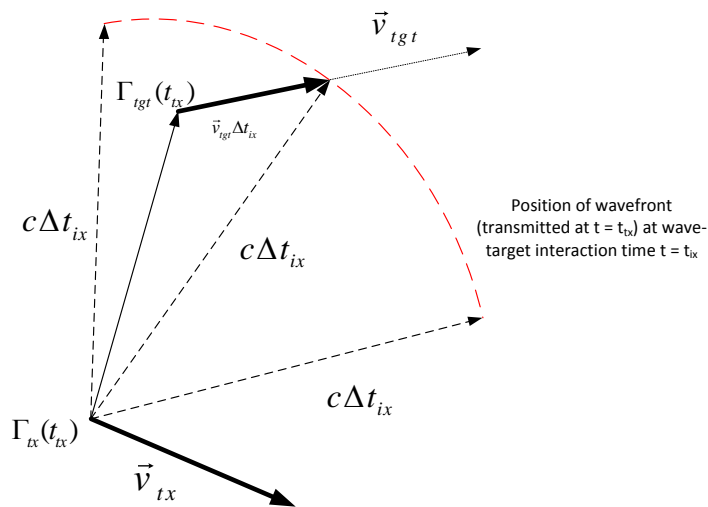


Figure 10. Illustration of geometry at interaction between wave and target.

Since we know the wave speed, as well as the position and velocity of the target, the time of interaction, t_{ix} , can be computed by solving for interception, that is:

$$R_{EMwave}(t_{ix} - t_{tx}) = R_{tgt}(t_{ix}) \quad (10)$$

We define $\Delta t_{ix} = t_{ix} - t_{tx}$ and compute the ranges from ranges from the radar's position at transmission:

$$c\Delta t_{ix} = \left| \vec{u}_{tgt}(t_{tx}) + \vec{v}_{tgt}\Delta t_{ix} - \vec{u}_{tx}(t_{tx}) \right| \quad (11)$$

For simplicity of writing, we define the relative positions between the radar and the target at the time of transmission, i.e., the expression $(\vec{u}_{tgt} + \vec{v}_{tgt}t_{tx} - \vec{u}_{tx} - \vec{v}_{tx}t_{tx})$, as $\vec{u}_t(t_{tx})$. Expanding Equation (11) yields the following equation, which is quadratic in terms of Δt_{ix} :

$$\left| \vec{u}_t(t_{tx}) \right|^2 + 2\vec{u}_t(t_{tx}) \cdot \vec{v}_{tgt}\Delta t_{ix} + \left(\left| \vec{v}_{tgt} \right|^2 - c^2 \right) \Delta t_{ix}^2 = 0 \quad (12)$$

We solve for the causal (i.e., $\Delta t_{ix} \geq 0$) solution (See Appendix A.I for full derivation) and thus obtain:

$$\Delta t_{ix}(t_{tx}) = \frac{\vec{u}_t(t_{tx}) \cdot \vec{v}_{tgt} + \sqrt{(\vec{u}_t(t_{tx}) \cdot \vec{v}_{tgt})^2 + (c^2 - \left| \vec{v}_{tgt} \right|^2) \left| \vec{u}_t(t_{tx}) \right|^2}}{(c^2 - \left| \vec{v}_{tgt} \right|^2)} \quad (13)$$

To determine t_{rx} , we apply similar reasoning with the roles of the source and target now reversed (i.e., the target is now the source of the wave and the radar is the interception point). For this, we define $\Delta t_{rx} = t_{rx} - t_{ix}$ so that $t_{rx} = t_{ix} + \Delta t_{ix} + \Delta t_{rx}$. We obtain

$$\Delta t_{rx}(t_{ix}) = \frac{-\vec{u}_t(t_{ix} + \Delta t_{ix}) \cdot \vec{v}_{tx} + \sqrt{(\vec{u}_t(t_{ix} + \Delta t_{ix}) \cdot \vec{v}_{tx})^2 + (c^2 - \left| \vec{v}_{tx} \right|^2) \left| \vec{u}_t(t_{ix} + \Delta t_{ix}) \right|^2}}{(c^2 - \left| \vec{v}_{tx} \right|^2)} \quad (14)$$

where $\vec{u}_t(t_{ix} + \Delta t_{ix})$ can be obtained by evaluating the position of the target at time $t_{ix} = t_{ix} + \Delta t_{ix}$, and Δt_{ix} can be computed using Equation (13).

E. WAVEFORM DISTORTION

From Equations (13) and (14), we see that both linear trajectories (Δt_{ix} and Δt_{rx}) are, in general, non-linear functions of t_{ix} . This has consequences on the shape of the waveform. To visualize this, we consider a pure sine waveform, $w_R(t)$, as made up of the sum of many samples separated by infinitesimally small, equally spaced, transmission time intervals, $t_{ix,n} = n\Delta t_{ix}$ i.e.,

$$w_R(t) = \lim_{\Delta t_{ix} \rightarrow 0} \sum_{n=-\infty}^{\infty} e^{i2\pi f n \Delta t_{ix}} \delta(t - n\Delta t_{ix}) \quad (15)$$

We note from the previous definitions that the reception times for two adjacent samples transmitted at times t_{ix} and $t_{ix} + \Delta t_{ix}$ can be expressed as

$$t_{rx}(t_{ix}) = t_{ix} + \Delta t_{ix}(t_{ix}) + \Delta t_{rx}(t_{ix}) \quad (16)$$

$$t_{rx}(t_{ix} + \Delta t_{ix}) = t_{ix} + \Delta t_{ix} + \Delta t_{ix}(t_{ix} + \Delta t_{ix}) + \Delta t_{rx}(t_{ix} + \Delta t_{ix}) \quad (17)$$

In order for the received waveform shape to remain distortion-free (i.e., the same as transmitted), it is required that upon reception, all samples have been scaled by the same scaling factor and that all samples continue to be separated by the time interval, Δt_{ix} . This requirement must be true for our free-space propagation and ideal target assumptions. Thus, for absence of waveform distortion at receive, it is necessary that

$$t_{rx}(t_{ix} + \Delta t_{ix}) - t_{rx}(t_{ix}) = \Delta t_{ix} \quad (18)$$

Or, from Equation (16) and (17), equivalently

$$\Delta t_{ix}(t_{ix} + \Delta t_{ix}) + \Delta t_{rx}(t_{ix} + \Delta t_{ix}) = \Delta t_{ix}(t_{ix}) + \Delta t_{rx}(t_{ix}) \quad (19)$$

We can see from Equations (13) and (14) that these quantities are non-linear functions of the transmission time and hence, in general, Equation (19) will not be satisfied and we can expect the waveform shape to be distorted due to changes in the spacing of the samples. This effect is akin to time dilation or expansion due to relative motion. Once the samples are no longer equally spaced as per the original signal, we can expect that $w_R(t)$ will no longer be a pure sinusoidal tone when viewed in the frequency domain. A special case exists when both radar and targets are stationary ($\vec{v}_{tx} = 0$ and $\vec{v}_{tgt} = 0$), resulting in:

$$\Delta t_{ix} + \Delta t_{rx} = \frac{2|u_{ix} - u_{tgt}|}{c} \quad (20)$$

which is the well-known time-of-flight formula used in radar analysis and is independent of the transmission time.

F. DOPPLER MODULATION EFFECT

Another common situation present in radar calculations is the scenario where the velocity vectors of the radar and target are parallel to their initial line-of-sight, $\Gamma_{tgt}(t_{ix}) - \Gamma_{ix}(t_{ix})$. In such cases, the velocities may be expressed as scalar multiples of the initial line-of-sight vector. For simplicity, we assume that the radar is stationary and note that all other such cases can be expressed as this basic case by converting to the radar's frame of reference. We consider the case of an inbound target so that

$$v_{tgt} = -|v_T| \hat{u}(t_{ix}) \quad \& \quad v_{ix} = 0 \quad (21)$$

Using Equations (21) in (13) and (14), we can see that the terms in the radical cancel out to yield a simple expression (See detailed derivation in Appendix A.III) :

$$\Delta t_{ix}(t_{ix}) = \frac{|\vec{u}_t(t_{ix})|}{(c + |\vec{v}_{tgt}|)} \quad (22)$$

Similarly,

$$\Delta t_{rx}(t_{tx}) = \frac{|\vec{u}_t(t_{tx})|}{(c + |\vec{v}_{tgt}|)} \quad (23)$$

We can express the change in propagation times between any two samples as

$$\Delta t_p(t_{tx} + n\Delta t_{tx}) - \Delta t_p(t_{tx}) = \frac{-2|\vec{v}_{tgt}|n\Delta t_{tx}}{(c + |\vec{v}_{tgt}|)} \quad (24)$$

Putting (24) back into (15), we have

$$\begin{aligned} E_{rx}(t) &= \lim_{\Delta t_{tx} \rightarrow 0} \sum_{n=-\infty}^{\infty} \cos(2\pi f n \Delta t_{tx}) \delta(t - n\Delta t_{tx} (1 + \frac{2|\vec{v}_{tgt}|}{(c + |\vec{v}_{tgt}|)})) \\ &= \cos(2\pi f (1 + \frac{2|\vec{v}_{tgt}|}{(c + |\vec{v}_{tgt}|)})t) \end{aligned} \quad (25)$$

The time dilation introduced can be seen equivalently as a Doppler frequency shift of a radar waveform by an inbound or outbound target when retaining the same time spacing at the receiver.

G. ROLE OF START-STOP APPROXIMATION

To examine the effects of motion, we take a closer look at the implications of the commonly assumed start-stop approximation vis-à-vis the received wave. The fundamental assumption here is that the radar and the target are both momentarily stationary when the wave is being transmitted and received.

From the previous discussion, it is clear that when the radar and the target are stationary, the received signal will be

$$E_{rx}(\vec{\Gamma}_R(t_{rx}), t) = w_R(t - t_{tx} - t_p) \quad \text{for } t_{tx} \leq t \leq t_{tx} + T_w \quad (26)$$

where $t_p = 2|\vec{\Gamma}_T(t_{rx}) - \vec{\Gamma}_R(t_{tx})|/c$

This means that at the receiver, the correlator can be implemented by performing matched filtering with a replica of the transmitted waveform. The output of the matched

filter is given by the autocorrelation function of $w_R(t)$, given by Equation (27), which has its peak when $\tau = t_{ix} + t_p$.

$$\rho(\tau) = \int w_R(t - t_{ix} - t_p) w_R^*(t - \tau) dt \quad (27)$$

where the asterisk denotes complex conjugation.

When the radar and target are moving, the distorted waveform will change the output of the correlation receiver. The exact effect of the distortion depends on the type of waveform employed. This is typically studied through the use of the radar ambiguity function, which is essentially the correlation function in the spatial domains, evaluated at different modulation frequencies, ν , as follows

$$\chi(\nu, \tau) = \int_{-\infty}^{\infty} w_R(t) w_R^*(t - \tau) \exp(2\pi\nu t) dt \quad (28)$$

H. ARTIFACTS FROM MOVING TARGETS

Imaging degradations, also termed artifacts, occur when the conditions of the actual scene do not correspond to the assumptions embodied within processing techniques. One such mismatch is the assumption of a stationary scene when there is in fact motion present. Typically, the moving radar will have its own means of knowing and compensating for its own motion, for example through the use of Inertial Navigation Systems (INS) and/or Global Positioning System (GPS), or through antenna phase center displacement. Hence, available literature mainly focuses on addressing the target motion and, to a lesser extent, the residual effects of imperfect radar motion compensation. We focus solely on target motion here.

Qualitatively, the outcome of target motion in a 2-D SAR image is generally as shown in Figure 11. These generally include smearing in range, smearing in cross-range, and a shift in the cross-range dimension.

The analysis from [16] and ([17], pp.152–154) illustrates that the effects of the waveform distortion leads to the shift in the cross-range dimension due to the Doppler shift introduced and a cross-range defocusing due to a non-linear phase term. Other

additional effects include the effect of range-walk (i.e., target crossing into a different range cell during the processing interval) and the effect of observing the target at different positions over the observation interval in the backprojection algorithm. We attempt to study these effects using the simulation model developed.

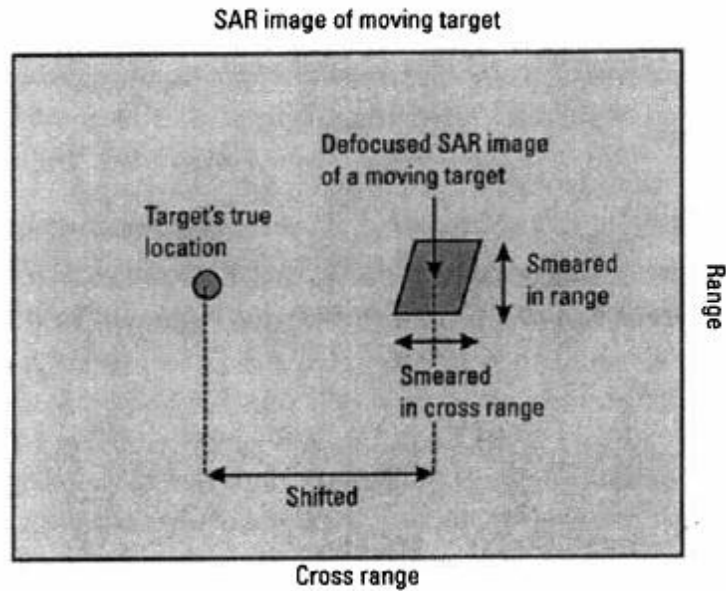


Figure 11. Effects of target motion on SAR imaging (From [17])

I. METHODS TO ADDRESS DE-FOCUSING

The topic of moving targets has been the focus of ongoing research interest on SAR over the past decades. A general survey of literature was made to provide brief backgrounds on past and current work in this area. Based on this survey, related research can be generally classified into the following areas.

1. Velocity Estimation Techniques in Single Channel SARs

Such SAR systems have only a single transmit/receive channel, and hence the Doppler shifted signals from moving targets are mixed in with the returns from stationary targets as part of the received signal. During matched filtering (typically matched for stationary scene), the returns from moving targets will lead to artifacts as a result of their

mismatch with the filter. With such systems, the focus is thus on obtaining an estimate of the target velocity using the radar returns [18], [19], [20] before applying the estimated velocity to achieve Doppler correction for the moving target. While the moving target becomes focused with such corrections, the rest of the scene not at the same velocity tends to become defocused.

2. Multichannel SAR (MSAR)

This class of SARs can generally be considered to include the Velocity SAR or VSAR proposed in [21], Displaced Phase Center Array (DPCA), as well as further work on the Multichannel SAR (MSAR) utilising Space Time-Adaptive Processing techniques (STAP) in SAR [22]. The key characteristic of this class of techniques is that the SAR system is set up to receive signals in multiple elements of the antenna arrays (space samples) and over different instances (time samples). Farina and Lombardo [22] provide a good overview of the evolution of MSAR architectures all the way through to the eventual incorporation of STAP techniques, including the use of time-frequency analysis methods [17]. MSARs are reported to provide better clutter suppression due to the additional degrees of freedom offered by the multiple antennas. This lends itself to Moving Target Indicator (MTI) processing; however, this is gained at the expense of greater hardware requirements.

3. Compressive Sensing

Compressive Sensing (CS) seems to be a recently explored technique introduced to the domain of SAR processing [23], [24], [25]. According to Patel [26], “compressed sensing enables the reconstruction of sparse or compressible signals from a small set of non-adaptive, linear measurements. If properly chosen, the number of measurements can be much smaller than the number of Nyquist rate samples.” Essentially, CS involves the selection of an appropriate sub-space basis set of functions that allow the SAR data set to be reduced. This method has been applied to the SAR imaging of uniformly moving targets in [23] “with higher resolution and lower sidelobes with fewer measurements.” We will not further investigate the application of CS in this thesis.

4. Linearized Theory by Cheney and Borden

The linearized theory from Cheney and Borden [15] is of particular interest to this thesis, as this thesis was motivated by study of this theory. This imaging procedure for moving targets is derived from the principles of wave scattering that combines the spatial, temporal and spectral aspects of scattered field based imaging. The work is an extension of the prior work from [12], which considered stationary sensors in multistatic configurations, to moving sensors. In essence, a linearized formulation of the phase (i.e., time argument) of the received signal is developed by making the following assumptions:

- The Born approximation is used to express the scattered wave as a simple function of the incident wave, since scatters are assumed to be non-interacting.
- The Platform and target motion are slow relative to the speed of light. The sensor is also much more distant than target from the origin and this range is much larger than the distance travelled between pulses by the sensor or the target. This approximation allows the higher order terms in the Taylor series expansion of the time dependent range between target and sensor to be dropped, thus linearizing the argument that appears in the phase function of the received wave.

With the following definitions adopted in [15],

$f_m(t - T_m^T)$ is the waveform for m -th pulse sent out at time $t = T_m^T$

$\gamma_m^T, \dot{\gamma}_m^T$: transmitter position and velocity vectors at the time of transmission

$\gamma_m^R, \dot{\gamma}_m^R$: transmitter location and velocity vectors at the time of reception

$\Gamma_m + v_m t$ is the trajectory vector of the target

$Q(\bar{\mathbf{z}})$ is the 3-D spatial reflectivity function of target

T_m' is the time of where the transmitted wave interacts with the target

These assumptions lead to the formulation of the imaging algorithm for each pulse based on matched filtering that is based on the signal that is expected from each point $\bar{\mathbf{p}}$ and each velocity \mathbf{v}_m in which the image I_m is given by

$$I_m(\bar{\mathbf{p}}, \vec{\mathbf{v}}_m) = \int f_m^*(\phi_m(t, \bar{\mathbf{p}}, \vec{\mathbf{v}}_m)) (4\pi)^2 |\gamma_m^T| |\gamma_m^R| (1 - \hat{\gamma}_m^T \cdot \vec{\mathbf{v}}_m / c) (1 + \beta_m^T) \epsilon_m^{sc}(t) dt \quad (29)$$

where

$$\phi_m(t, z, \mathbf{v}_m) \approx \frac{1}{1 + \beta_m^T} [\alpha_{\mathbf{v}_m} ([1 - \beta_m^R] t - R_m^R(z, \mathbf{v}_m) / c) - R_m^T(z, \mathbf{v}_m) / c] - T_m^T \quad (30)$$

$$\beta_m^T = \hat{\gamma}_m^T \cdot \dot{\gamma}_m^T / c \quad \& \quad \beta_m^R = \hat{\gamma}_m^R \cdot \dot{\gamma}_m^R / c \quad (31)$$

$$\alpha_{\mathbf{v}_m} = \frac{1 + \hat{\gamma}_m^T \cdot \mathbf{v}_m / c}{1 + \hat{\gamma}_m^R \cdot \mathbf{v}_m / c} \quad (32)$$

$$R_m^R(z, \mathbf{v}_m) = |\gamma_m^R| - \hat{\gamma}_m^R \cdot (z + \Gamma_m - \mathbf{v}_m T_m' + \dot{\gamma}_m^R T_m^R) \quad (33)$$

$$R_m^T(z, \mathbf{v}_m) = |\gamma_m^T| - \hat{\gamma}_m^T \cdot (z + \Gamma_m - \mathbf{v}_m T_m' + \dot{\gamma}_m^T T_m^T) \quad (34)$$

This method is similar to the ‘‘shift-varying filter’’ mentioned in ([13], pp. 212–215), but further accounts for shifts in the velocity domain, rather than just spatial locations. Full treatment of the derivation for the Cheney-Borden procedure can be found in [15]. The earlier work in [12] serves as a useful reference to provide further insights to the basis for the derivation.

THIS PAGE INTENTIONALLY LEFT BLANK

III. DESCRIPTION OF MODEL

This chapter provides design considerations and descriptions of the model that was implemented for the purpose of these studies. The model was implemented using MATLAB, R2011a 32-bit version.

A. OVERVIEW OF SINGLE PULSE MODEL

A key objective of this model is to allow the synthesis of a received waveform that has been distorted by effects of motion for analysis of effects on radar images. Figure 12 illustrates the general concept behind the model for single pulse generation.

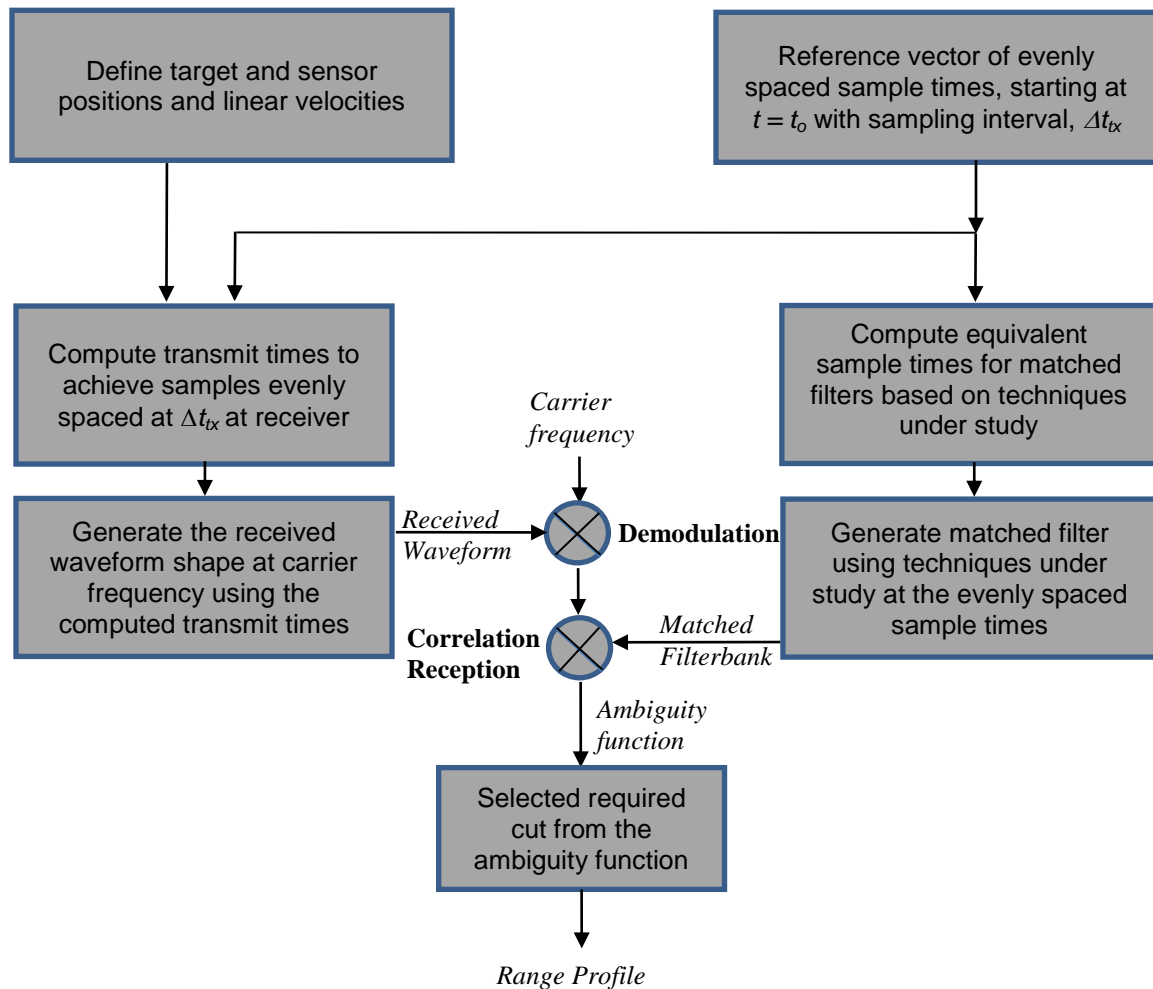


Figure 12. Block diagram for range profile generation

B. DEFINITION OF TARGET AND SENSOR TRAJECTORY

The implemented model allows for the definition of position and motion in three-dimension (3-D) spatial coordinates. As this model is intended for imaging, the origin is set at the center of the imaged scene. This model will only work for static or constant linear velocity scenarios due to the assumption made during the derivation of wave-interaction time and reception time. However, the positions of the transmitter, target, and receiver can be defined independently. This design is intended to allow for the possibility of defining different sensor configurations in different studies. Possible implementation methods for different configurations are provided in Table 2.

Table 2. Examples of possible sensor configuration that can be studied

Configuration	Possible Implementation Method
Stationary, Mono-static	Transmitter and receiver initial positions are defined to be the same, both with zero velocity. Each run provides the range profile for one pulse. This configuration may not be useful ² for SAR studies by itself, but serves as a useful case for model verification or a study on the performance of networked monostatic sensors.
Stationary, Multi-static	Transmitter and receiver initial positions are defined to be different, both with zero velocity. This can be used for multi-static SAR. In case of multiple receivers, a single pulse for each receiver position can be simulated separately for the same transmission instant to obtain the set of range profiles for <i>a single image</i>

² Although such a configuration can be practically used for Inverse-Synthetic Aperture Radar (ISAR), it is not useful here since the constraint of linear motion limits target rotational motion that ISAR requires.

Moving, Single-Channel Monostatic	Transmitter and receiver initial position are defined to be the same, both with the same non-zero velocity. This can be used for single channel SAR.
Moving, Multi-channel Monostatic (e.g., Displaced Phase Center Arrays)	Transmitter and receiver initial position are defined to be separated by the antenna displacement, both with the same non-zero velocity. Single pulse for each receiver position to be simulated separately for the same transmission instant to obtain the entire set of range returns for <i>a single pulse</i> . This can be used for multi-channel SAR.

C. WAVEFORM GENERATION CONCEPT

In order for the general waveform model to work, the continuous-time function of the waveform is required to be implemented so that the complex amplitude of the wave at any point in time can be computed. The reason for this will be clearer by the end of this section. These formulations are generally well known (e.g., in [27]) for typical practical waveforms for radar systems, and hence should typically not present difficulty in implementation. Examples for the rectangular and Linear Frequency Modulation (LFM or commonly known as chirp) waveforms are provided in Table 3.

Table 3. Examples of waveform functions

Name of waveform	Expression
Rectangular Pulse	$w_R(t) = A_m \text{rect}\left(\frac{t}{T_w} - \frac{1}{2}\right) \exp(i2\pi f_c t)$
Linear Frequency Modulated (Up-chirp)	$w_R(t) = A_m \text{rect}\left(\frac{t}{T_w} - \frac{1}{2}\right) \exp(-i\pi \frac{BW_w}{T_w} t^2) \exp(i2\pi f_c t)$

We also note that in general, the transmitted and received waveforms are continuous time functions, but for the purpose of digital simulations, these can only modeled through discrete time functions, typically by using evenly-spaced time samples. The use of evenly-spaced time samples is convenient as this allows easy signal and spectral analysis using the Discrete Fourier Transform (DFT) [28]. This simplification results in more cost-efficient hardware implementation. As a result, the Digital-to-Analog Convertors (DAC), Analog-to-Digital Convertors (ADC), and signal processing units employed as part of the sensor hardware largely use evenly-spaced time samples.

We see from the theory covered in Chapter II that, for moving sensors and targets, the propagation time for a wave is dependent on the geometry at the instants of wave transmission, interaction, and reception. For constant linear sensor and targets velocities, the relationship between the propagation time, Δt_p , for each sample can be determined as the sum of Equations (13) and (14). This propagation time, Δt_p , is in general a non-linear function of the transmission time. The implication of this non-linearity is that, following propagation, the corresponding amplitude samples arriving at the receiver may no longer be spaced at the same time intervals as the transmitted waveform, and may even be non-evenly spaced in time with respect to each other. Figure 13 illustrates an example of the relationship between the transmitted waveform samples and the distorted received waveform samples.

In digital correlation reception, the cross-correlation is used to measure the similarity between the sampled received signal, $w_{rx}(n)$, and the matched filtered, $f_m(n)$, and is computed as:

$$\rho_{rx,tx}(l) = \sum_{n=-\infty}^{\infty} w_{rx}(n) f_m^*(n-l) \text{ for } l \in \mathbb{Z} \quad (35)$$

where n , l indicate sample sequence numbers for each signal sequence. The matched filter, $f_m(n)$, is typically a sampled replica of the transmitted waveform.

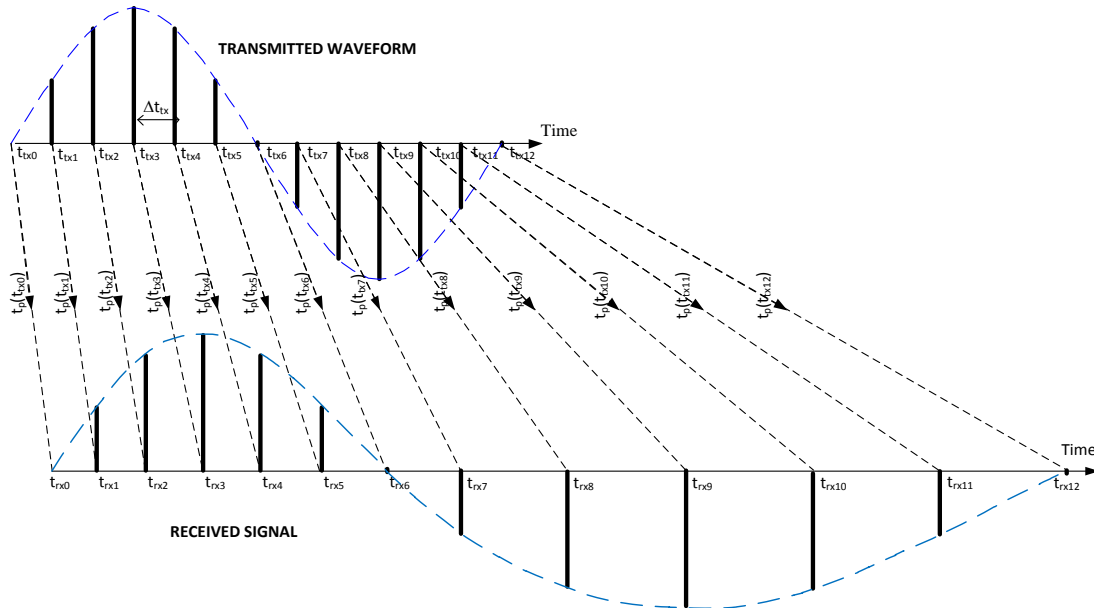


Figure 13. Illustration of relationship between transmitted and received waveforms

It is important to note that the summation in Equation (35) makes the assumption of equally spaced samples in both the received and matched filter sequences. When the received samples do not arrive with the same spacing in time as the transmitted waveform, these samples cannot be used directly in the correlation receiver to derive a meaningful range profile, since the transmitted and received time samples in fact exist at different instants in time, and thus do not contribute to the correlation summation correctly if equation (35) is simply applied. Hence, it is clear that some book-keeping in the time domain needs to be done, in order for the received signal to be processed correctly in a discrete simulation of the received waveform. Based on the preceding discussion, there is therefore good motivation to consider “resampling” the received signals to evenly spaced time intervals that match those of the transmitted waveform.

A number of methods for this “resampling” were initially considered. One possibility is to interpolate the received amplitude-time samples to obtain the required evenly spaced values of the received wave. In theory, sinc-interpolation provides a unique and perfect reconstruction of the bandlimited signals which have been sampled (at least) at Nyquist rate. The time shift properties of the Discrete Fourier Transform (as

given in Equation (36)) and “spectral interpolation (i.e., zero-padding in the frequency domain) also provide convenient means to obtain the value of a function at a different time instant through a given sampled time sequence.

$$x(n-l), (\text{mod } N) \xleftrightarrow{DFT} X(k)e^{i2\pi kl} \quad (36)$$

where N is the length of the sequence, l is the number of samples to be shifted by and n, k refer to the indices of the processed sample. These methods do not work when the arriving samples are non-uniform in time. The problem of interpolation of signals arriving at non-uniform instances in time is still an active area of ongoing research [28], [29]. Consequently, we do not consider these methods for implementation.

Another possibility is to make use of curve-fitting to achieve the interpolation. The values of $t_{tx,n}$ and $t_{rx,n}$ are known. Hence, it could be possible way to consider $t_{rx,n}$ as an arbitrary function of $t_{tx,n}$ and search for a function that fits the known data points. The forms Equations (13) and (14) suggest that the functional relationship is likely to include non-integer powers of $t_{tx,n}$. While it is possible to reconstruct the curve if the right parameters can be found for this curve fitting, the search space for these parameters is likely be large due to the degree of freedom. Hence, this approach, although theoretically possible, may be impractical.

Instead, we choose an approach based on the physical nature of the problem. For constant linear velocities, we can see that the geometry between transmitter, the target and the receiver is defined at the instant of transmission. By including the constraint of causality, we arrive at a unique solution mapping the transmission time, $t_{tx,n}$, to the reception time, $t_{rx,n}$ through the mathematics laid out in Chapter II. We now assert that a wave transmitted at a later instant will not be received earlier than the earlier transmission for a fixed geometrical relationship. This can be easily shown by noting that, for any given target speed v , the propagation time will decrease most rapidly from one transmission instant to the next when the target is moving directly towards the transmission source. In this scenario, assuming the initial range separation between source and target is R , we note from Equation (22) and (23) that the two-way propagation time is

$$t_p = \frac{2R}{c+v} \quad (37)$$

Hence, the reception times due to transmission at two instances separated by a small time interval Δt_{tx} are

$$t_{rx1} = t_{tx} + \frac{2R}{c+v} \quad (38)$$

$$t_{rx2} = t_{tx} + \Delta t_{tx} + \frac{R - v\Delta t_{tx}}{c+v} \quad (39)$$

$$t_{rx2} - t_{rx1} = \Delta t_{tx} - \frac{v\Delta t_{tx}}{c+v} = \Delta t_{tx} \left(\frac{c}{c+v} \right) > 0 \quad \forall \Delta t_{tx} > 0 \quad (40)$$

The difference in reception times in Equation (40) is always greater than zero for positive values of Δt_{tx} , hence proving that reception time is a monotonic increasing function of transmission time. With these observations, we can formulate a simple iterative search algorithm to find the values of transmission times that will provide evenly-spaced reception times as follows:

For each value of reception time to computed

Step 1: Set the desired reception time to be $\bar{t}_{rx,n} = t_{rx,0} + n\Delta t_{tx}$ where $t_{rx,0}$ is the reception time of the first sample, n is an integer and Δt_{tx} is the sampling interval used to generate the transmitted wave.

Step 2: Compute, as an initial reception time, $\tilde{t}_{rx,n}$, using equations (13) and (14) with the initial estimated transmission time $\tilde{t}_{tx,n}^{Current} = t_{tx,0} + n\Delta t_{tx}$.

Step 3: Compare the estimated reception time, $\tilde{t}_{rx,n}$, against the desired reception time, and do the following:

- If $|\tilde{t}_{rx,n} - \bar{t}_{rx,n}| > \Delta_e$, where Δ_e is the acceptable error, set the updated estimated transmission time as

$$\tilde{t}_{rx,n}^{New} = \tilde{t}_{rx,n}^{Current} - (\tilde{t}_{rx,n} - \bar{t}_{rx,n})$$

Compute the updated reception time, $\tilde{t}_{rx,n}$, using equations (13) and (14) with the updated estimated transmission time $\tilde{t}_{rx,n}^{New}$ and repeat Step 3.

- Else, end the iteration. $\tilde{t}_{rx,n}^{Current}$ is the required value for the current sample.

Step 4: Repeat from Step 1 for next sample until all samples in the range profile have been processed.

Once the entire set of corresponding transmission times have been determined, the functional relationship of the transmitted waveform can be used to obtain the associated amplitude values. It is for this reason that the continuous time representation of the waveform is a pre-requisite for this method to work. Figure 14 illustrates the implemented process.

We also note that in conventional implementations of digital matched filtering, the down-converted received signal is generally sampled at uniform rates. Hence, the received waveform generated would also be an approximate representation of waveforms received in actual systems; however, in practice, there are other practical effects that will affect the received signal.

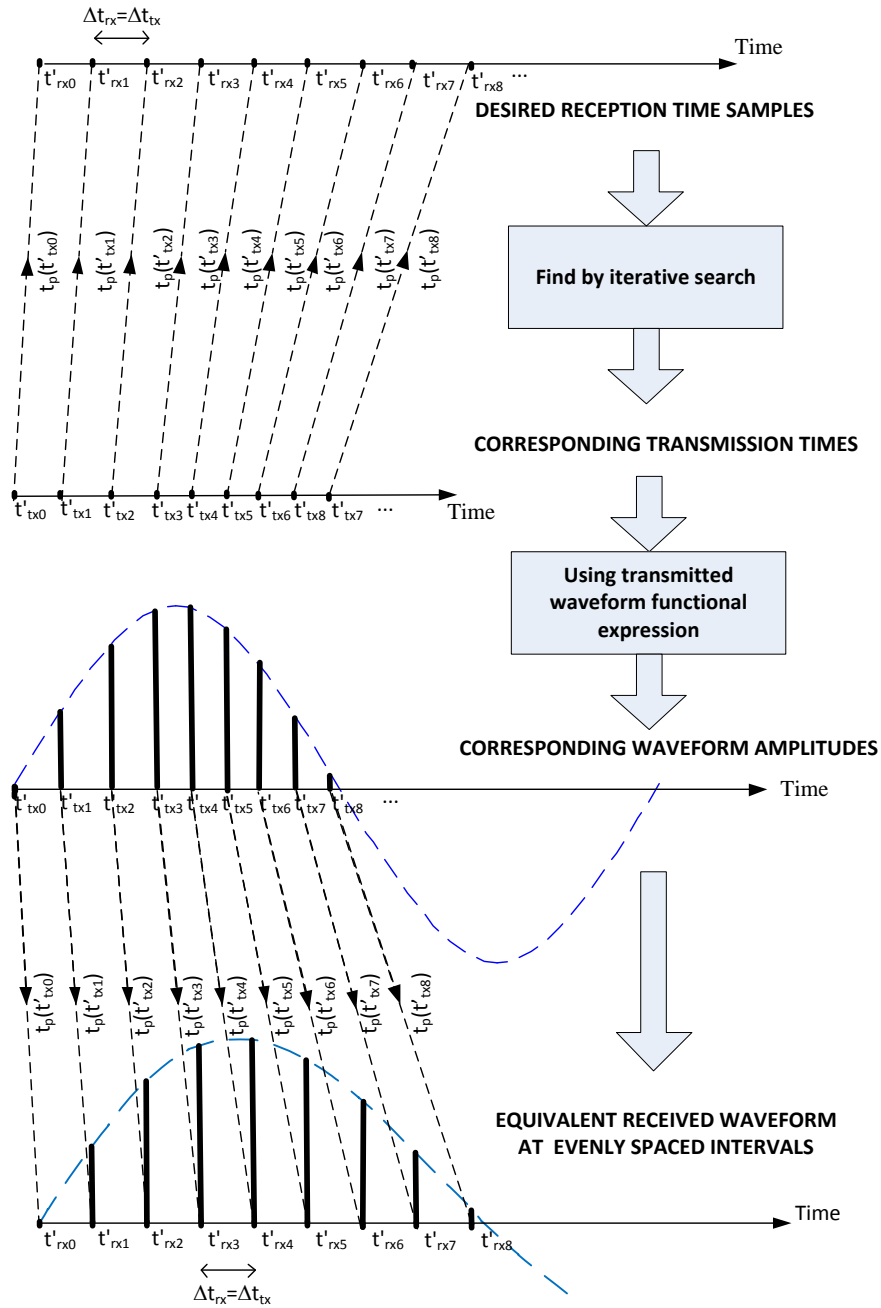


Figure 14. Illustration of received waveform generation process

D. MATCHED FILTERBANK AND RANGE PROFILE

The intent of matched filtering is to maximize the Signal-to-Noise Ratio (SNR) ratio at the receiver end in the presence of noise. When only white noise is considered, it can be shown ([30], pp. 22–28) that the ideal matched filter is a template of received signal free from white noise, but including distortions such as Doppler effect encountered during propagation. Matched filtering in radar is commonly understood as using a replica of the transmitted signal or its Doppler-shifted version to recover the transmitted signal amidst noise. However, this model is not always true, although it is frequently assumed in radar signal processing. This matched filter is a replica of the transmitted signal or its Doppler-shifted version only in scenarios with stationary, radially ingressing, or egressing targets when viewed from the sensor’s frame of reference. More generally, the formulation in [15] provides a linearized model that can be used to derive the matched filter that accounts for phase-space (or equivalently, time domain) distortions due to target and sensor motions. Nevertheless, many systems continue to use the transmitted signal replica or its Doppler-shifted version as this greatly simplifies signal processing implementations, yet at the same time yields relatively accurate results.

In this study, as the intent is to examine the artifacts due to motion, we only implement the matched filter as a bank of the transmitted signal replica and its Doppler-shifted versions to observe the outcomes of wrongly assuming the start-stop approximation. With such a bank of Doppler-shifted filters, the output of the correlation filter in the absence of distortion is simply the waveform’s ambiguity function. This also provides a useful check for the correctness of the simulation. To provide the best signal for imaging, the output from the filter within the banks that provides highest peak should be chosen as the range profile to be used for imaging since this filter is the one that best corrects for the signal modulation that has been introduced into the received signal. We note that the simulation is sufficiently flexible to allow the use of other forms of matched or mismatched filters that the user generates.

The output of the digital correlation receiver can be described by Equation (35). In a practical simulation, suitable limits need to be placed on the time domain for summation. For calculating the cross-correlation between two sequences of lengths M

and N respectively, the final sequence length will be $M+N-1$. For a time-limited waveform, we can make use of the fact that the signal is zero outside the pulse width. Hence, the matched filter length is determined by pulse width divided by the sampling interval. The length of the received waveform will need to consider the time expansion or compression introduced during propagation. We estimated the required length by taking the worst case time expansion to ensure that the entire received signal is modeled. This can be done by deriving the time expansion for the case of an egressing target. We obtain

$$t_{rx2} - t_{rx1} = \Delta t_{tx} + \frac{v\Delta t_{tx}}{c-v} = \Delta t_{tx} \left(\frac{c}{c-v} \right) > 0 \quad \forall \Delta t_{tx} > 0 \quad \text{for } v < c \quad (41)$$

Hence, for a transmitted signal sequence with M samples within its pulse width, at least $M(c/c-v)$ samples (including zero-valued samples outside the pulse width) should be generated for the received pulse, in order for the received waveform to be completely simulated. We add to this discussion a few words about the importance of choosing the right sampling rate. In general, in order to reproduce a signal without aliasing, the required sampling rate should be at least twice the signal bandwidth (i.e., Nyquist rate). This choice of sampling needs to consider the added bandwidth due to the effects of distortion in order to avoid aliasing. In our study, we select a sampling rate much higher than the Nyquist rate to avoid this.

E. IMAGE RECONSTRUCTION

In image reconstruction, the objective is to create a representation of the reflectivity of the scene in the 2-D spatial domain by using several observations of the desired scene. So far, the generation of range profile outputs needed for image reconstruction have been covered in the previous sections. Image reconstruction is discussed here. The concept of image reconstruction is presented in Figure 15 and requires two important processes, namely, Range Alignment, and Image Formation.

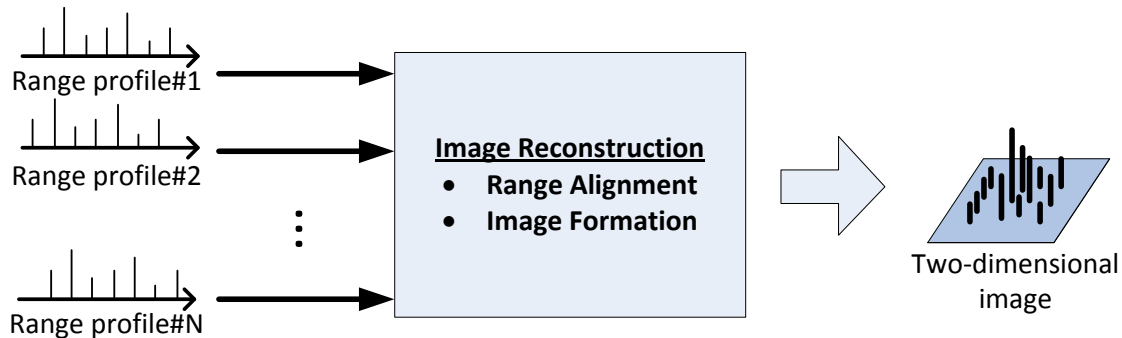


Figure 15. Block diagram illustrating concept of image reconstruction

1. Range Alignment

Typically in radar imaging, it is necessary to range align all the range profiles prior to passing the data set to the algorithm. This is required as the radar data is collected at different start ranges and hence the same sample numbers in each of the range profile sequences correspond to different reception times (and hence spatial samples). The intent of range alignment is to ensure that when processed, the respective samples in the range profiles represent the same range when processed together side-by-side. In order to range align the data, the amount of range shift required can be worked out by keeping track of the propagation time to the scene center and subtracting this from the reception time of the signal from the target. When this is done, what remains is the time position of each sample relative to the scene center. Thus, the signal sample with time reference nearest to zero will be the nearest sample to the scene center in terms of range (or bistatic range for multi-static radars). All the different range profiles can thus be aligned by “placing” this sample at the middle of each sequence and zero-padding the sequence where necessary in order to achieve the same sequence length for all the range profiles to be processed. As the range profiles consist of evenly-spaced samples, the range alignment to correct for fractional steps (i.e., to shift by fractions of a single range cell) can be done by using the Fourier time shift property presented in Equation (36). We note that this range alignment is exact for stationary sensors (mono-static and multi-static) since the time to scene center remains unchanged through all the collected samples. This is no longer true in the case

with moving sensors; in such cases, the time to scene center at the start of transmission is used as an approximation. We note that a separate range alignment process is no longer required when using the implemented backprojection method for image formation.

2. Image Reconstruction Using Backprojection

The concept of backprojection was presented in Chapter I. One implementation of a backprojection algorithm is the Inverse Radon Transform that is implemented in MATLAB as the function *iradon.m* [31]. The Inverse Radon Transform is used in computerised tomography and is equivalent to the backprojection of a scene to form a spatial image when given a series of one-dimensional views. This is similar in application to the use of a series of range profiles that are collected at different aspect angle to a target, in order to form an image of the target reflectivity distribution.

A further simplification of the Inverse Radon Transform involves using the two-dimensional Inverse Discrete Fourier Transform (2-D IDFT) to achieve imaging. This method can be shown to be approximately equal to the back projection method under the assumption that the observation angle is small. This is because when the observation angle is small, the data collected appears on a nearly-rectangular grid, and hence, is suitable for processing using Fourier methods as a spatial transform. When the data collection deviates sufficiently from a rectangular grid (monostatic radar data are normally collected on a polar grid and multi-static data on an elliptical grid), pre-processing to interpolate the data to a rectangular grid should be done prior to using the FFT method for imaging.

We note that the Inverse Radon Transform implemented in MATLAB is limited to the use of uniformly spaced observation aspect angles. The use of 2D-FFT also requires evenly spaced sampling in both the range and angular domains. Since it is impractical to expect radar data to be always collected from uniformly spaced aspect angles in both multistatic and moving SAR configurations, an imaging algorithm was developed and implemented as part of this study to overcome this limitation.

The key concept behind this imaging algorithm is also the backprojection method. This algorithm is inspired by existing literature describing this method ([13], pp.357–

359). However, the implementation here was developed and tailored to fit the rest of the model. The rationale and implementation of this model are further explained here.

Physically, the received signal is the result of the transmitted pulse travelling to an object and being backscattered to the receiver. The reception time is simply the transmission time with two-way propagation time of the receiver. For each signal received at a given reception time, the propagation time can be deduced if there is knowledge of the transmission time. It is therefore possible to reconstruct, based on the transmitter and receiver geometry, the set of possible spatial locations that this signal has been backscattered from.

For a monostatic radar, this procedure involves solving for the set of possible position coordinates $[x,y,z]$ that satisfy the following:

$$t_p = 2\sqrt{(x-x_r)^2 + (y-y_r)^2 + (z-z_r)^2} / c \quad (42)$$

where $[x_r, y_r, z_r]$ are the position coordinates of the radar. This turns out to be the equation for circles with the radar at the origin and radius equal to $ct_p/2$. For a multi-static radar, the bistatic range equation has to be used.

$$t_p = \sqrt{(x-x_{tx})^2 + (y-y_{tx})^2 + (z-z_{tx})^2} / c + \sqrt{(x-x_{rx})^2 + (y-y_{rx})^2 + (z-z_{rx})^2} \quad (43)$$

where $[x_{tx}, y_{tx}, z_{tx}]$ and $[x_{rx}, y_{rx}, z_{rx}]$ are the position coordinates of the transmitter and receiver respectively. The set of points corresponding to the same reception times are ellipses with the transmitter and receiver locations at the focal points, corresponding to the well-known ‘‘ovals of Cassini,’’ and is a generalisation of the case of monostatic radar. For a moving sensor, the exact process is more complicated due to the dynamic change of positions from range sample to range sample. Ideally, the time map should be recomputed for each range sample before being used to update the image map. In the implemented model, we assume that the time map does not change significantly during the pulse in order to reduce the computational load and simply use the time map based on the sensor positions at the start of transmission. This assumption is likely to be valid as long as the sensor moves much less than the required imaging resolution cell during the pulse duration.

The implemented model makes use of the mapping of reception time to each sample point in the desired scene, as defined by a set of contiguous known coordinates. This map of reception times is used to compare against reception times associated with the range profiles in order to assign these range profiles values to the right spatial location. Figure 16 illustrates the concept of this algorithm, which is described as follows:

Step 1: Create a matrix of spatial coordinate points representing the desired scene. The separation between each of the points shall be smaller than the sampling cell of the range profile data to be used.

Step 2: Create a matrix of the same size to store imaging data corresponding to the scene. This is matrix hereinafter referred to as the “image map.”

Step 3: Using the known transmitter and receiver location, the signal reception time after travelling to each spatial coordinate point is computed. This set of reception times, each corresponding to a spatial coordinate in the desired scene is hereinafter called “time map.”

Step 4: For a single range profile, process each range sample (with amplitude, A_n and reception time, $t_{rx,n}$) as follows:

Step 4a: Search for all position indices in the time map with receptions times between $t_{rx,n} - T_s / 2$ and $t_{rx,n} + T_s / 2$.

Step 4b: Add the amplitude value, A_n , to the corresponding points on the image map.

When completed, the set of $\{A_n\}$ in the image map forms the “image” provided by a single pulse.

Step 5: Repeat Step 4 for all available range profiles and cumulatively sum the image maps from all the range profiles. When completed, the image can be visualized by plotting the magnitude of the image map.

One major advantage of this algorithm is that it automatically performs the polarimetric (or ellipsoidal) interpolation and range alignment through the reception time

mapping, whereas a separate step is typically required for the FFT methods to work. Furthermore, since the time map is re-computed based on sensor configuration for each range profile, this method overcomes the limitation present in both the FFT and Inverse Radon Transform methods of requiring data to be collected at uniformly spaced angles. This method is also very flexible in the sense that the image map can be easily recomputed for a different scene of interest using the same range profile data by re-computing the time map corresponding to the new scene. Furthermore, different waveforms may be used in the generation of each range profile, since the correlation receiver takes care of the characteristics of each waveform when generating each range profile.

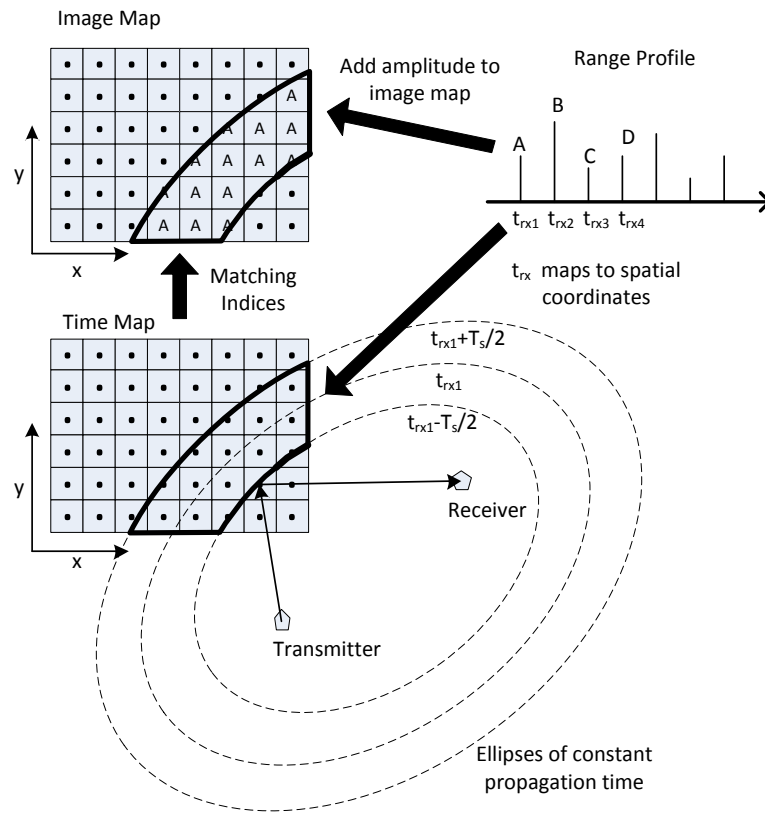


Figure 16. Illustration of the backprojection method

IV. RESULTS

In this chapter, the results produced by the implemented model are presented. Source codes are appended in Appendix B for reference.

A. SIMULATION PARAMETER SELECTION

The key limitation of the simulation model is its heavy computational resource requirements, in terms of both time and memory. MATLAB also places restrictions on the maximum size of vectors and matrices, which limits the scenarios that can be simulated. In this Section, we describe the effect of simulation parameter choices on the simulations so that appropriate choices may be made regarding scenarios.

1. Waveform Definition

The waveform parameters to be defined include the carrier frequency, pulse width, pulse bandwidth, and pulse repetition interval. The pulse width defines the time interval—according to Equation (41)—for which samples need to be generated for each range profile of a point target, since samples outside of this interval will be zero. The pulse bandwidth defines the necessary sample time interval to recover the baseband signal since it is necessary to sample the pulse sequence minimally at the Nyquist rate in order to avoid aliasing. In order to ensure that the sampling interval is sufficient taking into account effects such as target motion, we oversample the time sequence beyond Nyquist sampling.

The number of samples per pulse width is given by pulse width divided by the sampling interval. For a pulse width of 1 μs and a pulse bandwidth of 150 MHz (i.e., for 1 meter down-range resolution), a sampling rate of 1 GHz is selected. This translates to about 1000 samples per range profile. This number of samples is multiplied by the number of pulses to be simulated per run, which can be large in the case of a moving SAR. Furthermore, to resample the received pulse to obtain evenly spaced samples, the search algorithm is processed sample-by-sample within the range profile. Thus, the

simulation of a long pulse and/or a pulse with high bandwidth will lead to range profiles with large numbers of time samples, and hence, require long simulation times and also heavy use of memory.

2. Imaged Scene Definition

The scene to be imaged in the simulation is defined by the scene center location, down-range width, and cross-range width, as well as the resolution steps in down range and cross range. The down range and cross range widths, together with the respective resolution steps, defines the number of cells in the image map used in the backprojection algorithm. The resolution steps in the image map need to be of the same order as the range profile sampling interval, in order to maintain the resolution present in the range profile samples. If the image map resolution is too coarse, the range profile samples may not map correctly to the spatial locations in the image map, and thus affect the imaging outcome. It is not desirable to have an overly fine resolution, as this greatly increases the demand on computational resources. For example, consider the 100 x 100 meter scene. With a sampling rate of 1 GHz, the range sampling interval works out to be 0.3 meters. This means that the image map is a 334 x 334 matrix (111556 samples). In the backprojection algorithm, the updating of the image map is processed on a sample-by-sample basis for each range profile to obtain the image map for a single pulse. This process is repeated for all range profiles.

We conclude this section by noting that, while the implemented algorithm is sufficiently flexible to allow for simulation of a wide range of scenarios, judicious choice of simulation parameters is necessary to manage the computational load, and thus, this consideration limits the types of scenarios that can be simulated using this model.

B. ONE-DIMENSION MODEL VERIFICATION

This section focuses on the verification of processes leading up to the range profile generation. In order to check the correctness of the model, the outputs from the model are checked against known theoretical predictions. The results from these checks are consistent with theoretical predictions. This lends confidence that the model is accurate. The results are presented as follows:

1. Doppler Shift for Approaching and Receding Target

The geometry of scenarios involving approaching and receding targets is illustrated in Figure 17. The theoretical outcome for such scenarios is well known from literature and was also presented in Chapter II. The change in propagation time from sample to sample should correspond to the predictions from Equation (24), when uniformly spaced transmission samples are used to generate the reception times. Equation (24) should continue to be valid even when non-uniform transmission times are used to obtain the required uniformly spaced reception times. Figure 18 shows the results obtained for approaching and receding targets at various speeds. As expected, the propagation time changes as a linear function of the transmission time, with the slope determined by the radial velocity. The differences obtained between the obtained Doppler (by computing the gradient of the propagation time change) and predicted Doppler shifts are less than 10^{-6} Hz.

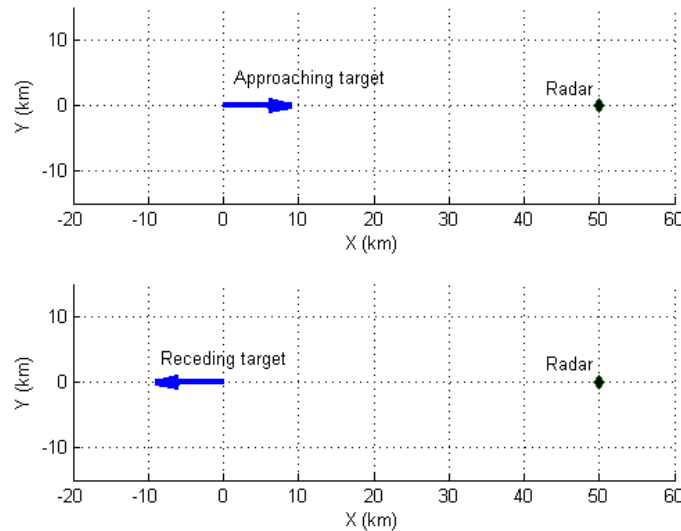


Figure 17. Geometry of the approaching target (Top) and receding target (Bottom) scenarios

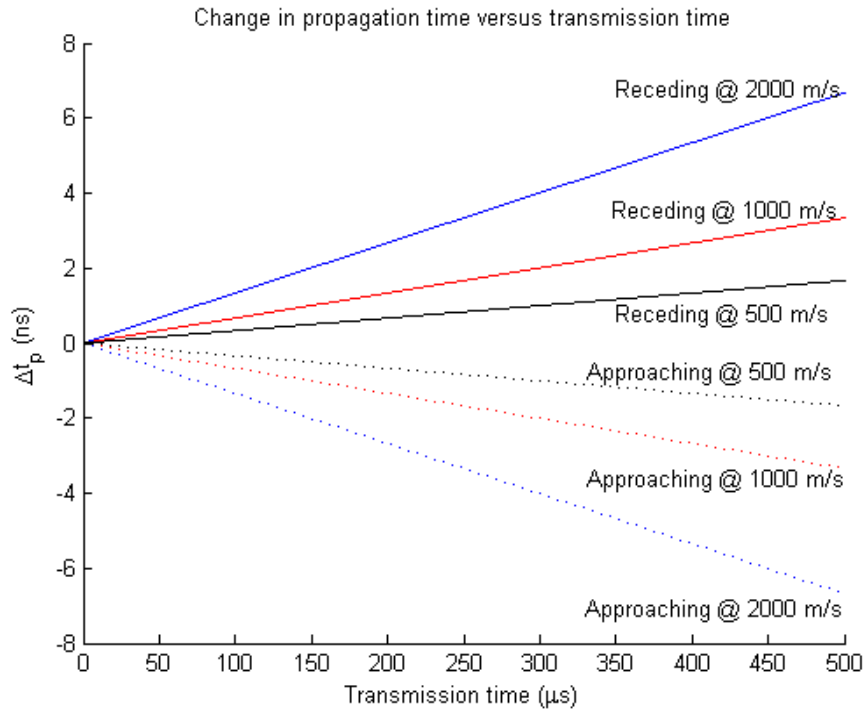


Figure 18. Change in propagation time as a function of transmission time for various approaching and receding radial velocities.

To check for minute non-linearities that cannot be seen from observing the “straight line” graphs observed in Figure 18, the difference between the change in propagation time and a linear line based on theoretical predictions is computed and plotted. A result of zero across all transmission times should be obtained if the results conform to theory. If the relationship were non-linear, then a non-linear relationship should be apparent from the curve. The results from this “deviation from linear” curve, shown in Figure 19, look fairly noisy, although the magnitude of the deviation, at $10^{-13} \mu s$, is very small.

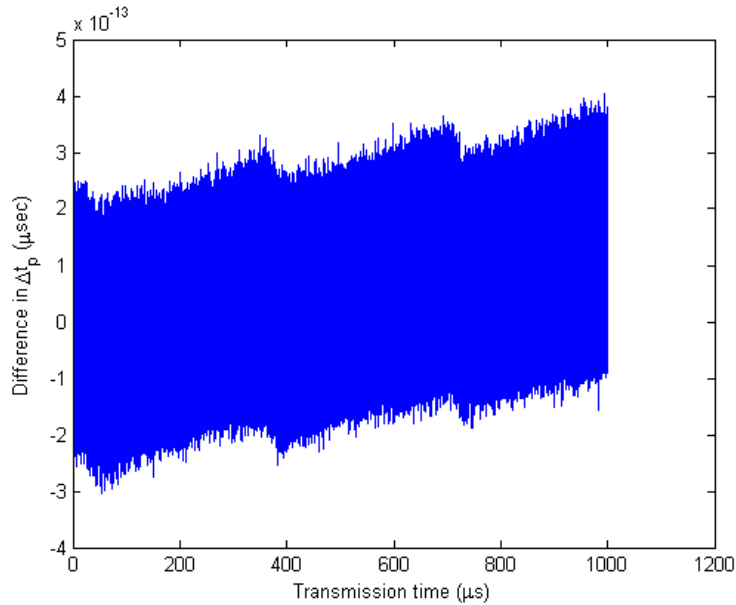


Figure 19. Difference between the simulated change in propagation time versus theoretically predicted linear line as a function of transmission time

Following some investigation, it was confirmed that this is due to quantizing noise from double precision floating point arithmetic used in MATLAB. We provide a short explanation here. MATLAB—and in general, double precision floating point calculations—have a computational dynamic range of around 15–17 digits. This essentially means that when we have two numbers whose difference in magnitude is greater than 10^{16} , the smaller number cannot be represented correctly. This is a consequence of the digital representation of such floating point numbers in 64 bits. MATLAB’s Symbolic Computation Toolbox provides a function that implements Variable Precision Arithmetic (VPA), which allows for the computation of results to beyond double precision accuracy. The main tradeoff in the use of VPA is a great increase in the amount of computer memory and simulation times required. The result of a short study on the use of VPA versus double precision arithmetic is provided in Appendix C for information. These accuracies are mainly required only when a combination of low Doppler speeds and very short sampling intervals are involved. As such, we have scoped our simulation scenario to avoid long simulation times due to the use of VPA. The use of VPA is not further considered in this thesis.

2. Non-linear Relationship Between Transmission and Reception Times

The main cases of interest for study using the model are moving targets which are not directly ingressing or egressing. Hence, we attempt to verify the model with a representative scenario. We pick the case of a single crossing target, starting at $[0;-20;0]$ km and ending at $[0;+20;0]$ km. The target is simulated at various constant speeds along the cross-range axis. The radar is 100km from the origin. Figure 20 illustrates this scenario.

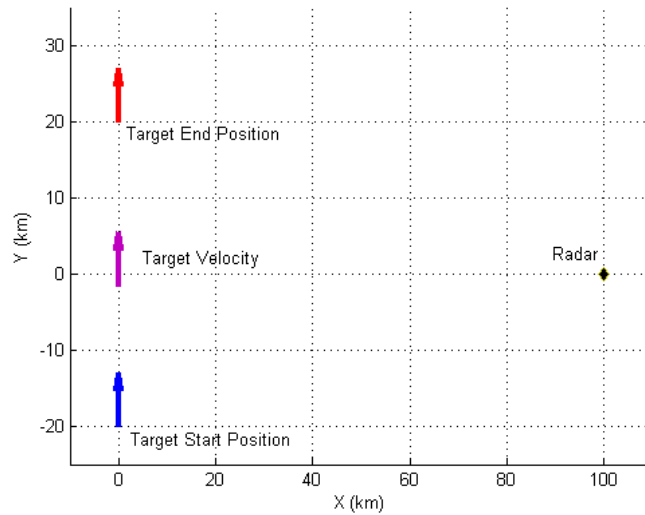


Figure 20. Geometry for scenario with crossing target. This is for the case of a target with crossing speed of 7.8 km/s

From the derivation in Chapter II, we can expect the initial variation in propagation time to be non-linear a function of transmission time. Figure 21 shows the results obtained, which are as expected. We can observe that the magnitude of the change in propagation time does not depend on the speed, but rather on the location of the target at the point of interaction as expected. As a check, we can compute the difference in slant range from the radar between the start position and closest point of approach and compute the difference in propagation time. This difference works out to be $13.2\mu\text{s}$, which is consistent with the simulation results.

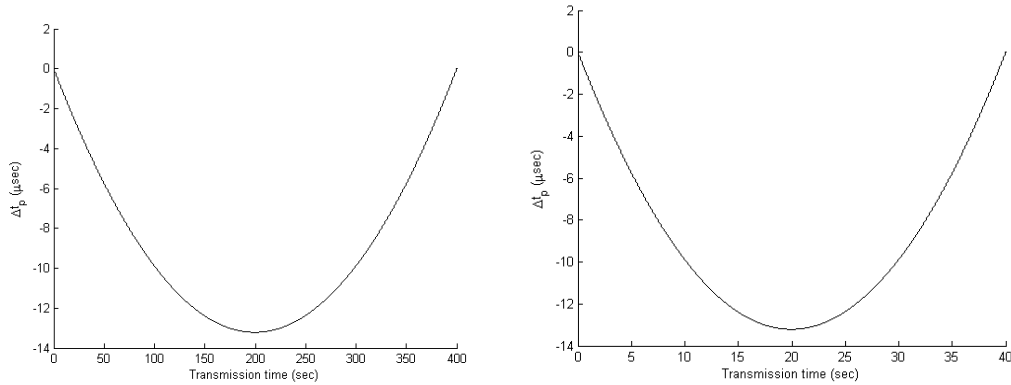


Figure 21. Change in propagation time (referenced to first transmitted sample) for crossing targets at 100 m/s (Left) and 1000 m/s (Right).

Figure 22 shows the change in propagation time over the period of a 500 μs pulse transmission period for a 100 m/s target crossing at closest point of approach 100km away. Based on these results, we can see that the change in propagation time is less than a femtosecond. Compared to the period of waves at microwave frequencies, this variation could be insignificant, and thus justifies the adoption of the start-stop approximation for slow moving targets. However, when a longer pulse is adopted, the non-linearity will become more significant. Figure 23 shows the change in propagation time over the period of a 50 millisecond pulse for a 250 m/s crossing at closest point of approach 50km away. In this case, the deviation is a hundred-th of a nanosecond, which is significant compared to the period of a 10 GHz wave. Hence, it can be seen that for longer waveforms, there may be a further need to examine whether the start-stop approximation is appropriate.

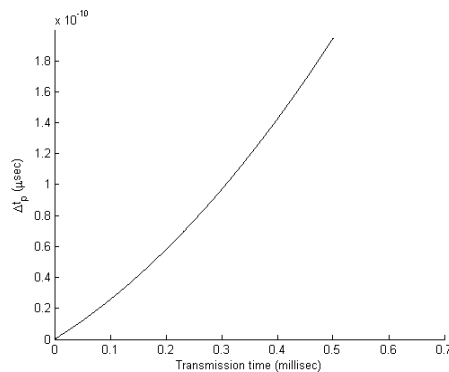


Figure 22. Change in propagation time (referenced to start of transmission sample) for a 500 μs pulse on a 100m/s crossing target at 100km away.

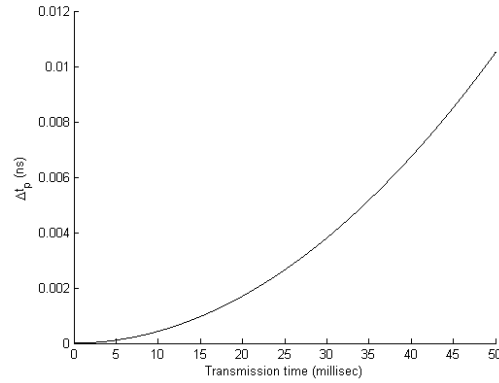


Figure 23. Change in propagation time (referenced to start of transmission sample) for a 50 millisec pulse on a 250m/s crossing target at 50km away.

3. Ambiguity Functions for Known Waveforms

The ambiguity functions of waveforms are useful tools for analyzing the characteristics of a radar waveform in the spatial and Doppler domains. To check the reception process, we generated the ambiguity functions for a monostatic setup by allowing the received signal to be the same as the transmitted signal and passing this through the matched filter. This is done for a rectangular pulse, a Barker-13 binary phase coded pulse, and a LFM pulse. Figure 24, Figure 25, and Figure 26 show the ambiguity functions obtained. These compare well with known ambiguity function plots found in literature ([27], pp.55, pp. 114 and pp.58).

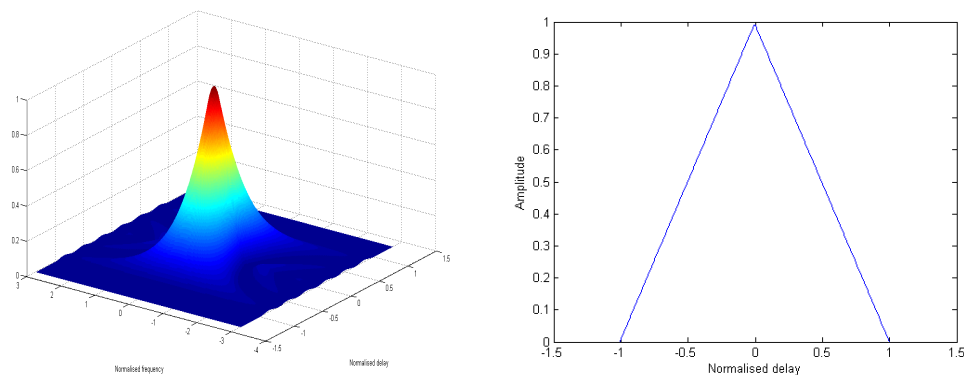


Figure 24. Ambiguity function and associated zero Doppler cut for a rectangular pulse from model. The delay and frequency axes have been normalized using the simulated pulse width and pulse bandwidth (= reciprocal of pulse width in this case), respectively.

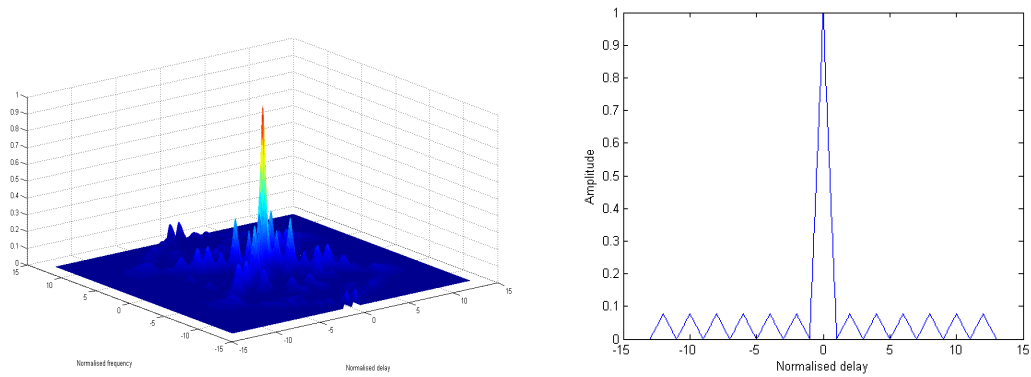


Figure 25. Ambiguity function and associated zero Doppler cut for a Barker 13 binary phased coded pulse from model. The delay and frequency axes have been normalized using the subpulse width and pulse bandwidth, respectively.

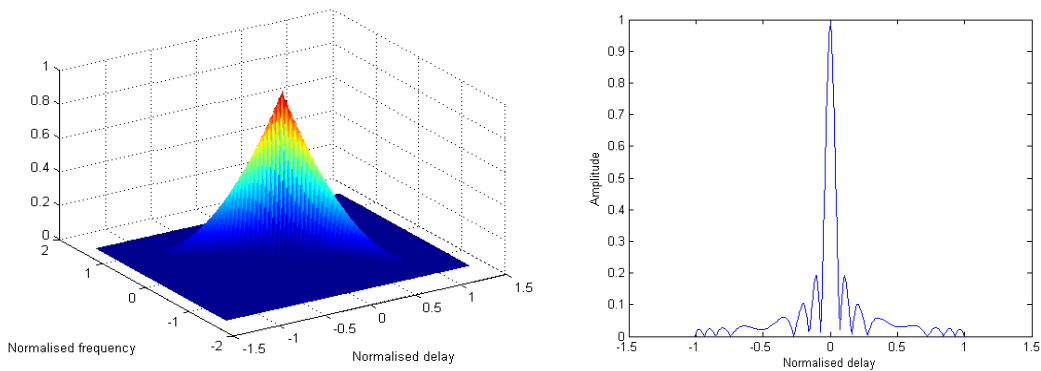


Figure 26. Ambiguity function and associated zero Doppler cut generated for a LFM pulse (Bandwidth=15MHz) from model. The delay and frequency axes have been normalized using the pulse width and pulse bandwidth, respectively.

C. TWO-DIMENSION IMAGING MODEL VERIFICATION

This section focuses on the verification of processes related to image reconstruction.

1. Time Map Implementation for 2-D Imaging

The correct generation of the time map is critical for image reconstruction using the backprojection method. Figure 27 and Figure 28 show the time map generated for both monostatic and bistatic radar configurations. These maps were generated with coarse

spatial sampling at 1km intervals to provide a “big picture” view of the time map. As expected, the monostatic radar presented a circular time map and the multistatic radar provided an ellipsoidal map.

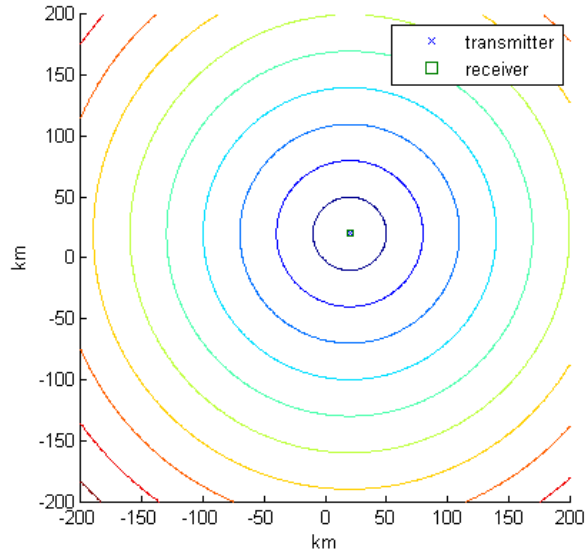


Figure 27. Contour plot of time map for a monostatic radar located at [20km,20km].

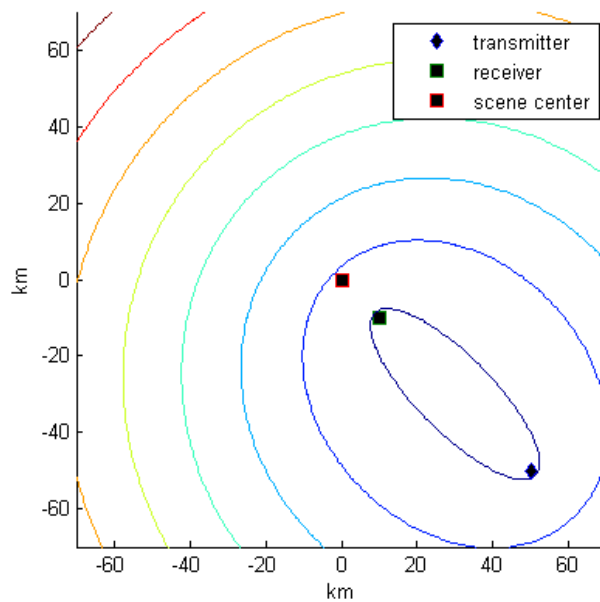


Figure 28. Contour plot of time map for bistatic radar with transmitter at [50km,-50km] and receiver at [10km,-10km].

Figure 29 shows the typical time map that will be used in the imaging process. This is a detailed time map generated for a scene of 400m x 400m in size at 10cm intervals. One observation here is that, although the time map looks fairly elliptical in Figure 28, the contour plots here look fairly linear even though the scene center is only about 14km away from the receiver. This means that there could be potential for linear mapping between the spatial and time domains over such small scenes that could simplify the implementation of backprojection algorithms.

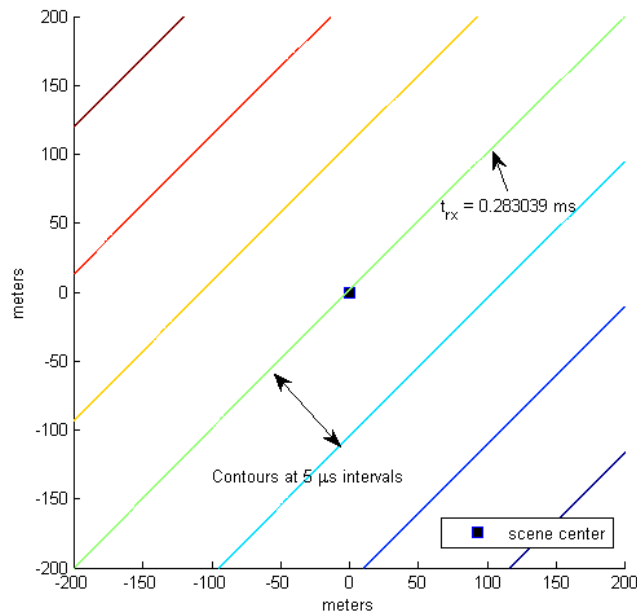


Figure 29. Detailed time map for 400m x 400m area around scene center based on the geometry shown in Figure 28. Contours are set at 5 μ s intervals for display only. Samples are generated at 10cm intervals.

2. Single Pulse Image Map

The image map due to a single pulse is checked to ensure proper mapping between the time map results and the image map. A target is placed at [-50m,50m] for this check. Figure 30 and Figure 31 show the image map generated using the monostatic and bistatic sensor, respectively.

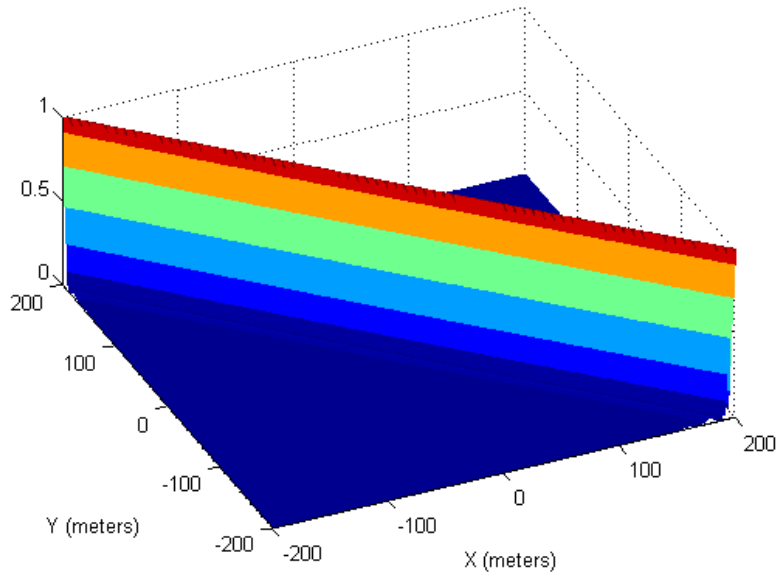


Figure 30. Single LFM pulse (15 MHz bandwidth) image map using monostatic configuration, with target at [-50m,50m] using the backprojection algorithm.

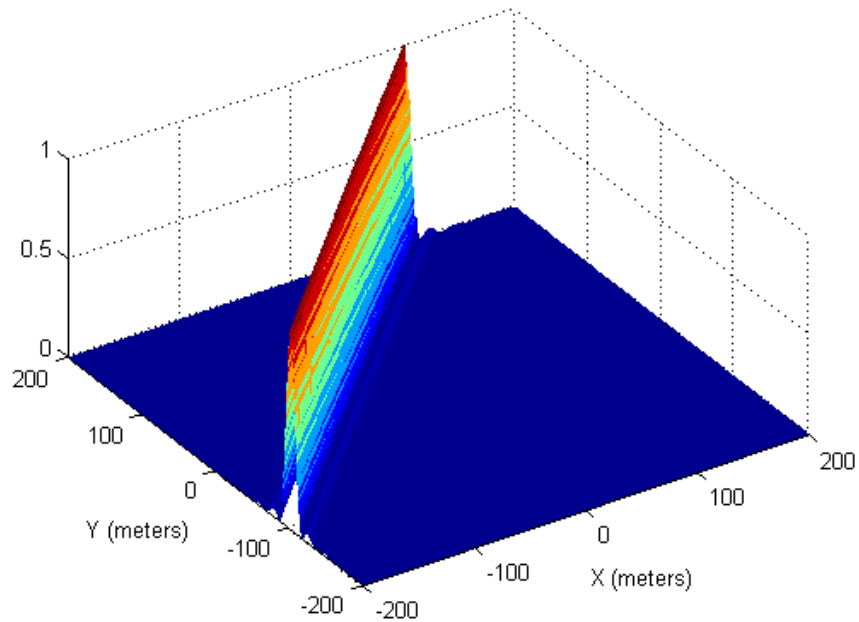


Figure 31. Single LFM pulse (15 MHz bandwidth) image map using bistatic configuration, with target at [-50m,50m] using the backprojection algorithm.

The combined image map is shown in Figure 32. It can be seen that the target is clearly localized at its true location with just two pulses in this case.

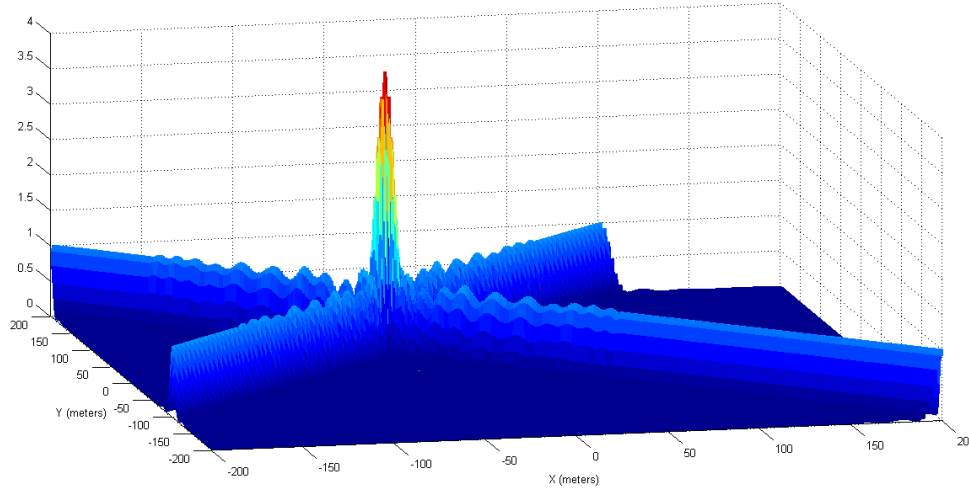


Figure 32. Combined image map formed from the outputs of the monostatic and bistatic radars. The target is clearly localized at its true location, [-50m, 50m].

D. EFFECT OF TARGET SPEED ON RANGE PROFILE

Cheney and Borden [15] listed, as a guideline, a validity domain for start stop approximation as $v < \lambda / T_w$ where v is the relative speed between sensor and target, λ is the wavelength at the center frequency and T_w is the pulse width. This essentially means that the motion between sensor and target over a single pulse width is less than a wavelength and sets limits on the desired target speed or pulse-width, given that the transmission frequency is typically chosen based on other considerations previously discussed. The effects within the validity domain are examined here.

As a reference, a single LFM pulse with pulse width of $1\mu\text{s}$ and bandwidth of 15 MHz is used. A carrier frequency of 1 GHz is chosen, thus the wavelength is 30 cm. The radar is 100km from the target. The effects on the range profile are observed when the speed for an inbound target is varied from 1km/s to 100km/s, or equivalently v varies from $0.003 \lambda / T_w$ to $0.3 \lambda / T_w$. The range profile is selected at the zero Doppler cut of the correlation filter bank. Figure 33 shows the results.

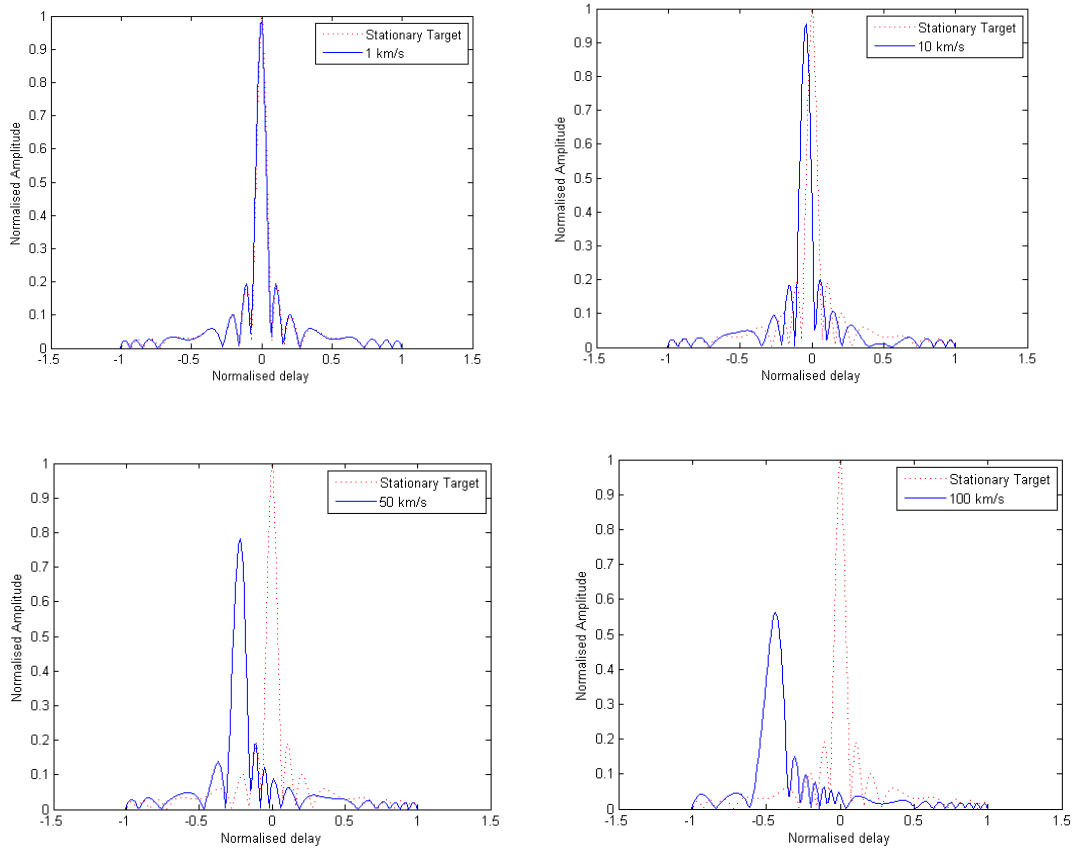


Figure 33. Effect of target speed (inbound target) from 1 km/s to 100 km/s on the range profile output for LFM pulse with $T_w = 1\mu s$, bandwidth = 15 MHz. The delay axis is normalized by the pulse width, the amplitude is normalized using the peak of the auto-correlation function.

It can be clearly seen that the range profile peak is shifted from the “correct” range in the profile and the peak amplitude is reduced by more than 3dB even when the target speed is still much smaller than λ / T_w . These effects will contribute to artifacts in the radar imaging processes.

Figure 34 shows the output for the same waveform with a 100km/s target when the radar is at 45 degree aspect angle to the target and a target with velocity at 90 deg to the down-range direction. It can be seen that the range profile output is less impacted even though the speed is the same. This is because the target is not approaching head-on, and so the radar waveform is experiencing correspondingly less Doppler modulation.

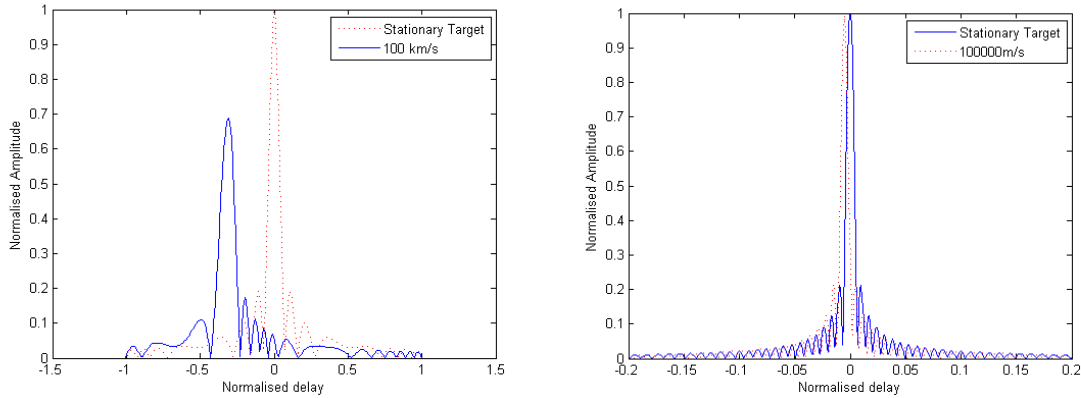


Figure 34. Effect on the range profile output for LFM pulse with $T_w = 1\mu s$, bandwidth = 15 MHz when a 100km/s target is at 45 degree aspect angle (Left) and when velocity is at 90 deg to the down-range direction (Right). The delay axis is normalized by the pulse width, the amplitude is normalized using the peak of the auto-correlation function.

The effects of changing the LFM pulse are examined. Figure 35 shows the output with an inbound target at 100km/s, with a longer pulse width of $T_w = 10\mu s$, bandwidth = 15 MHz. It can be seen that, in both cases, the distortions introduced by the target's motion are reduced. In the case of a longer pulse, it can be seen that the actual range shift introduced by the Doppler shift remains about the same as the reference, since the pulse width has increased ten-fold.

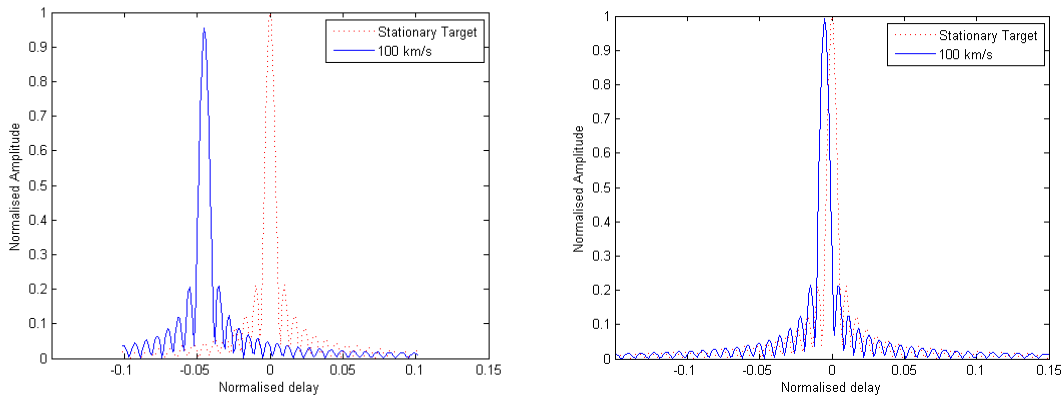


Figure 35. Effect on the range profile output for LFM pulse with longer pulse, $T_w = 10\mu s$ (Left) and higher bandwidth = 15 MHz (Right) with an 100km/s inbound target. The delay axis is normalized by the pulse width, the amplitude is normalized using the peak of the auto-correlation function.

To explore the dependence on waveforms, the effects of the same scenario on a Barker-13 binary phase coded signal are examined. The Barker code is often stated in literature as having poor ‘‘Doppler tolerance.’’ [27] The bandwidth of this waveform is kept at 15 MHz to maintain the same range resolution; this gives a slightly shorter pulse width of $0.867 \mu\text{s}$. Figure 36 shows the effect of target motion on this waveform at higher target speeds of 50km/s and 100km/s. It can be seen that the effect of target motion essentially is to raise the range sidelobes and lower the peak response of the return, but does not introduce a range error. This is likely to cause artifacts that are different from that of LFM pulses in the imaging outcome—for example, the raised sidelobes from large targets masking out other nearby features in the image.

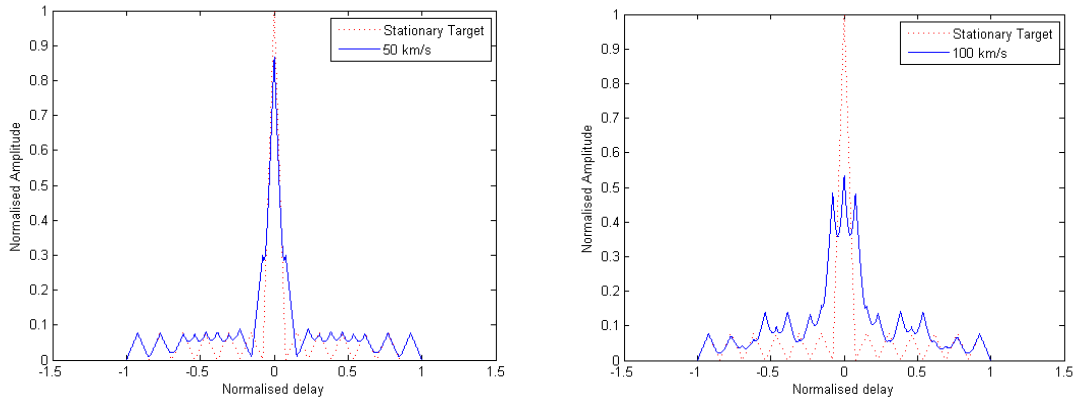


Figure 36. Effect on the range profile output for Barker-13 binary phase coded pulse with subpulse width, $T_w = 0.667 \mu\text{s}$ for a 50 km/s and 100 km/s inbound target. The delay axis is normalized by the *subpulse* width, the amplitude is normalized using the peak of the auto-correlation function.

Hence, it can be seen that the artifacts due to imaging will be dependent on the characteristics of the waveform chosen, in addition to the target characteristics.

E. MULTI-STATIC RADAR CASE STUDY

In this section, we present the imaging outcomes for two different configurations of multistatic radar systems. The first is a collection of monostatic radars, assumed to be perfectly synchronized; and the second, a true multi-static system where the transmitter and receiver are not collocated.

1. Multiple Monostatic Radars

This configuration consists of four monostatic radars arranged as follows: Radar 1 is at $[-100,100,0]$ km, Radar 2 is at $[0,100,0]$ km, Radar 3 is at $[50,0,0]$ km, and Radar 4 is at $[50,86.6,0]$ km. This corresponds to observation angles of $-30, 0, 45,$ and 90 degrees, but at differing ranges. LFM pulses with pulsewidths of $1\mu\text{s}$ and bandwidth of 15 MHz are used in all the radars.

A point target located at initial position $[-50,50,0]$ meters is observed. The sensor and target layout is shown in Figure 37. The imaging outcome, i.e., Point Spread Function (PSF), for a stationary target is shown in Figure 38. The target is well localized at its true position with the expected resolution from a 15 MHz bandwidth (i.e., 10 meters). The lines of backprojection from the radar positions are clearly observable.

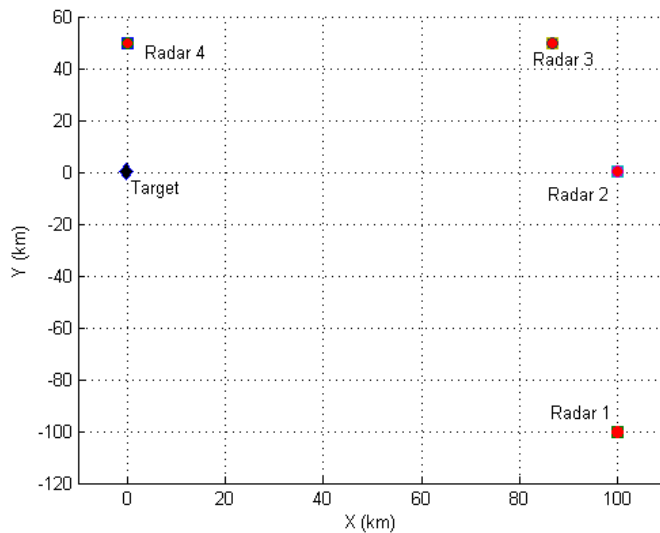


Figure 37. Layout of radars for multiple monostatic imaging case study

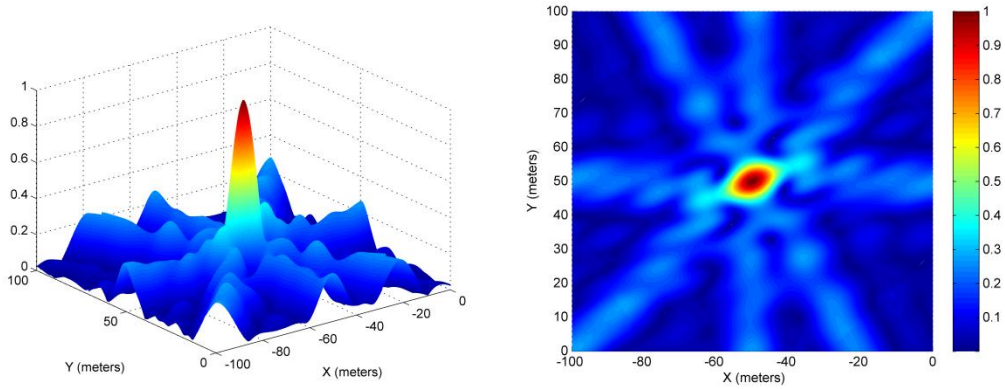


Figure 38. Point Spread Function for stationary target at $[-50,50]$ meters. Radars are at $[-100,100,0]$ km, $[0,100,0]$ km, $[50,0,0]$ km and $[50,86.6,0]$ km. Amplitudes are normalized by the number of pulses processed.

The effect of target motion is now investigated. Figure 39 shows the PSF for a target moving at 7.5 km/s parallel to the Y and X-axes. A close-up view of the imaging PSF for the stationary target is provided for reference. We note that during the interaction with the pulse, the target moves less than 1cm. It can be seen that the imaging responses are clearly shifted away from the true target location by approximate 2.5 meters in each case. Visually, it can be seen that the shape of the PSF has broadened slightly across the axis of motion. The peak responses in both cases have also decreased compared to the stationary target.

A hypothetical high speed target travelling at 50km/s in the direction of the +Y axis has been used to illustrate its impact on the imaging PSF. The target moves 5cm during the $1\mu\text{s}$ pulse duration. The observed PSF is shown in Figure 40. This image clearly shows the same degradations shown in the previous figures, including a wrong target location and decrease in the peak responses. In addition, it can be clearly observed that the backprojected range profiles fail to converge at the same focal point, which ideally should be at the true location of the target. In effect, the target has become defocused, resulting in multiple spurious peak responses. This is because different radars “see” different radial velocities due to their aspect angle, and thus the range error introduced varies between different range profiles. When this deviation is sufficiently large, the projection lines will no longer intersect at the same location.

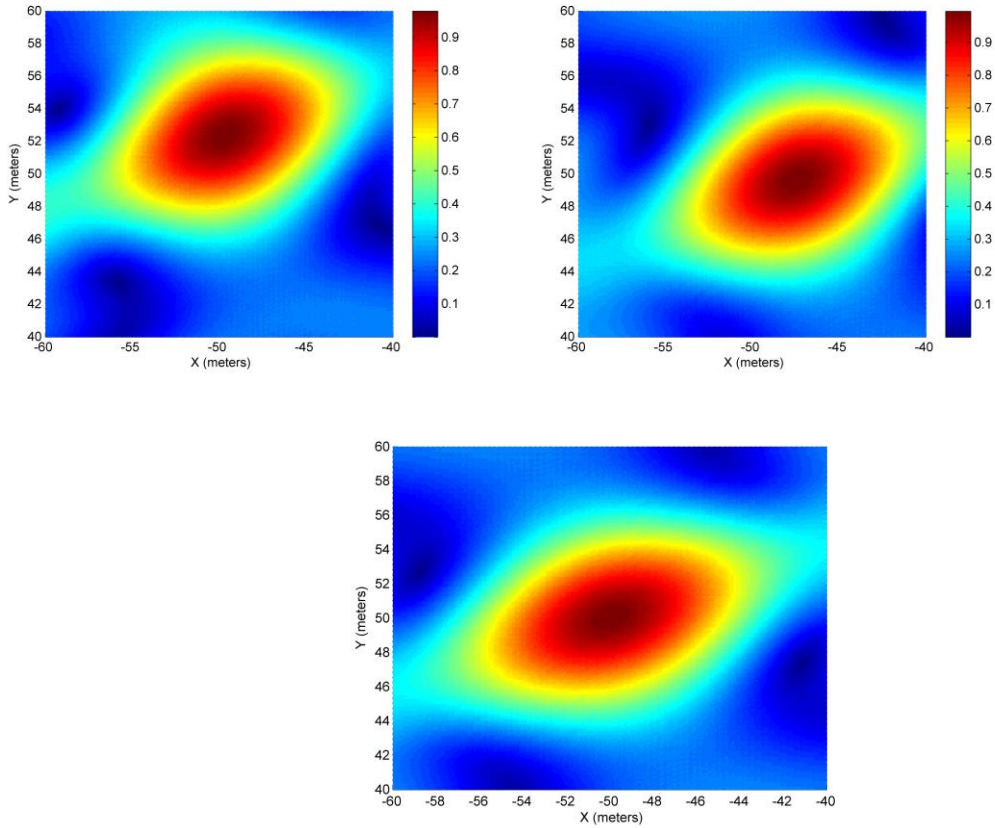


Figure 39. Point Spread Function for target with initial position $[-50,50,0]$ meters moving at 7.5 km/s, (a) parallel to $+Y$ -axis (Top Left), (b) parallel to $+X$ -axis (Top Right). The PSF for the stationary target (Bottom) is shown for reference.

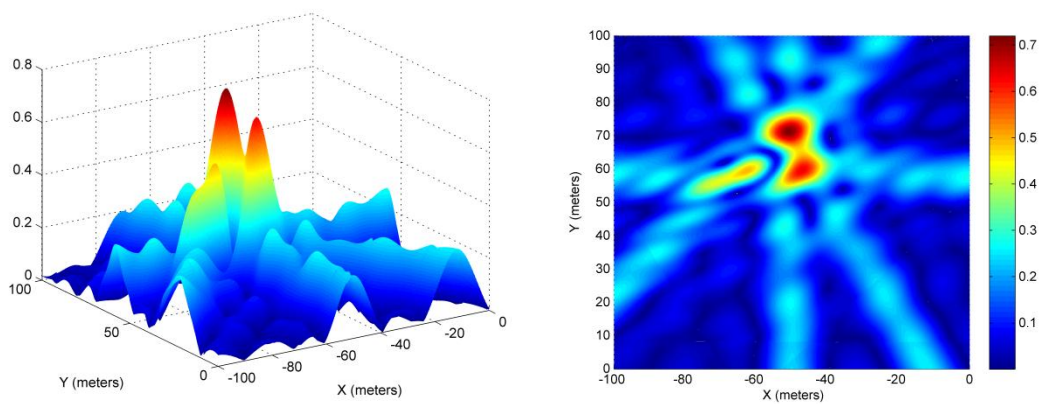


Figure 40. Point Spread Function for target with initial position $[-50,50,0]$ meters moving at 50 km/s.

The same simulations are repeated on a set of radars using Barker-13 binary phase coded waveforms. As expected, it can be seen that the range sidelobes appear more prominently in the imaging results. The results are shown in Figure 41. The observed effects are similar to the case of the LFM waveform.

2. Multistatic Radars

In this case, we check an actual multi-static configuration where the transmitter and receiver are not co-located. The locations of the receivers are the same as the radar locations in the previous scenario: $[-100,100,0]$ km, $[0,100,0]$ km, $[50,0,0]$ km, and $[50,86.6,0]$ km. The transmitter is located at $[0,100,0]$ km and transmits LFM pulses with pulsewidths of $1\mu\text{s}$ and bandwidth of 15 MHz. Again, the target is placed at $[-50,50,0]$ meters. Figure 42 shows the layout of the scenario and the PSF for a stationary target. Again, the target is well localized at its true position with the expected resolution from a 15 MHz bandwidth (i.e., 10 meters). The lines of backprojection from the radar positions are clearly observable and clearly different in orientation from that of the multiple monostatic radar case. This is because the backprojections of the multistatic radar wavefronts are aligned to ellipses with the transmitter and receiver as the foci, unlike circular arcs in the monostatic radar case.

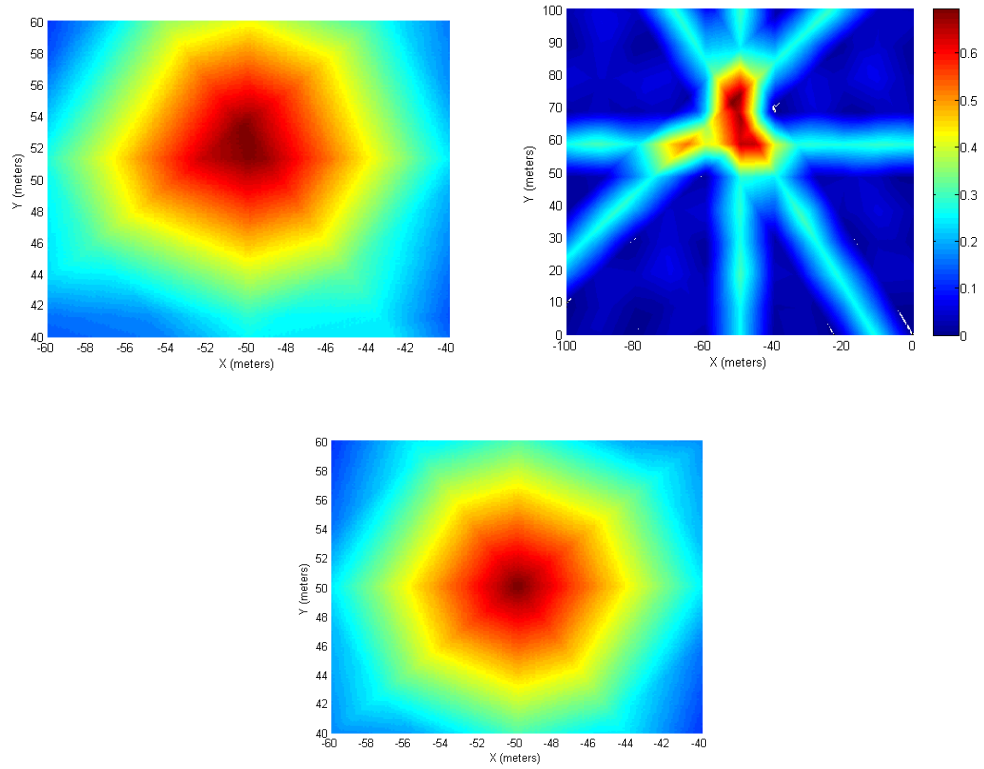


Figure 41. Point Spread Function for configuration using Barker-13 binary phase coded signal for target towards +Y direction at, (a) 7.5 km/s (Top Left), (b) 50 km/s. The point spread function for a stationary target (Bottom) is shown for reference.

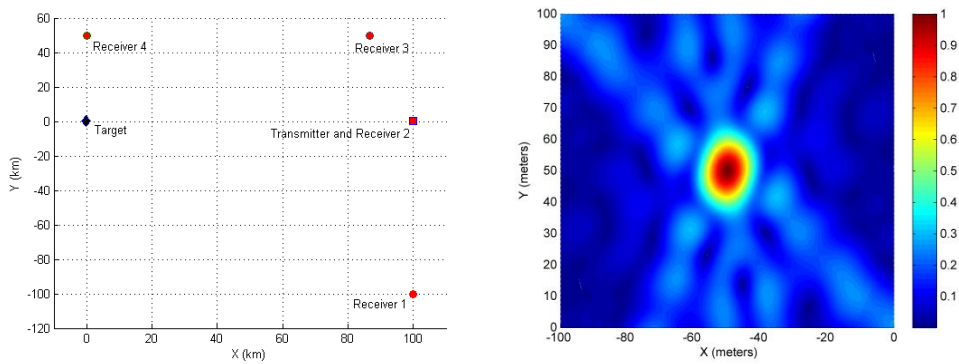


Figure 42. Layout of target, transmitter and receivers (Left) and Point Spread Function (Right) for the multistatic radar scenario.

It can be seen from Figure 43 that the effects of a moving target are similar to the multiple monostatic radar case.

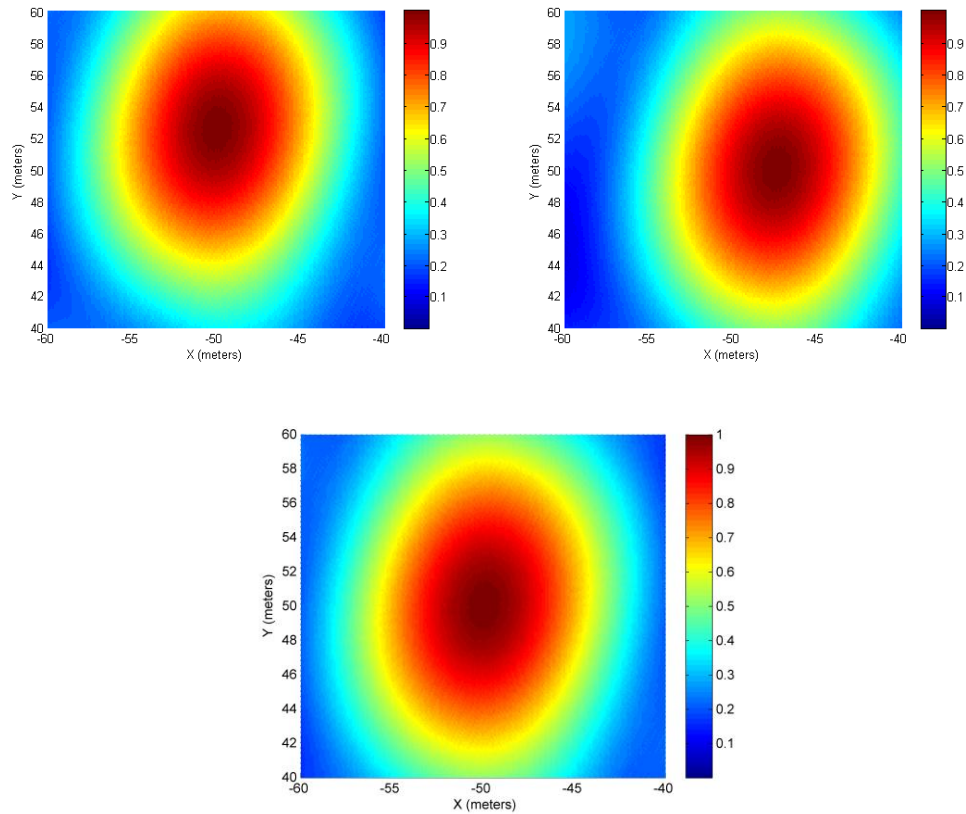


Figure 43. Multistatic configuration Point Spread Function for target with initial position $[-50,50,0]$ meters moving at 7.5 km/s, (a) parallel to +Y-axis (Top Left), (b) parallel to +X-axis (Top Right). The PSF for the stationary target (Bottom) is shown for reference.

We conclude this section by summarizing the observations that have been made. It has been observed that moving targets may introduce a shift in the location of the target image. This follows from the distortions in the range profile that have been observed in the previous section. When the target is sufficiently fast, the range shift introduced varies between different range profile. This deviation may cause standard backprojection to fail, since the backprojected range profiles will no longer intersect at the same point, leading to image defocusing.

F. MONO-STATIC SINGLE CHANNEL SAR CASE STUDY

In this section, we examine the effects of a moving target on single channel SAR.

1. SAR Cross Range Resolution

Prior to observing the effects of a moving target, the SAR model is checked to verify that the model conforms to theoretical predictions for known cases. A LFM waveform with pulse-width of $1\mu\text{s}$ and modulation bandwidth of 15 MHz (corresponding to down-range resolution of 10 meters) is used in this series of verifications. A carrier frequency of 100 MHz, with sampling frequency of 1 GHz, is chosen for a manageable computation load. The expected cross-range resolution of this model can be computed using Equation (4). When processing the SAR imagery, a salient point to note is that the SAR data needs to be processed at the carrier frequency in order to achieve the full resolution as predicted [13].

The effect of observation width, L , (i.e., SAR speed multiplied by observation time) is first examined. As a reference case, L is chosen to be 3km. The SAR is positioned with a down-range of 10km, with a speed of 50 m/s (i.e., 100 kts). The SAR path is chosen such that the target, located at the origin, appears broadside in the middle of the observation width and samples are taken at half-wavelength intervals in the synthetic aperture domain. This geometry is illustrated in Figure 44. With these parameters, the PSF obtained is shown in Figure 45. It can be seen that the cross-range resolution achieved is around 10 meters (null-to-null), which is as expected.

The PSF is generated for observation widths of 1.5km and 6km. The results shown correspond well to theory, with cross range resolutions (null-to-null) of 20m and 5m, respectively. The PSF is also observed for carrier frequencies of 75MHz and 150MHz, using the reference observation width of 3km. The results shown in Figure 47 again correspond well to theory with cross range resolutions (null-to-null) of 13.3 meters and 6.7 meters, respectively. These verifications show that the implemented model is consistent with theory, in terms of both the expected down-range and cross-range resolutions.

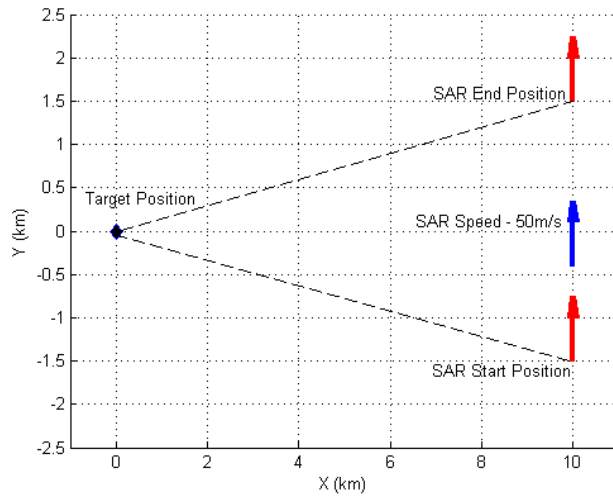


Figure 44. Geometry of reference SAR scenario. The SAR's speed is chosen to be 50m/s. The X and Y axes are the down-range and cross-range directions, respectively.

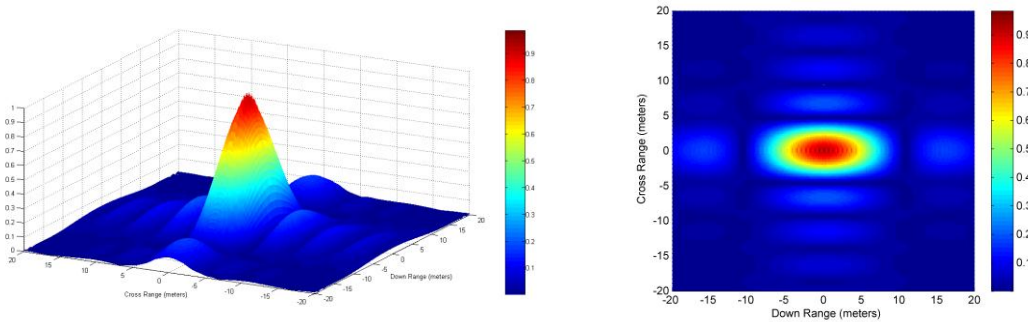


Figure 45. Point Spread Function for reference SAR scenario.

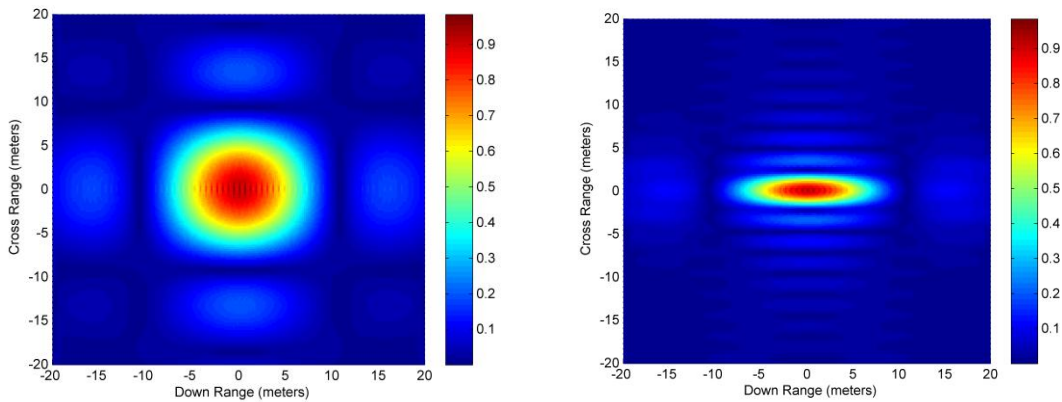


Figure 46. Point Spread Function for SAR scenario with observation widths of 1.5km (Left) and 6km (Right)

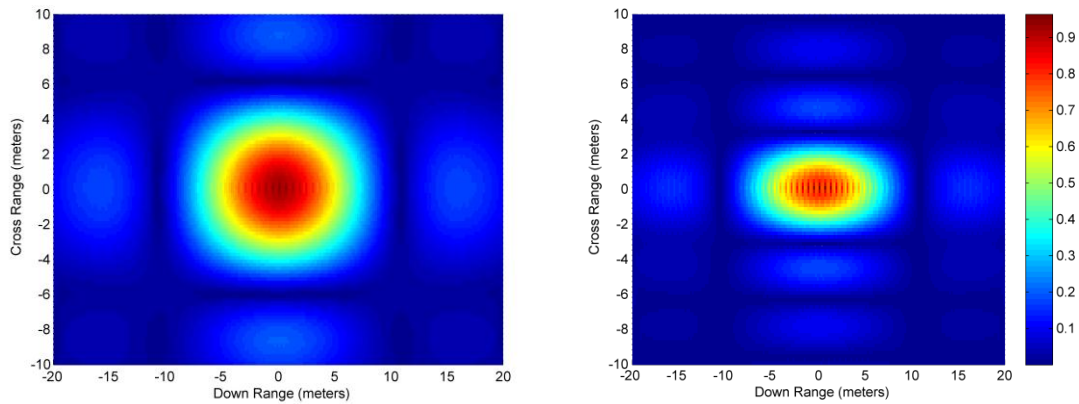


Figure 47. Point Spread Function for SAR scenario with carrier frequencies of 50 MHz (Left) and 150 MHz (Right)

2. Point Spread Function for a Moving Target

Here, the PSF is observed for a moving target. Figure 48 and Figure 49 show the PSFs for a SAR scenario with target, initially located at $[0,0,0]$ meters, moving at 0.1 m/s in the downrange (positive X) and cross-range (positive Y) directions, respectively. The targets move 0.1 μ m during a single pulse duration and 6 meters during the entire observation period. This slow speed is chosen to illustrate cases where there is very little Doppler modulation, which results in negligible range shift of the range profile's peak output compared to a stationary target. It can be clearly seen in both cases of down-range and cross-range motions, that there are errors introduced in the location of the target and the peak output of the responses have slightly decreased. For the target moving in the downrange direction, the error in the cross-range location is 20 meters as predicted with the formula in [16].

In the case of the cross-range motion, the resolution of the PSF has been degraded, as the original main lobe of the PSF has merged with its adjacent sidelobes to create a broadened response. This is the defocusing effect that is discussed in [16] and [17].

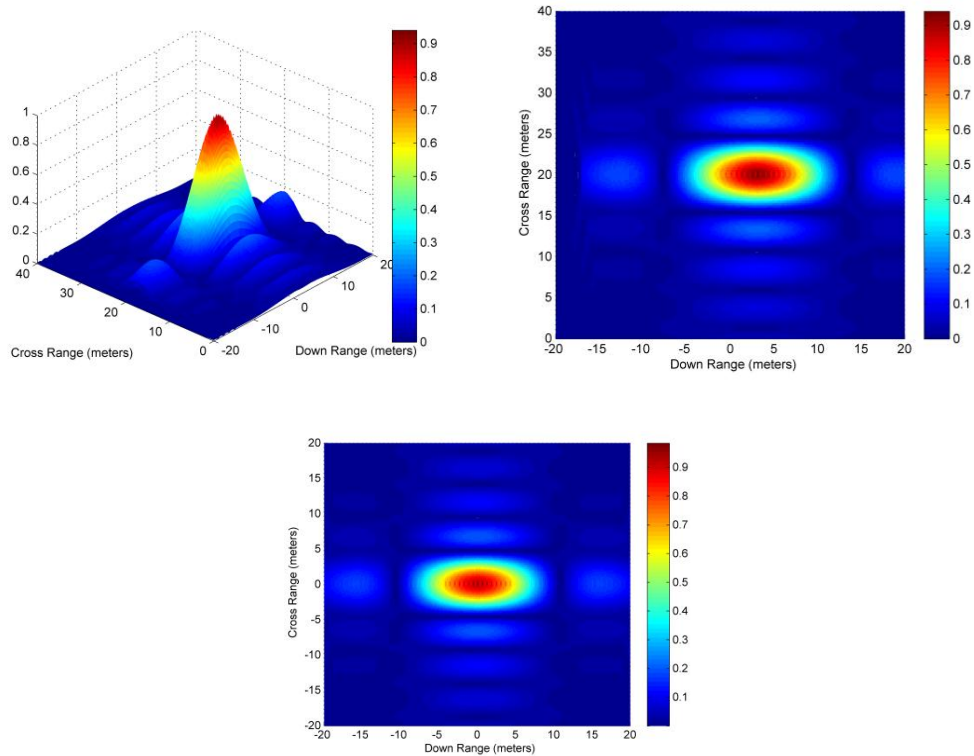


Figure 48. Point Spread Function for SAR scenario with target, initially located at $[0,0,0]$ meters, moving at 0.1 m/s in the down-range direction. The PSF for a stationary target is shown (Bottom) for reference.

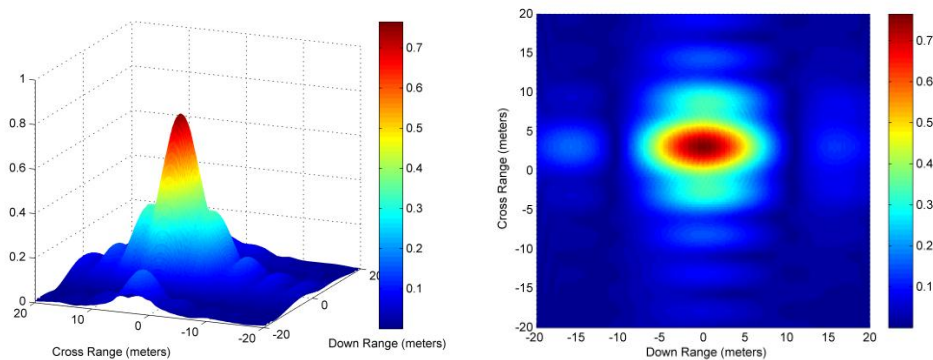


Figure 49. Point Spread Function for SAR scenario with target, initially located at $[0,0,0]$ meters, moving at 0.1 m/s in the cross-range direction.

We now examine the PSF for a faster target which is moving at 10m/s. Figure 50 shows the PSF for a SAR scenario with a target initially located at $[0,0,0]$ meters, moving at 10 m/s in the downrange (positive X) and cross-range (positive Y) directions. The

target moves $100\mu\text{m}$ during a single pulse duration and 600 meters during the entire observation period. This speed is chosen to illustrate cases where the target moves a distance which is much greater than the imaging resolution during the observation period. The peak response is again shifted in cross-range by the amount predicted using [16]. We see that the PSF is smeared out, the peak response is greatly reduced, and there are multiple peaks in the response. This is due to the fact that the target continuously varies its physical location throughout the observation period, resulting in an effect similar to “motion blur” in optical cameras.

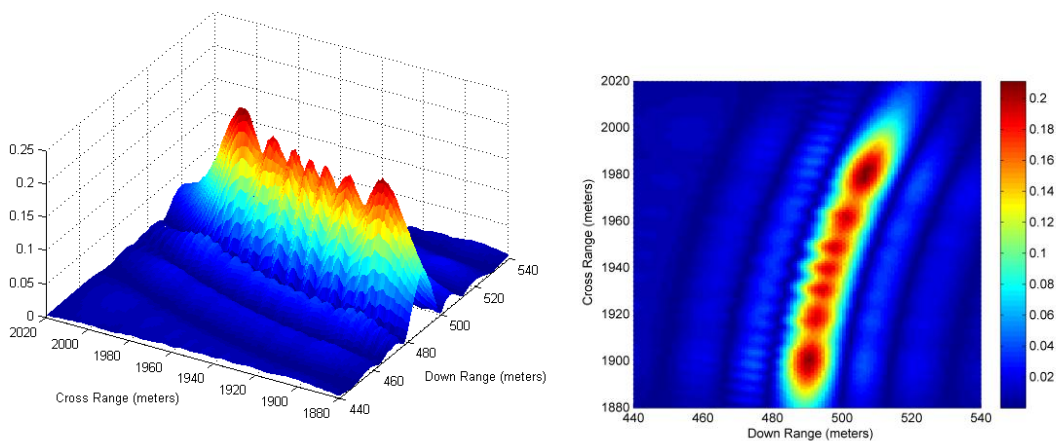


Figure 50. Point Spread Function for SAR scenario with target, initially located at $[0,0,0]$ meters, moving at 10 m/s in the down-range direction.

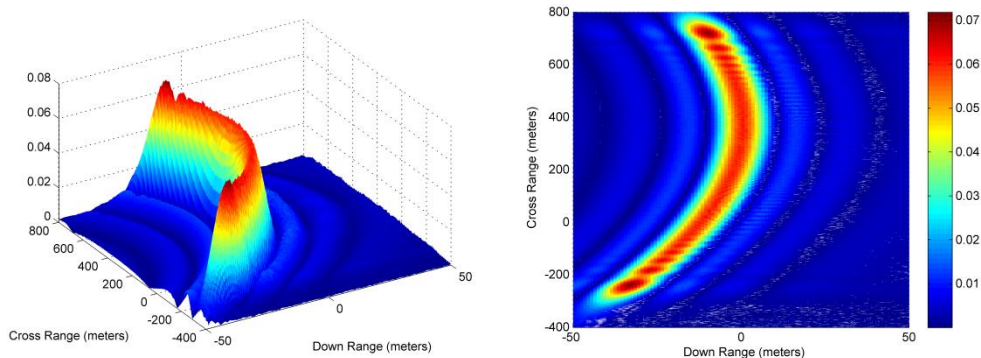


Figure 51. Point Spread Function for SAR scenario with target, initially located at $[0,0,0]$ meters, moving at 10 m/s in the cross-range direction.

The PSF for targets moving at 10m/s is now further examined with a faster SAR speed of 250m/s to reduce the observation time. Target motion during a single pulse duration remains the same, but the target now moves only 120 meters during the entire observation period. Figure 52 and Figure 53 show the PSF for a SAR scenario with target, initially located at [0,0,0] meters, moving at 10 m/s in the downrange (positive X) and cross-range (positive Y) directions, respectively. It can be observed that the smearing and cross-range error is greatly reduced in both cases despite the greater relative motion between the SAR and the target. This is consistent with Raney's [16] conclusion that a large SAR speed reduces the artifacts induced by target motion.

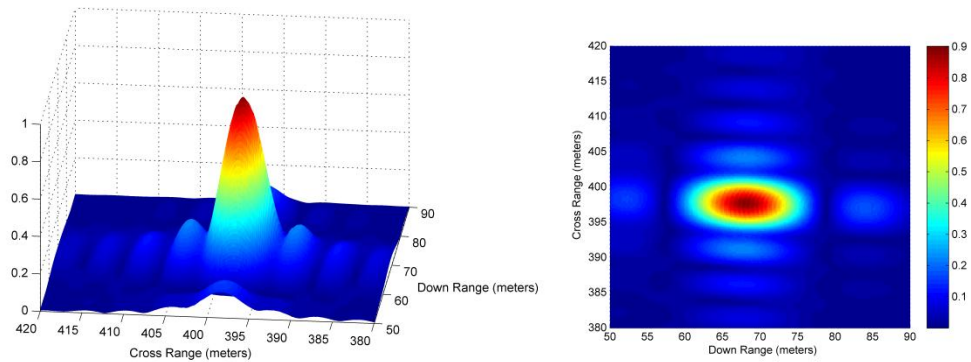


Figure 52. Point Spread Function for SAR scenario with target, initially located at [0,0,0] meters, moving at 10 m/s in the down-range direction and with SAR moving at 250 m/s.

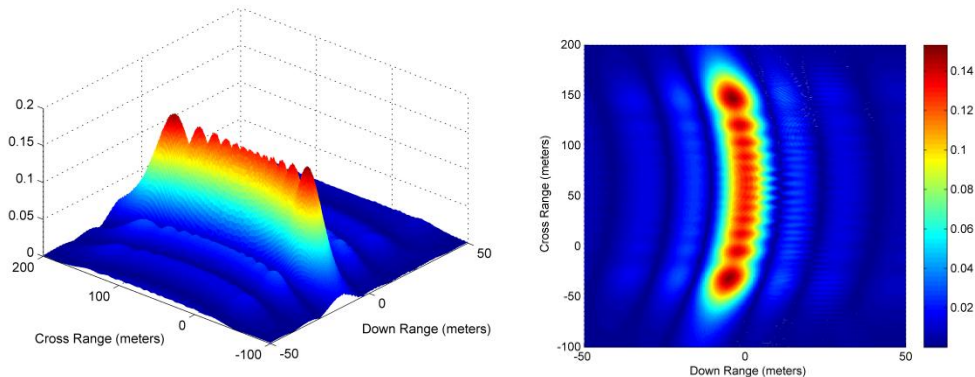


Figure 53. Point Spread Function for SAR scenario with target, initially located at [0,0,0] meters, moving at 10 m/s in the cross-range direction and with SAR moving at 250 m/s.

In summary, the effects of target motion on SAR imaging have been examined. The phase distortions introduced by a motion target will lead to an error in the cross-range location of the target and defocusing. In addition, when the target moves over a long distance during the observation period, the resultant imaging response is smeared. In such cases, a higher SAR speed will help to reduce the artifacts caused by target motion. However, in practical systems, higher SAR speeds will require the use of higher Pulse Repetition Frequencies (PRF) to maintain the sampling distance in the synthetic aperture domain. There are other practical constraints on PRF selection considerations, such as the required radar unambiguous range, as well as radar hardware limitations. These other considerations have not been factored into our simulations, but will nevertheless need to be addressed in a real system.

THIS PAGE INTENTIONALLY LEFT BLANK

V. CONCLUSIONS

In this thesis, we study the imaging degradations or artifacts that occur when a scene to be imaged by radar contains moving targets.

The physics of interaction between radar waves and moving targets were studied, and a simulation was developed, using MATLAB to model the resultant signal received. A backprojection algorithm was also implemented for radar image reconstruction from multiple one-dimensional range profiles, each corresponding to the output from a single radar pulse. The model implemented is flexible and provides the means to study the effects of target motion at different stages in the image formation process, and also for different radar configurations, including multistatic radars and Synthetic Aperture Radar (SAR). Most importantly, this model also does not rely on the commonly used start-stop approximation which assumes that the target and sensor are both stationary throughout the transmission and reception process.

Validations were performed, with results checked against established theories or literature to provide confidence in the model. The key limitation of this model is its high computational resource requirements for high bandwidth or long pulses, due to the sample sequence lengths that need to be simulated for proper results.

Through these studies, it was noted that there are a few main effects that lead to the degradation of a radar image. The first effect is the distortion introduced to range profiles due to the mismatch of the received waveform vis-à-vis the “matched filter.” This exact effect is waveform-dependent, but in the commonly used Linear Frequency Modulated (LFM) waveforms, other than a broadening of the main lobe which results in smearing in the final image, a range shift is introduced. This leads to the object being placed in the wrong location on the final image, commonly known as the “train off the tracks” or “ship off its wake” phenomenon by SAR image analysts. The second effect, evident from the studies on multi-static imaging, stems from the range error from range profiles affecting the intersection points of the back-projection algorithm, resulting in defocusing. Lastly, for a moving SAR platform, as the samples are taken from different

instants in time, the actual physical position of the target varies throughout the imaging process. In the case of slow targets, this leads to defocusing and positional errors, especially in the cross-range domain. For faster targets, the intersections of the backprojections do not intersect correctly, even if the location error due to the Doppler shift has been corrected, resulting in a smeared imaging response. This is similar to “motion blur” experienced in optical cameras with a fast object. A faster SAR speed may help to reduce these artifacts. These observed effects are consistent with descriptions from literature, but have been observed in detail due to the flexibility of the implemented model.

The implemented model is sufficiently flexible to allow for the study of different waveforms distorted by propagation, without first having to derive closed-form expressions, which are typically difficult to derive in the moving target and multi-static radar cases. Hence, the model is useful for further studies into artifacts introduced by motion in radar imaging, as well as methods to address these artifacts. Possible opportunities for future work to extend or apply this model include the following:

- Using the model to further study aspects of radar imaging under motion using different waveforms and/or matched filter generation.
- Using the model to generate matched filters across both spatial and velocity domains corresponding to the *Borden Cheney* procedure so that its performance on SAR data can be analyzed.
- Using the model to investigate the effects of time synchronization errors on the imaging outcomes of multistatic radars. This could possibly be done by adding such errors to the time map for image formation.
- Developing a model to exactly represent the “time map” of moving targets and study the “time-map” distortions introduced due to motion vis-à-vis static sensors and targets.
- Attempt the derivation of similar expressions as Equations (13) and (14) for circular flight paths and geo-centric circular orbits (e.g., useful for satellites)

APPENDIX A. DERIVATION OF EQUATIONS

This appendix provides the detailed derivations of key equations that were presented in Chapter II.

A. PROPAGATION TIME FROM TRANSMITTER TO TARGET

Definition of terms:

Δt_{ix} = one way propagation time from transmitter to target

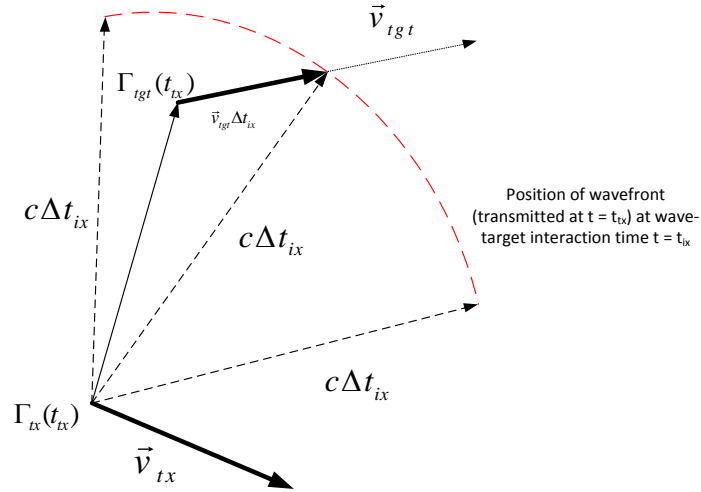
t_{ix} = transmission time

Target position at $t = 0$: $\vec{u}_{tgt} = [u_{x,tgt}; u_{y,tgt}; u_{z,tgt}]$

Target velocity (constant): $\vec{v}_{tgt} = [v_{x,tgt}; v_{y,tgt}; v_{z,tgt}]$

Transmitter position at $t = 0$: $\vec{u}_{tx} = [u_{x,tx}; u_{y,tx}; u_{z,tx}]$

Target velocity (constant): $\vec{v}_{tx} = [v_{x,tx}; v_{y,tx}; v_{z,tx}]$



Since the wave has the same speed in all directions, the wave intercepts the target when their ranges are equal from the transmitter. From the frame of the transmitter, we have

$$R_{EMwave}(t_{ix} + \Delta t_{ix}) = c\Delta t_{ix} \text{ and } R_{tgt}(t_{ix} + \Delta t_{ix}) = \left| \vec{u}_{tgt}(t_{ix}) + \vec{v}_{tgt}\Delta t_{ix} - \vec{u}_{tx}(t_{ix}) \right|$$

Equating the two ranges:

$$R_{tgt}(t_{ix} + \Delta t_{ix}) = R_{EMwave}(t_{ix} + \Delta t_{ix})$$

$$\Rightarrow c\Delta t_{ix} = \left| \vec{u}_{tgt}(t_{ix}) + \vec{v}_{tgt}\Delta t_{ix} - \vec{u}_{tx}(t_{ix}) \right|$$

$$\Rightarrow c^2 \Delta t_{ix}^2 = \left| \vec{\mathbf{u}}_{igt}(t_{ix}) + \vec{\mathbf{v}}_{igt} \Delta t_{ix} - \vec{\mathbf{u}}_{tx}(t_{ix}) \right|^2$$

$$\text{Define } \vec{\mathbf{u}}_t(t_{ix}) = \vec{\mathbf{u}}_{igt}(0) + \vec{\mathbf{v}}_{igt} t_{ix} - \vec{\mathbf{u}}_{tx}(0) - \vec{\mathbf{v}}_{igt} t_{ix}$$

$$\Rightarrow c^2 \Delta t_{ix}^2 = (\vec{\mathbf{u}}_t(t_{ix}) + \vec{\mathbf{v}}_{igt} \Delta t_{ix}) \cdot (\vec{\mathbf{u}}_t(t_{ix}) + \vec{\mathbf{v}}_{igt} \Delta t_{ix})$$

$$\Rightarrow 0 = \left| \vec{\mathbf{u}}_t(t_{ix}) \right|^2 + 2 \vec{\mathbf{u}}_t(t_{ix}) \cdot \vec{\mathbf{v}}_{igt} \Delta t_{ix} + \left(\left| \vec{\mathbf{v}}_{igt} \right|^2 - c^2 \right) \Delta t_{ix}^2$$

Solving the quadratic equation for t_p and choosing the causal solution where $\Delta t_{ix} > 0$:

$$\begin{aligned} \Delta t_{ix}(t_{ix}) &= \frac{-2 \vec{\mathbf{u}}_t(t_{ix}) \cdot \vec{\mathbf{v}}_{igt} \pm \sqrt{4 \left(\vec{\mathbf{u}}_t(t_{ix}) \cdot \vec{\mathbf{v}}_{igt} \right)^2 - 4 \left(\left| \vec{\mathbf{v}}_{igt} \right|^2 - c^2 \right) \left| \vec{\mathbf{u}}_t(t_{ix}) \right|^2}}{2 \left(\left| \vec{\mathbf{v}}_{igt} \right|^2 - c^2 \right)} \\ &= \frac{\vec{\mathbf{u}}_t(t_{ix}) \cdot \vec{\mathbf{v}}_{igt} + \sqrt{\left(\vec{\mathbf{u}}_t(t_{ix}) \cdot \vec{\mathbf{v}}_{igt} \right)^2 + \left(c^2 - \left| \vec{\mathbf{v}}_{igt} \right|^2 \right) \left| \vec{\mathbf{u}}_t(t_{ix}) \right|^2}}{\left(c^2 - \left| \vec{\mathbf{v}}_{igt} \right|^2 \right)} \end{aligned}$$

This yields Equation (13) from Chapter II.

B. PROPAGATION TIME FROM TARGET TO RECEIVER

Definition of terms:

Δt_{rx} = one way propagation time from target to receiver

Δt_{ix} = one way propagation time from transmitter to target

t_{ix} = transmission time

Target position at $t = 0$: $\vec{\mathbf{u}}_{igt} = [u_{x,igt}; u_{y,igt}; u_{z,igt}]$

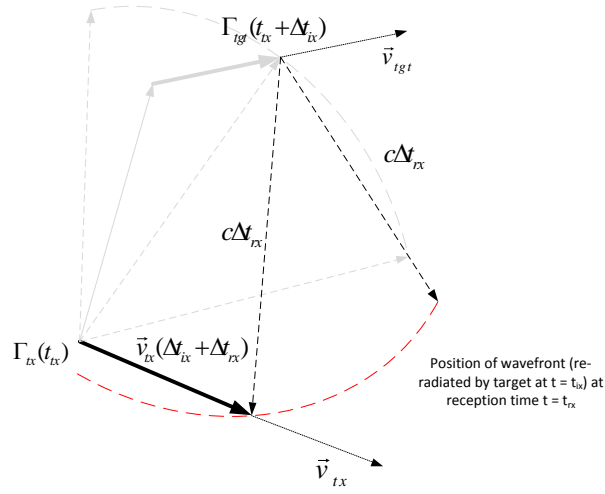
Target velocity (constant): $\vec{\mathbf{v}}_{igt} = [v_{x,igt}; v_{y,igt}; v_{z,igt}]$

Transmitter position at $t = 0$: $\vec{\mathbf{u}}_{tx} = [u_{x,tx}; u_{y,tx}; u_{z,tx}]$

Target velocity (constant): $\vec{\mathbf{v}}_{tx} = [v_{x,tx}; v_{y,tx}; v_{z,tx}]$

Receiver position at $t = 0$: $\vec{\mathbf{u}}_{rx} = [u_{x,rx}; u_{y,rx}; u_{z,rx}]$

Receiver velocity (constant): $\vec{\mathbf{v}}_{rx} = [v_{x,rx}; v_{y,rx}; v_{z,rx}]$



The key difference from the case in Appendix A.I is that the target is now the source of the EM wave, which it emits at time $t_{tx} + \Delta t_{ix}$, and the receiver is the object to be intercepted by the wave, which is received at $t_{rx} = t_{tx} + \Delta t_{ix} + \Delta t_{rx}$. Since the wave has the same speed in all directions, the wave intercepts the target when their ranges are equal from the target.

From the frame of the target, we have

$$R_{EMwave}(t_{rx}) = c\Delta t_{rx} \text{ and } R_{igt}(t_{rx}) = \left| \vec{u}_{rx}(t_{tx} + \Delta t_{ix}) + \vec{v}_{rx}\Delta t_{rx} - \vec{u}_{igt}(t_{tx} + \Delta t_{ix}) \right|$$

Equating the two ranges:

$$\begin{aligned} R_{igt}(t_{rx}) &= R_{EMwave}(t_{rx}) \\ \Rightarrow c\Delta t_{rx} &= \left| \vec{u}_{rx}(t_{tx} + \Delta t_{ix}) + \vec{v}_{rx}\Delta t_{rx} - \vec{u}_{igt}(t_{tx} + \Delta t_{ix}) \right| \\ \Rightarrow c^2\Delta t_{rx}^2 &= \left| \vec{u}_{rx}(t_{tx} + \Delta t_{ix}) + \vec{v}_{rx}\Delta t_{rx} - \vec{u}_{igt}(t_{tx} + \Delta t_{ix}) \right|^2 \\ \text{Define } \vec{u}_r(t_{tx} + \Delta t_{ix}) &= \vec{u}_{rx}(0) + \vec{v}_{rx}t_{tx} + \vec{v}_{igt}\Delta t_{ix} - \vec{u}_{igt}(0) - \vec{v}_{igt}t_{tx} - \vec{v}_{igt}\Delta t_{ix} \\ \Rightarrow c^2\Delta t_{rx}^2 &= (\vec{u}_r(t_{tx} + \Delta t_{ix}) + \vec{v}_{igt}\Delta t_{rx}) \cdot (\vec{u}_r(t_{tx} + \Delta t_{ix}) + \vec{v}_{igt}\Delta t_{rx}) \\ \Rightarrow 0 &= \left| \vec{u}_r(t_{tx} + \Delta t_{ix}) \right|^2 + 2\vec{u}_r(t_{tx} + \Delta t_{ix}) \cdot \vec{v}_{igt}\Delta t_{rx} + \left(\left| \vec{v}_{igt} \right|^2 - c^2 \right) \Delta t_{rx}^2 \end{aligned}$$

Solving the quadratic equation for t_p and choosing the causal solution where $\Delta t_{rx} > 0$:

$$\Delta t_{rx}(t_{tx}) = \frac{\vec{u}_r(t_{tx} + \Delta t_{ix}) \cdot \vec{v}_{rx} + \sqrt{(\vec{u}_r(t_{tx} + \Delta t_{ix}) \cdot \vec{v}_{rx})^2 + (c^2 - |\vec{v}_{rx}|^2) |\vec{u}_r(t_{tx})|^2}}{(c^2 - |\vec{v}_{rx}|^2)}$$

This is the general case where the transmitter and receiver are not assumed to be co-located or moving with the same speed.

In the case of a monostatic radar, $\vec{u}_r(t_{tx} + \Delta t_{ix}) = -\vec{u}_t(t_{tx} + \Delta t_{ix})$ and $\vec{v}_{rx} = \vec{v}_{tx}$. This yields Equation (14) from Chapter II.

$$\Delta t_{rx}(t_{tx}) = \frac{-\vec{u}_t(t_{tx} + \Delta t_{ix}) \cdot \vec{v}_{tx} + \sqrt{(\vec{u}_t(t_{tx} + \Delta t_{ix}) \cdot \vec{v}_{tx})^2 + (c^2 - |\vec{v}_{tx}|^2) |\vec{u}_t(t_{tx})|^2}}{(c^2 - |\vec{v}_{tx}|^2)}$$

C. DOPPLER-SHIFT FOR INCOMING TARGET

In the case of an incoming target,

$$\vec{u}_t(t_{tx}) \cdot \vec{v}_{tgt} = |\vec{u}_t(t_{tx})| \cdot |\vec{v}_{tgt}| \cos(180) = -|\vec{u}_t(t_{tx})| \cdot |\vec{v}_{tgt}|$$

Starting from Equation (13), the derivation of Equation (22) is as follows:

$$\begin{aligned} \Delta t_{ix}(t_{tx}) &= \frac{\vec{u}_t(t_{tx}) \cdot \vec{v}_{tgt} + \sqrt{|\vec{u}_t(t_{tx})|^2 \cdot |\vec{v}_{tgt}|^2 + (c^2 - |\vec{v}_{tgt}|^2) |\vec{u}_t(t_{tx})|^2}}{(c^2 - |\vec{v}_{tgt}|^2)} \\ &= \frac{-|\vec{u}_t(t_{tx})| |\vec{v}_{tgt}| + \sqrt{|\vec{u}_t(t_{tx})|^2 |\vec{v}_{tgt}|^2 - |\vec{u}_t(t_{tx})|^2 |\vec{v}_{tgt}|^2 + c^2 |\vec{u}_t(t_{tx})|^2}}{(c^2 - |\vec{v}_{tgt}|^2)} \\ &= \frac{-|\vec{u}_t(t_{tx})| \cdot |\vec{v}_{tgt}| + c |\vec{u}_t(t_{tx})|}{(c^2 - |\vec{v}_{tgt}|^2)} \\ &= \frac{|\vec{u}_t(t_{tx})| (c - |\vec{v}_{tgt}|)}{(c - |\vec{v}_{tgt}|)(c + |\vec{v}_{tgt}|)} \end{aligned}$$

$$= \frac{|\bar{u}_t(t_{ix})|}{(c + |\bar{v}_{igt}|)}$$

Equation (23) can be derived from Equations (14) and (22) similarly as follows:

$$\begin{aligned} \Delta t_{rx}(t_{ix}) &= \frac{-|\bar{u}_t(t_{ix} + \Delta t_{ix})| |\bar{v}_{ix}| + \sqrt{|\bar{u}_t(t_{ix} + \Delta t_{ix})|^2 |\bar{v}_{ix}|^2 + (c^2 - |\bar{v}_{ix}|^2) |\bar{u}_t(t_{ix} + \Delta t_{ix})|^2}}{(c^2 - |\bar{v}_{ix}|^2)} \\ &= \frac{|\bar{u}_t(t_{ix} + \Delta t_{ix})| c}{c^2} \quad [\text{Since } |\bar{v}_{ix}| = 0] \\ &= \frac{|\bar{u}_t(t_{ix})| - |\bar{v}_{igt}| \Delta t_{ix}}{c} \quad [\text{By definition of } \bar{u}_t(t_{ix}) \text{ and since } |\bar{v}_{ix}| = 0] \\ &= \frac{(|\bar{u}_t(t_{ix})| - |\bar{v}_{igt}| \frac{|\bar{u}_t(t_{ix})|}{c + |\bar{v}_{igt}|})}{c} \quad [\text{Using Equation (17) for } \Delta t_{ix}] \\ &= \frac{c |\bar{u}_t(t_{ix})| + (|\bar{v}_{igt}| - |\bar{v}_{igt}|) |\bar{u}_t(t_{ix})|}{c (c + |\bar{v}_{igt}|)} \\ &= \frac{|\bar{u}_t(t_{ix})|}{(c + |\bar{v}_{igt}|)} \end{aligned}$$

The result of Equation (24) can then simply be shown as follows

$$\begin{aligned} \Delta t_p(t_{ix}) &= \Delta t_{ix}(t_{ix}) + \Delta t_{rx}(t_{ix}) = \frac{2|\bar{u}_t(t_{ix})|}{(c + |\bar{v}_{igt}|)} \\ \Delta t_p(t_{ix} + n\Delta t_{ix}) &= \frac{2|\bar{u}_t(t_{ix} + n\Delta t_{ix})|}{(c + |\bar{v}_{igt}|)} = \frac{2(|\bar{u}_t(t_{ix})| - n\Delta t_{ix} |\bar{v}_{igt}|)}{(c + |\bar{v}_{igt}|)} \\ \Delta t_p(t_{ix} + n\Delta t_{ix}) - \Delta t_p(t_{ix}) &= \frac{-2|\bar{v}_{igt}| n\Delta t_{ix}}{(c + |\bar{v}_{igt}|)} \end{aligned}$$

THIS PAGE INTENTIONALLY LEFT BLANK

APPENDIX B. MATLAB CODES

The MATLAB codes used in for this study are listed in this Appendix.

A. FUNCTIONS

The MATLAB functions written for the model are listed here.

1. Generation of Linear Trajectory Path

```
function [Pos] = linear_trajectory(P_start, Vel, time)

% This function is to calculate the position of an object at
% a given value of time (or a row vector of time values).
% Assumes (for the moment) that the object is travelling linearly
% with constant speed, Vel
%
% Inputs:
% - Vel = speed vector, 3x1 column vector of [vx;vy;vz]
% - P_start = Position at time = 0, 3x1 column vector of [x0;y0;z0]
% - time = time instants to compute position for [any row vector]
%
% Outputs:
% - P = Matrix of positions [X;Y;Z] corresponding to [time]
%
% By: Tng YS (Jul 2012)

[A1,B1] = size(time);
if (A1 ~= 1)
    error('Only single values or row vectors allowed')
end

Pos = repmat(P_start,1,B1) + repmat(Vel,1,B1).*repmat(time,3,1);
```

2. Computation of Wave Interception Time

```
function [t_i] =
intercept_time(obj_start_pos,obj_velocity,wave_start_pos)
%
% This function computes the time that a wavefront travelling at
% speed of light from tx_pos takes to intercept an object tgt starting
from
% tx_pos.
%
```

```

% Inputs:
% - obj_start_pos = Object position at wave transmission,3xN column
vector
% - obj_velocity = Obj (linear) velocity, 3xN column vector
% - wave_start_pos = Wave start position, 3xN column vector
%
% Outputs:
% - t_i = 1xN row vector of intercept times
%
% By: Tng YS (Jul 2012)

[A1,A2] = size(obj_start_pos);
[A3,A4] = size(obj_velocity);
[A5,A6] = size(wave_start_pos);
if (A1 ~= 3 || A3 ~= 3 || A5 ~= 3 || A4 ~= 1)
    error('All position inputs must be 3xN matrices, velocity is 3x1 ')
end
if (A2 ~= A6)
    error('Dimensions of the position matrices must be the same.')
end

c = 299792458; % m/s - EM wave speed = Speed of light in vaccuum

u = obj_start_pos - wave_start_pos;

% This assumes constant velocity. If variable velocity, change function
% to accept the velocity vector accordingly.
v = repmat(obj_velocity,1,A6);

u_dot_v = dot(u,v);
v_dot_v = dot(v,v);
u_dot_u = dot(u,u);
c2_minus_v2 = c^2 - v_dot_v;

t_i = (u_dot_v + sqrt( u_dot_v.^2 + c2_minus_v2.*u_dot_u))./c2_minus_v2;

end

```

3. Generation of Rectangular Pulse

```

function [t,f_t,mf] = rect_pulse(time_vec,fc,fs,pw,PRI,t_start)

% This code is used to generate the values of a single (amplitude
modulated)
% rectangular pulse transmit waveform at the time instances specified
by time vector
% The matched filter for a single pulse duration is also returned
%
% The waveform is described by a carrier frequency, pulse width,
repetition
% period, transmission start time (relative to t = 0).

```

```

% time_vec is the vector of time values to compute waveform for;
% fc is the carrier frequency
% pw is pulse width
% PRI is the interval between pulses
% t_start is the start transmission time

% Calculate length of t
[Nrow,Ncol] = size(time_vec);
num_samples = Ncol;
if(Nrow == 1)
    num_samples = Ncol;
elseif(Ncol == 1)
    num_samples = Nrow;
    time_vec = time_vec';
else
    error('time must be a vector');
end

check_time_vec(time_vec,t_start,pw,PRI);

t = double(time_vec);

if (pw >= PRI)
    % This becomes a CW signal ...
    f_t = ones(1,num_samples);
    if (t_start >= t(1))
        start_ind = find(t < t_start);
        f_t(1:start_ind) = 0;
    end
else
    % Compute the intervals where the pulses occur & set these to 1
    f_t = zeros(1,num_samples);
    pulse_start = t_start;
    pulse_end = t_start + pw;
    start_ind = max(1,find(t >= pulse_start,1,'first')); % Find
smallest index
    if (t(end) > pulse_end)
        end_ind = find(t <= pulse_end,1,'last'); % Find largest index
    else
        end_ind = num_samples;
    end
    f_t(start_ind:end_ind) = 1;
end
first_start_ind = start_ind;

% Generate matched filter baseband response
mf = conj(f_t(first_start_ind:end_ind));
Nmf_orig = length(mf); Nmf = 2^nextpow2(Nmf_orig);
mf = [mf,zeros(1,Nmf-Nmf_orig)];

% Upconversion to RF
f_t = f_t.*exp(1i * 2 * pi * fc * (time_vec + t_start)); % Multiply
Baseband with Carrier

```


4. Generation of Barker-Coded Binary Phase Modulated Pulse

```
function [t,f_t,mf] =
BarkerCode(time_vec,fc,fs,codelength,subpw,PRI,t_start)

% This code is used to generate the values of a single Barker coded
% pulse transmit waveform at the time instances specified by time
vector
% The matched filter for a single pulse duration is also returned
%
% The waveform is described by a carrier frequency, pulse width,
repetition
% period, transmission start time (relative to t = 0).

% time_vec is the vector of time values to compute waveform for;
% fc is the carrier frequency
% fs is the sampling frequency
% code length is the length of the Barker code desired (Up to 13)
% subpw is sub-pulse width
% PRI is the interval between pulses
% t_start is the start transmission time

% Calculate length of t
[Nrow,Ncol] = size(time_vec);
num_samples = Ncol;
if(Nrow == 1)
    num_samples = Ncol;
elseif(Ncol == 1)
    num_samples = Nrow;
    time_vec = time_vec';
else
    error('time must be a vector');
end

% The actual pulse width is 7 sub-pulse widths
pw = codelength * subpw;
check_time_vec(time_vec,t_start,pw,PRI);

t = double(time_vec);

switch(codelength)
    case 2
        Code = [+1,-1];
    case 3
        Code = [+1,+1,-1];
    case 4
        Code = [+1,+1,-1,+1];
    case 5
        Code = [+1,+1,+1,-1,+1,];
    case 7
        Code = [+1,+1,+1,-1,-1,+1,-1];
    case 11
        Code = [+1,+1,+1,-1,-1,-1,+1,-1,-1,+1,-1];
    case 13
```

```

        Code = [+1,+1,+1,+1,+1,-1,-1,+1,+1,-1,+1,-1,+1];
    otherwise
        error('Not a valid Barker code');
end

if (pw >= PRI)
    error('PW cannot be greater than PRI for the chosen Barker code');
else
    f_t = zeros(1,num_samples);
    % pulse_index_len = zeros(1,codelength); % For debug
    for nn = 1:codelength
        % Compute the intervals where the subpulses occur & set these
to
        % the Barker code
        pulse_start = t_start + (nn-1)*subpw;
        pulse_end = t_start + nn*subpw;
        start_ind = max(1,find(t >= pulse_start,1,'first')); % Find
smallest index
        if(nn == 1)
            first_start_ind = start_ind;
        end
        if (t(end) > pulse_end)
            end_ind = find(t <= pulse_end,1,'last'); % Find largest
index
        else
            end_ind = num_samples;
        end
        % pulse_ind_length(nn) = end_ind - start_ind; % For debug
        f_t(start_ind:end_ind) = Code(nn);
    end
end

% Generate matched filter baseband response
mf = conj(f_t(first_start_ind:end_ind));
Nmf_orig = length(mf); Nmf = 2^nextpow2(Nmf_orig);
mf = [mf,zeros(1,Nmf-Nmf_orig)];

% Upconversion to RF
f_t = f_t.*exp(1i * 2 * pi * fc * (time_vec + t_start)); % Multiply
Baseband with Carrier

```

5. Generation of Linear-Frequency-Modulated Pulse

```

function [t,f_t,mf,mf_freq_ind] = lfm(time_vec,...
    fc,fs,PulseBW,pw,PRI,t_start,direction)

% This code is used to generate the values of a single Linear FM
% rectangular pulse transmit waveform at the time instances specified
by time vector
% The matched filter for a single pulse duration is also returned
%

```

```

% The waveform is described by a carrier frequency, pulse width,
repetition
% period, transmission start time (relative to t = 0).

% time_vec is the vector of time values to compute waveform for;
% fc is the carrier frequency
% PulseBW is the chirp BW
% pw is pulse width
% PRI is the interval between pulses
% direction ('up' or 'down' is the chirp direction)
% t_start is the start transmission time

% Set chirp direction
switch (direction)
    case 'down'
        downchirp = 1;
    case 'up'
        downchirp = 0;
    otherwise
        error('Select chirp up or down');
end

% Calculate length of t
[Nrow,Ncol] = size(time_vec);
num_samples = Ncol;
if(Nrow == 1)
    num_samples = Ncol;
elseif(Ncol == 1)
    num_samples = Nrow;
    time_vec = time_vec';
else
    error('time must be a vector');
end

check_time_vec(time_vec,t_start,pw,PRI);

t = double(time_vec);
mu = PulseBW/pw;

if (pw >= PRI)
    % This becomes a CW signal ...
    f_t = ones(1,num_samples);
    if (t_start >= t(1))
        start_ind = find(t < t_start);
        f_t(1:start_ind) = 0;
    end
else
    % Compute the intervals where the pulses occur & set these to 1
    f_t = zeros(1,num_samples);
    pulse_start = t_start;
    pulse_end = t_start + pw;
    start_ind = max(1,find(t >= pulse_start,1,'first')); % Find
smallest index

```

```

    if (t(end) > pulse_end)
        end_ind = find(t <= pulse_end,1,'last'); % Find largest index
    else
        end_ind = num_samples;
    end
    % Chirp Up
    f_t(start_ind:end_ind) = exp(1i*pi*mu*(t(start_ind:end_ind)-
t(start_ind)).^2);
    % Chirp Down
    if(downchirp)
        f_t(start_ind:end_ind) = f_t(end_ind:-1:start_ind);
    end
end

% Generate the unshifted baseband matched filter response & zero pad to
% length that is power of 2 (for fft & easy computation of freq index)
mf = conj(f_t(start_ind:end_ind));
Nmf_orig = length(mf); Nmf = 2^nextpow2(Nmf_orig);
mf = [mf,zeros(1,Nmf-Nmf_orig)];

% This is the rectangular pulse where f_t is simply the amplitude
modulation
f_t = f_t.*exp(1i * 2 * pi * fc * (time_vec + t_start)); % Multiply
Baseband with Carrier

```

6. Correlation Receiver

```

function [corr_out_r,delay_ind,freq_ind] ...
=
corr_rx(w_r,m_f,rng_width_desired,f_width_desired,fstep_desired,fs,Ts)
%
% w_r is the received waveform
% m_f is the baseband matched filter
% f_width_desired (Hz) is the range of frequencies to generate on each
side
% fstep_desired (Hz) is the desired frequency shift between each row
% Ts is the sampling interval

%
*****
% Relevant Physics Constants (from NIST)
%
*****
c = 299792458; % m/s - EM wave speed = Speed of light in vaccuum

Nmf = length(m_f);
Nwr = length(w_r);

% *****
% Generate the bank of matched filters matched to shifted frequencies
% *****

```

```

% Compute number of range cells around scene center to compute on each
side
rng_sample = c*Ts/2; % Two-way range (Correct for monostatic)
N_rng_cell = ceil(rng_width_desired/rng_sample); % cells

fstep = fs/Nmf;% Hz per frequency index step in FFT output
nshift = fstep_desired/fstep;
Nf = ceil(f_width_desired/fstep_desired); % No. of freq rows on each
side
Nf_limit = 5000; % To limit and avoid out of memory problems
if (Nf > Nf_limit)
    Nf = Nf_limit;
    disp('*** WARNING: Frequency steps truncated to 5000 on each side
***');
end
mf_freq_vec = 1i*2*pi*[-Nf:1:Nf]'*nshift/Nmf;
index_vec = 1-Nmf/2:1:Nmf/2;
n_shift_mat = repmat(mf_freq_vec,1,Nmf);
index_mat = repmat(index_vec,2*Nf+1,1);
f_shift_mat = exp(n_shift_mat.*index_mat);
mf_mat = f_shift_mat.*repmat(m_f,2*Nf+1,1);
mf_conj = conj(mf_mat); % MATLAB dot product will conjugate it again

% Generate associated frequency indices
freq_ind = [-Nf:1:Nf]'*nshift*fstep;

% Size of mf_mat is needed later
col_mf = Nmf; row_mf = 2*Nf+1;

% Ensure that received signal is at least same length as the matched
filter
% for correlation to work (This can happen between mf is always
extended
% to 2^N lengths for efficient FFT)
if(Nwr < col_mf)
    w_r = [w_r,zeros(1,col_mf-Nwr)]; % Append zeros
end

% *****
% Correlation Receiver
% *****
w_r2 = repmat([zeros(1,N_rng_cell),w_r,zeros(1,N_rng_cell)],row_mf,1);
[~,Nwr2] = size(w_r2);
corr_out_r = zeros(row_mf,2*N_rng_cell);

for nn = 1:(2*N_rng_cell+1)
    mf2 = [zeros(row_mf,(nn-1)),mf_conj,zeros(row_mf,Nwr2-col_mf-(nn-
1))];
    corr_out_r(:,nn) = dot(mf2,w_r2,2);
end

% Generate associated time delay indices (referenced to start of w_f)

```

```

delay_ind = [-N_rng_cell:1:N_rng_cell]*Ts; % Associated delay from
center

% Normalise by the waveform energy
r_0 = dot(m_f,m_f);
corr_out_r = corr_out_r/r_0;

end

```

7. Create the Time Map for Given Target-Sensor Geometry

```

function [time_map,img_map,x_ind,y_ind] = ...

create_timemap(scene_ctr,x_width,x_step,y_width,y_step,tx_pos,rx_pos);

% Compute a reception time map for the transmitter & reception geometry
% based on cartesian coordinates around a scene and initialise an image
map

%
*****
% Relevant Physics Constants (from NIST)
%
*****
c = 299792458; % m/s - EM wave speed = Speed of light in vaccuum

% Form N_r x N_xr x 2 matrix to capture x,y-coord for each pt
N_x = ceil(x_width/x_step);
N_y = ceil(y_width/y_step);
x_ind = [-N_x:N_x]*x_step+scene_ctr(1);
y_ind = [-N_y:N_y]*y_step+scene_ctr(2);
spatialmap = zeros(2*N_y+1,2*N_x+1,2);
spatialmap(:,:,1) = repmat(x_ind,2*N_y+1,1);
spatialmap(:,:,2) = repmat(y_ind',1,2*N_x+1);
img_map = zeros(2*N_y+1,2*N_x+1,1);

% For each point on spatial map, compute the propagation time.
tx2pos_x = spatialmap(:,:,1) - tx_pos(1,:);
tx2pos_y = spatialmap(:,:,2) - tx_pos(2,:);
tx2_pos = sqrt(tx2pos_x.^2 + tx2pos_y.^2);

rx2pos_x = spatialmap(:,:,1) - rx_pos(1,:);
rx2pos_y = spatialmap(:,:,2) - rx_pos(2,:);
rx2_pos = sqrt(rx2pos_x.^2 + rx2pos_y.^2);

time_map = (tx2_pos + rx2_pos)/c;

```

8. Update the Image Map based on Current Range Samples

```
function [img_map_updated] = update_img_map(img_map,time_map,fr,trx,Ts)

% Updates the img_map with the (a single) function value based on
% given reception time instant.

temp_img_map = zeros(size(img_map));

g1 = find(time_map < (trx+Ts/2));
temp_img_map(g1) = fr;
g2 = find(time_map < (trx-Ts/2));
temp_img_map(g2) = 0;

img_map_updated = img_map + temp_img_map;
```

9. Check Time Vector for Required Length Constraints before Processing

```
function check_time_vec(time_vec,t_start,pw,PRI);

% Convert back to double precision for easy processing
% ** Watch out for lost accuracy beyond 16th significant digit !!
% ** Use only the actual symbolic time vector for calculations !!
t = double(time_vec);

% Check that the time vector contains only a single pulse
if (t(end) > t_start + PRI || t(end) > t(1) + PRI)
    error('Time vector contains more than 1 PRI. Please separate the
pulses for calculations!');
    % Processing the PRI separately makes matched filtering easy to
implement.
    % This is what is done in practical receiver systems as well.
end

% Check that time vector is sufficient to complete 1 pulse
if (t(end) < t_start + pw)
    error('Time vector contains less than 1 Pulse Width. Will not yield
correct matched filtering!');
end

%disp('Checked OK');
```

B. SCRIPTS

This Section provide examples of scripts which make use of the implemented functions to simulate different imaging radar configurations

1. Example of Multistatic Radar

a. Scenario Definition

```
% This script defines the target characteristics
% It should be called for all M-files to ensure a consistent sensor
% definition

% Simulation parameters
plot_scene = 1; % This is to set whether to do the quiver plot or not.

%
*****
% Relevant Physics Constants (from NIST)
%
*****
c = 299792458; % m/s - EM wave speed = Speed of light in vaccuum

%
*****
% Imaging Parameters
%
*****

% Set Region of Interest around pulse and scene
scene_ctr = [-50,50,0];

rng_width_desired = 50; % meters (on each side)
rng_step = 0.1; % meters (per cell)
rng_resol_desired = 10; % meters

cr_rng_width_desired = 50; % meters (on each side)
cr_step = 0.1; % meters (per cell)
cr_rng_resol_desired = 10; % meters (on each side)[Not used in
Multistatic]

%
*****
% Sensor Waveform & Sampling Time Definition
%
*****
fc = 150e6; % Carrier frequency in Hz
fs = 1e9; % Sampling frequency; Should be at least Nyquist+
Ts = 1/fs;
PRF = 0.1; % Hz
PRI = 1/PRF; % sec
```



```

waveform_choice = waveform_choice_vec(qq);
switch(waveform_choice)
    case 1 % Rectangular Pulse
        PW = 1e-7; % sec
        PulseBW = 1/PW; % Hz
    case 2 % Barker Code
        SubPW = (2/3)*1e-7; % sec
        codelength = 13; % No. of sub-pulse widths
        PulseBW = 1/SubPW; % Hz
        PW = codelength*SubPW; % sec
    case 3 % Linear FM
        PW = 1e-6; % sec
        PulseBW = c/(2*rng_resol_desired); %Hz
        lfm_direction = 'up';
end

% For matched filter generation
rng_sample = c*Ts/2; % meters (based on sampling rate)
f_width_desired = 0*PulseBW; % Hz (on each side on zero Doppler cut)
fstep_desired = ...
    max(10e3,round(f_width_desired/500)); %Hz (difference betw each row)

%
*****
% Sensor Position, Velocity Definition
%
*****
% Notes:
% - All theta are measured counter-clockwise from x-axis
% - tx_range is distance measured from sensor to scene center
% - velocity bearing = 0 => moving away from scene center along x
% - velocity bearing = 180 => moving away from scene center along -x

tx_pos_theta = 0; % deg - Angle between tx & scene center at start
tx_init_height = 0; % meters
tx_init_range = 100e3; % meters
tx_init_pos = tx_init_range*[cosd(tx_pos_theta);...
    sind(tx_pos_theta);tx_init_height]; %meters - @ time = 0;
tx_spd = 0; % m/s
tx_vel_theta = 180; %deg -velocity bearing
tx_vel = tx_spd*[cosd(tx_vel_theta);sind(tx_vel_theta);0]; % m/s

% Set to same as tx for 1-channel mono-static radar. Adjust according
% otherwise
rx_pos_theta = theta_vec(qq); % deg - Angle between tx & scene center
at start
rx_init_height = 0; % meters
rx_init_range = rx_init_rng_vec(qq);
rx_init_pos = rx_init_range*[cosd(rx_pos_theta);...
    sind(rx_pos_theta);rx_init_height]; %meters - @ time = 0;
rx_spd = 0; % m/s
rx_vel_theta = 180; %deg - velocity bearing
rx_vel = rx_spd*[cosd(rx_vel_theta);sind(rx_vel_theta);0]; % m/s

```

```

%
*****
% Target Position, Velocity Definition
%
*****
% Notes:
% - All theta are measured counter-clockwise from x-axis
% - velocity bearing = 0 => moving away from scene center along x
% - velocity bearing = 180 => moving away from scene center along -x

tgt_spd = 0; % m/s
tgt_init_pos = [-50;50;0]; %meters - @ time = 0;
%savefile_id = [num2str(tgt_spd/1e3),'k']; % Used in script for
analysis
tgt_vel_theta = 0; % deg - velocity bearing
tgt_vel = tgt_spd*[cosd(tgt_vel_theta);sind(tgt_vel_theta);0]; % m/s

%
*****
% Plot the relative positions and vel on a quiver plot if selected
%
*****
if(plot_scene)
    scale = 1000;
    v_scale = 200;
    if(qq == 1)
        h_scene = figure;
    else
        figure(h_scene);
    end
    if (qq == 1 && tgt_spd == 0)
        scatter(tgt_init_pos(1)/scale,tgt_init_pos(2)/scale,60,...
            'd','Markerfacecolor','k');
    elseif (qq == 1)
        quiver(tgt_init_pos(1)/scale,tgt_init_pos(2)/scale,...
            tgt_vel(1)/v_scale,tgt_vel(2)/v_scale,'MaxHeadSize',10,...
            'LineWidth',3,'color','k')
    end
    hold on
    if (tx_spd == 0)
        scatter(tx_init_pos(1)/scale,tx_init_pos(2)/scale,40,...
            's','Markerfacecolor','r');
    else
        quiver(tx_init_pos(1)/scale,tx_init_pos(2)/scale,...
            tx_vel(1)/v_scale,tx_vel(2)/v_scale,'MaxHeadSize',2,...
            'LineWidth',3,'Color','r');
    end
    if (rx_spd == 0)
        scatter(rx_init_pos(1)/scale,rx_init_pos(2)/scale,40,...
            'o','Markerfacecolor','r');
    else
        quiver(rx_init_pos(1)/scale,rx_init_pos(2)/scale,...
            tx_vel(1)/v_scale,tx_vel(2)/v_scale,'MaxHeadSize',2,...

```

```

        'LineWidth',3,'Color','r');
    end
    hold off;
%   xlim([-5,15]); ylim([-15,15]);
    grid on
    xlabel('X (km)');
    ylabel('Y (km)');
end

```

b. Main Script

```

% This script is used to generate the multistatic config in the thesis
%
%close all; % Close all figures (These take up memory too!)
format long; % Set MATLAB display format
clock = tic; % To keep track of the script's run time

% These define the angles and ranges for the receivers (for multistatic)
theta_vec = [-45,0,30,90]; % degrees
rx_init_rng_vec = [sqrt(2)*100e3,100e3,100e3,100e3*sind(30)];
waveform_choice_vec = [3,3,3,3]; % waveform selection for each tx/rx
pair
N_sys = length(theta_vec); % No. of systems simulated in this script

for qq = 1:N_sys

scenario_definition_multistatic; % Call scenario file (multistatic)

if (qq == 1)
    rng_sample = c*Ts/2;
    N_rng_cell = ceil(rng_width_desired/rng_sample); % cells
    range_profile = zeros(N_sys,2*N_rng_cell+1);
    trx_range_profile = zeros(N_sys,2*N_rng_cell+1);
    range_alignment_ind = zeros(N_sys,1);
    tx_pos = zeros(3,N_sys);
    rx_pos = zeros(3,N_sys);
end

% *****
% Create the time range to simulate based on PW
% *****

t_start = 0; %sec - Required start time (integral multiple of Ts needed)
t_end = t_start+PW+Ts; %sec - Required end time(integral multiple of Ts
needed)

% *****
% Generation of Time Sequences
% *****

n = round(t_start/Ts);

```

```

N_desired = round(t_end/Ts);
% For actual N, adjust number of samples for time expansion due to
motion
N = ceil(c/(c-(tx_spd+rx_spd+tgt_spd))*N_desired); % worst case
if ((N-n) > 5e6+1000)
    n_samples = N-n
    fprintf(['Too many samples simulated. Memory problems may occur.
',...
',...
'It is recommended to reduce sequence size to < 5 million ',...
'samples. \n']);
fprintf(['For longer sequences, alternative is to simulate as \'...
'separate vectors and combine subsequently if needed. \n']);
A1 = 0;
while (A1 ~= 1 && A1 ~= 2)
    A1 = input('Continue ? (1 to continue, 2 to stop): ');
    if (A1 == 2)
        return % exit the script
    end
end
end

% Create evenly spaced (@ Ts) reference time vector
% -- Time vector starts from nTs and ends at N*Ts to allow flexibility
%   in the start transmission time
% -- Length is N-n+1 samples
ttx = n*Ts:Ts:N*Ts; % sec

% Compute propagation time
[trx,tp,t_ctr] = total_propagation_time(tgt_init_pos,tgt_vel,...
    tx_init_pos,tx_vel,rx_init_pos,rx_vel,ttx);

% *****
% Recreate evenly spaced receive samples using search
% *****

% Desired outcome
trx_desired = tp(1) + ttx;
trx_original = trx;
ttx_original = ttx;
tp_original = tp;
t_ctr_original = t_ctr;

% Search algorithm
alpha = 0.99; % This controls how fast search converges

for curr_sample = 2:N+1

    curr_sample

    % Initialise before entering while loop
    desired_time = trx_desired(curr_sample);
    actual_time = trx(curr_sample);
    diff_from_desired = actual_time-desired_time;
    ttx(curr_sample) = ttx(curr_sample) - alpha * diff_from_desired;

```

```

iterations = 0; % This is to prevent infinite loops
threshold = max(1e-16*desired_time,...
               1e-18);% 1e-16 is the limit of double precision

while ((abs(diff_from_desired) > threshold) && (iterations < 1000))

    iterations = iterations + 1;

    % Compute propagation time
    [trx(curr_sample),tp(curr_sample),t_ctr(curr_sample)]...
    =
total_propagation_time(tgt_init_pos,tgt_vel,tx_init_pos,...
                      tx_vel,rx_init_pos,rx_vel,ttx(curr_sample));
    % Compute difference from desired
    actual_time = trx(curr_sample);
    diff_from_desired = actual_time-desired_time;

    % Update for next iteration
    ttx(curr_sample) = ttx(curr_sample) - alpha * diff_from_desired;
end
end

% *****
% Create Transmitted Waveform & Matched Filter
% *****

switch(waveform_choice)
    case 1 % Rectangular Pulse
        [~,f_t,mf] = rect_pulse(ttx_original-
ttx_original(1),fc,fs,PW,...
                              PRI,t_start);
    case 2 % Barker Code
        [~,f_t,mf] = BarkerCode(ttx_original-ttx_original(1),fc,fs,...
                                codelength,SubPW,PRI,t_start);
    case 3 % Linear FM
        [~,f_t,mf] = lfm(ttx_original-ttx_original(1),fc,fs,...
                          PulseBW,PW,PRI,t_start,lfm_direction);
end

% *****
% Propagation
% *****

switch(waveform_choice)
    case 1 % Rectangular Pulse
        [~,f_r,~] = rect_pulse(ttx-ttx(1),fc,fs,PW,PRI,0);
    case 2 % Barker Code
        [~,f_r,~] = BarkerCode(ttx-ttx(1),fc,fs,...
                                codelength,SubPW,PRI,0);
    case 3 % Linear FM
        [~,f_r,~] = lfm(ttx-ttx(1),fc,fs,...
                          PulseBW,PW,PRI,0,lfm_direction);
end

```

```

% *****
% Reception
% *****

% Demodulate the carrier frequency using the original time vector
mixer_phase = 0; % Assumes Ideal mixer (Perfect phase & timing)
f_r_demod = f_r.*exp(-1i*2*pi*fc*ttx)*exp(-1i*mixer_phase);

% Sampling/Decimation/Downsampling (if required)
sample_start = 1; % To allow sampling at different start samples
N_dec = 1; % This is the number of times to downsample.
m_f = mf(sample_start:N_dec:end);
f_r_demod = f_r_demod(sample_start:N_dec:end);
Ts = Ts*N_dec;
fs = fs/N_dec;

% Correlation receiver
[corr_out_r,delay_ind,mf_freq_ind] ...
    = corr_rx(f_r_demod,mf,rng_width_desired,f_width_desired,...
        fstep_desired,fs,Ts);

% Select range profile (Max is selected)
[Nrow,Ncol] = size(corr_out_r);
zero_cut = floor(Nrow/2+1);
range_profile(qq,:) = corr_out_r(zero_cut,:); % Zero-Doppler cut
range_alignment_ind(qq) = find_range_alignment(trx-t_ctr(1),Ts);

trx_range_profile(qq,:) = delay_ind + trx(1);

% *****
% Image Reconstruction
% *****

% Create Time Map
tx_pos(:,qq) = tx_init_pos + t_start*tx_vel;
rx_pos(:,qq) = rx_init_pos + t_start*rx_vel;
[time_map,img_map,x_ind,y_ind] = ...
    create_timemap(scene_ctr, rng_width_desired, rng_step, ...
        cr_rng_width_desired, cr_step, tx_pos(:,qq), rx_pos(:,qq));

% Check and Update Time Map for each sample in range profile
Max_trx = max(max(time_map)); % Max trx in desired scene
Min_trx = min(min(time_map)); % Min trx in desired scene
for ll = 1:Ncol
    if((trx_range_profile(qq,ll) > Min_trx) && ...
        (trx_range_profile(qq,ll) < Max_trx))
        [img_map] = update_img_map(img_map,time_map,...
            range_profile(qq,ll),trx_range_profile(qq,ll),Ts);
    end
end

if(qq == 1)

```

```

        img_map_cum = zeros(size(img_map));
end
img_map_cum = img_map_cum+img_map;

eval(['img_map_',num2str(qq),' = img_map;']);

end

h_img2 = surf(x_ind,y_ind,abs(img_map_cum)/N_sys,'edgecolor','none');
xlabel('X (meters)');
ylabel('Y (meters)');

elapsed_time = toc(clock)

```

2. Example of SAR

a. Scenario Definition

```

% This script defines the target characteristics
% It should be called for all M-files to ensure a consistent sensor
% definition

% Simulation parameters
plot_scene = 1; % This is to set whether to do the quiver plot or not.

%
*****
% Relevant Physics Constants (from NIST)
%
*****
c = 299792458; % m/s - EM wave speed = Speed of light in vaccuum

%
*****
% Imaging Parameters
%
*****

% For moving SAR
SAR_speed = 50.0; %m/s
SAR_halfwidth = 1.5e3; % meters
SAR_downrange = 10e3; % meters

% Set Region of Interest around pulse and scene
scene_ctr = [0,200,0];

rng_width_desired = 100; % meters (on each side)
rng_step = 2; % meters (per cell)

cr_rng_width_desired = 100; % meters (on each side)

```

```

cr_step = 2; % meters (per cell)

%
*****
% Sensor Waveform & Sampling Time Definition
%
*****
fc = 100e6; % Carrier frequency in Hz
fs = 1000e6; % Sampling frequency; Should be at least Nyquist+
Ts = 1/fs;

wavelength = c/fc; % m
rng_resol_desired = 10; % meters
cr_rng_resol = wavelength/...
    (2*(atan(SAR_halfwidth/SAR_downrange))); % meters (on each side)

waveform_choice = 3;
switch(waveform_choice)
    case 1 % Rectangular Pulse
        PW = 1e-7; % sec
        PulseBW = 1/PW; % Hz
    case 2 % Barker Code
        SubPW = 2/3*1e-8; % sec
        codelength = 13; % No. of sub-pulse widths
        PulseBW = 1/SubPW; % Hz
        PW = codelength*SubPW; % sec
    case 3 % Linear FM
        PW = 1e-6; % sec
        PulseBW = c/(2*rng_resol_desired); %Hz
        lfm_direction = 'up';
end

Nyquist_sampling = wavelength/2;
PRI = Nyquist_sampling/SAR_speed; % sec
PRF = 1/PRI; % Hz

% For matched filter generation
rng_sample = c*Ts/2; % meters (based on sampling rate)
f_width_desired = 0*PulseBW; % Hz (on each side on zero Doppler cut)
fstep_desired = ...
    max(10e3,round(f_width_desired/500)); %Hz (difference betw each row)

%
*****
% Sensor Position, Velocity Definition
%
*****
% Notes:
% - All theta are measured counter-clockwise from x-axis
% - tx_range is distance measured from sensor to scene center
% - velocity bearing = 0 => moving away from scene center along x
% - velocity bearing = 180 => moving away from scene center along -x

tx_init_height = 0; % meters

```



```

tx_init_pos = [SAR_downrange;-SAR_halfwidth;...
               tx_init_height]; %meters - @ time = 0;
tx_spd = SAR_speed;
tx_vel = [0;SAR_speed;0]; % m/s

% Set to same as tx for 1-channel mono-static radar. Adjust according
% otherwise
rx_init_height = tx_init_height; % meters
rx_init_pos = tx_init_pos;
rx_spd = tx_spd;
rx_vel = tx_vel; % m/s

%
*****
% Target Position, Velocity Definition
%
*****
% Notes:
% - All theta are measured counter-clockwise from x-axis
% - velocity bearing = 0 => moving away from scene center along x
% - velocity bearing = 180 => moving away from scene center along -x

tgt_spd = 0; % m/s
tgt_init_pos = [0;0;0]; %meters - @ time = 0;
tgt_vel_theta = 0; % deg - velocity bearing
tgt_vel = tgt_spd*[cosd(tgt_vel_theta);sind(tgt_vel_theta);0]; % m/s

%
*****
% Plot the relative positions and vel on a quiver plot if selected
%
*****
if(plot_scene == 1)
    scale = 1000;
    v_scale = 60;
    h_scene = figure;
    if (tgt_spd == 0)
        scatter(tgt_init_pos(1)/scale,tgt_init_pos(2)/scale,60,...
                'd','Markerfacecolor','k');
    else
        quiver(tgt_init_pos(1)/scale,tgt_init_pos(2)/scale,...
               tgt_vel(1)/v_scale,tgt_vel(2)/v_scale,'MaxHeadSize',15,'LineWidth',3)
    end
    hold on
    if (tx_spd == 0)
        scatter(tx_init_pos(1)/scale,tx_init_pos(2)/scale,40,...
                'd','Markerfacecolor','k');
    else
        quiver(tx_init_pos(1)/scale,tx_init_pos(2)/scale,...
               tx_vel(1)/v_scale,tx_vel(2)/v_scale,'MaxHeadSize',15,...
               'LineWidth',3,'Color','r');
    end
end

```

```

    hold off;
    xlim([-1,11]); ylim([-2,2]);
    grid on
    xlabel('X (km)');
    ylabel('Y (km)');
end

```

b. Main Script

```

% This script is used to simulate a moving SAR config for the thesis
%
%close all; % Close all figures (These take up memory too!)
format long; % Set MATLAB display format
clock = tic; % To keep track of the script's run time

plot_scene = 0; % This is to set whether to do the quiver plot or not.
scenario_definition_SAR; % Call scenario definition file
plot_scene = 0; % This is to set whether to do the quiver plot or not.

N_pulses = ceil(2*SAR_halfwidth/wavelength*2);
t_start_vec = (0:(N_pulses-1))*PRI;
for qq = 1:N_pulses

qq

scenario_definition_SAR; % Call scenario definition file
if (qq == 1)
    rng_sample = c*Ts/2; % Two-way range (Correct for monostatic)
    N_rng_cell = ceil(rng_width_desired/rng_sample); % cells
    range_profile = zeros(N_pulses,2*N_rng_cell+1);
    range_alignment_ind = zeros(N_pulses,1);
    tx_pos = zeros(3,N_pulses);
    rx_pos = zeros(3,N_pulses);
    trx_range_profile = zeros(N_pulses,2*N_rng_cell+1);
end

% *****
% Create the time range to simulate based on PW
% *****

t_start = t_start_vec(qq); %sec - Required start time (integral
multiple of Ts needed)
t_end = t_start+PW+Ts; %sec - Required end time(integral multiple of Ts
needed)

% *****
% Generation of Time Sequences
% *****

n = round(t_start/Ts);
N_desired = round(t_end/Ts);
% For actual N, adjust number of samples for time expansion due to
motion
N = ceil(c/(c-(tx_spd+rx_spd+tgt_spd))*(N_desired-n)); % worst case

```

```

if ((N-n) > 5e6+1000)
    n_samples = N-n
    fprintf(['Too many samples simulated. Memory problems may occur.
',...
        '\n',...
        '\tIt is recommended to reduce sequence size to < 5 million \n',...
        '\tsamples. \n']);
    fprintf(['For longer sequences, alternative is to simulate as \n',...
        '\tseparate vectors and combine subsequently if needed. \n']);
    A1 = 0;
    while (A1 ~= 1 && A1 ~= 2)
        A1 = input('Continue ? (1 to continue, 2 to stop): ');
        if (A1 == 2)
            return % exit the script
        end
    end
end

% Create evenly spaced (@ Ts) reference time vector
% -- Time vector starts from nTs and ends at N*Ts to allow flexibility
%   in the start transmission time
% -- Length is N-n+1 samples
ttx = n*Ts:Ts:(N+n)*Ts; % sec

% Compute propagation time
[trx,tp,t_ctr] = total_propagation_time(tgt_init_pos,tgt_vel,...
    tx_init_pos,tx_vel,rx_init_pos,rx_vel,ttx);

% *****
% Recreate evenly spaced receive samples using search
% *****

% Desired outcome
trx_desired = tp(1) + ttx;
trx_original = trx;
ttx_original = ttx;
tp_original = tp;
t_ctr_original = t_ctr;

% Search algorithm
alpha = 0.99; % This controls how fast search converges

for curr_sample = 2:(N+1)
    % Initialise before entering while loop
    desired_time = trx_desired(curr_sample);
    actual_time = trx(curr_sample);
    diff_from_desired = actual_time-desired_time;
    ttx(curr_sample) = ttx(curr_sample) - alpha * diff_from_desired;

    iterations = 0; % This is to prevent infinite loops
    threshold = max(1e-16*desired_time,...
        1e-18);% 1e-16 is the limit of double precision

    while ((abs(diff_from_desired) > threshold) && (iterations < 1000))

```

```

iterations = iterations + 1;

% Compute propagation time
[trx(curr_sample),tp(curr_sample),t_ctr(curr_sample)]...
    = total_propagation_time(tgt_init_pos,tgt_vel,...
        tx_init_pos,tx_vel,rx_init_pos,rx_vel,ttx(curr_sample));
% Compute difference from desired
actual_time = trx(curr_sample);
diff_from_desired = actual_time-desired_time;

% Update for next iteration
ttx(curr_sample) = ttx(curr_sample) - alpha * diff_from_desired;
end
end

% *****
% Create Transmitted Waveform & Matched Filter
% *****

switch(waveform_choice)
    case 1 % Rectangular Pulse
        [~,f_t,mf] = rect_pulse(ttx_original,fc,fs,PW,...
            PRI,t_start);
    case 2 % Barker Code
        [~,f_t,mf] = BarkerCode(ttx_original,fc,fs,...
            codelength,SubPW,PRI,t_start);
    case 3 % Linear FM
        [~,f_t,mf] = lfm(ttx_original,fc,fs,...
            PulseBW,PW,PRI,t_start,lfm_direction);
end

% *****
% Propagation
% *****

switch(waveform_choice)
    case 1 % Rectangular Pulse
        [~,f_r,~] = rect_pulse(ttx-ttx(1),fc,fs,PW,PRI,0);
    case 2 % Barker Code
        [~,f_r,~] = BarkerCode(ttx-ttx(1),fc,fs,...
            codelength,SubPW,PRI,0);
    case 3 % Linear FM
        [~,f_r,~] = lfm(ttx-ttx(1),fc,fs,...
            PulseBW,PW,PRI,0,lfm_direction);
end

% *****
% Reception
% *****

% Demodulate the carrier frequency using the original time vector
mixer_phase = 0; % Assumes Ideal mixer (Perfect phase & timing)
f_r_demod = f_r.*exp(-1i*2*pi*fc*ttx)*exp(-1i*mixer_phase);

```

```

% Correlation receiver
[corr_out_r,delay_ind,mf_freq_ind] ...
    = corr_rx(f_r_demod,mf,rng_width_desired,f_width_desired,...
        fstep_desired,fs,Ts);

% Select range profile
[Nrow,Ncol] = size(corr_out_r);
zero_cut = floor(Nrow/2+1);
trx_range_profile(qq,:) = delay_ind + trx(1) - t_start;
range_alignment_ind(qq) = find_range_alignment(trx-t_ctr(1),Ts);

% Based on Soumekh (pp 359)
% Reverse baseband conversion - Note this requires sampling rate to
% be much higher than the carrier frequency
range_profile(qq,:) = corr_out_r(zero_cut,:).*...
    exp(1i*2*pi*fc*(delay_ind+t_start));

% *****
% Image Reconstruction
% *****

% Create Time Map
tx_pos(:,qq) = tx_init_pos + t_start*tx_vel;
rx_pos(:,qq) = rx_init_pos + t_start*rx_vel;
[time_map,img_map,x_ind,y_ind] = ...
    create_timemap(scene_ctr, rng_width_desired, rng_step, ...
        cr_rng_width_desired, cr_step, tx_pos(:,qq), rx_pos(:,qq));

% Check and Update Time Map for each sample in range profile
Max_trx = max(max(time_map)); % Max trx in desired scene
Min_trx = min(min(time_map)); % Min trx in desired scene
for ll = 1:Ncol
    if((trx_range_profile(qq,ll) > Min_trx) && ...
        (trx_range_profile(qq,ll) < Max_trx))
        [img_map] = update_img_map(img_map,time_map,...
            range_profile(qq,ll),trx_range_profile(qq,ll),Ts);
    end
end

if(qq == 1)
    [Nrow_img,Ncol_img] = size(img_map);
    img_map_cum = zeros(Nrow_img,Ncol_img);
end
img_map_cum = img_map_cum+img_map;

end

% *****
% Analysis and Graph plotting
% *****

h_img = surf(x_ind,y_ind,abs(img_map_cum)/N_pulses,'edgecolor','none');
xlabel('Down Range (meters)'); ylabel('Cross Range (meters)');
view([0,90]);

```

```

if (plot_scene == 1)
    figure(h_scene)
    hold on
    quiver((tx_init_pos(1)+tx_vel(1)*trx(end))/scale,...
           (tx_init_pos(2)+tx_vel(2)*trx(end))/scale,...
           tx_vel(1)/v_scale,tx_vel(2)/v_scale,...
           'MaxHeadSize',2,'LineWidth',3,'Color','r');
    hold off
end

elapsed_time = toc(clock)

```

3. Script for Re-imaging the Scene After Generation

```

% This script to allow processing the range profile matrix with a
different
% scene of interest following completion of the original run

[Nrow,Ncol] = size(range_profile);

% Set Region of Interest around pulse and scene
scene_ctr = [0,200,0];

rng_width_desired = 50; % meters (on each side)
rng_step = 1; % meters (per cell)

cr_rng_width_desired = 600; % meters (on each side)
cr_step = 1; % meters (per cell)

% For movie creation
mov(1:Nrow) = struct('cdata', [], 'colormap', []);

for qq = 1:Nrow

qq

% *****
% Image Reconstruction
% *****

% Create Time Map
[time_map,img_map,x_ind,y_ind] = ...
    create_timemap(scene_ctr,rng_width_desired,rng_step,...
        cr_rng_width_desired,cr_step,tx_pos(:,qq),rx_pos(:,qq));

% Check and Update Time Map for each sample in range profile
Max_trx = max(max(time_map)); % Max trx in desired scene
Min_trx = min(min(time_map)); % Min trx in desired scene

```

```

for ll = 1:Ncol
    if((trx_range_profile(qq,ll) > Min_trx) && ...
        (trx_range_profile(qq,ll) < Max_trx))
        [img_map] = update_img_map(img_map,time_map,...
            range_profile(qq,ll),trx_range_profile(qq,ll),Ts);
    end
end

if(qq == 1)
    img_map_cum = zeros(size(img_map));
end
img_map_cum = img_map_cum+img_map;
h_img2 = surf(x_ind,y_ind,abs(img_map_cum)/Nrow,'edgecolor','none');
xlabel('X (meters)');ylabel('Y (meters)');
mov(qq) = getframe(gcf); % For movie creation
pause(.03);
end

% For movie creation
movie2avi(mov, 'SAR50_tgt10_90deg#1.avi', 'compression', 'None');

% Display the image map
h_img3 = surf(x_ind,y_ind,abs(img_map_cum)/Nrow,'edgecolor','none');
xlabel('Down Range (meters)'); ylabel('Cross Range (meters)');
view([0,90]);

```

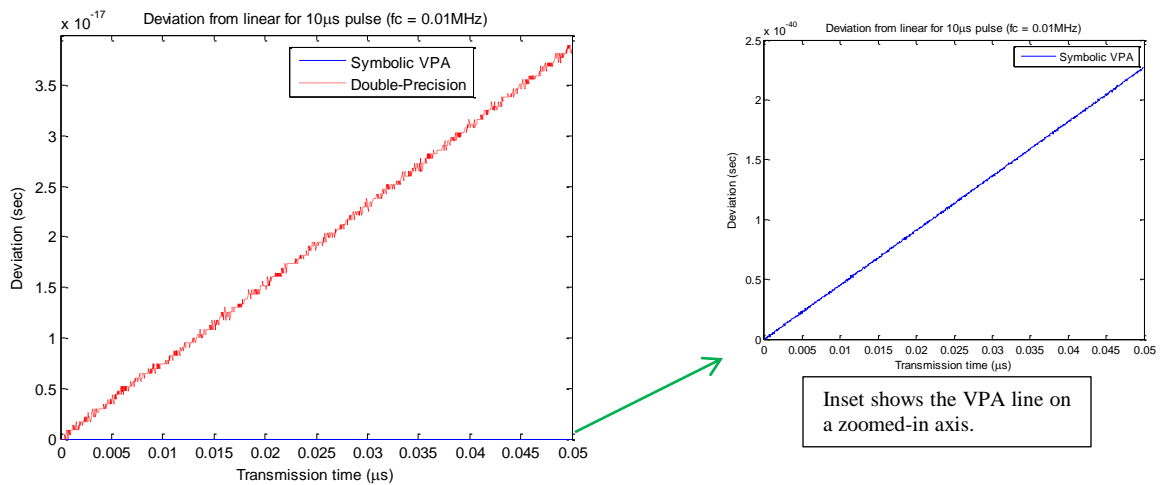
APPENDIX C. STUDY ON FLOATING POINT PRECISION

This appendix is mainly to highlight, for reference purposes, the effect of computational precision on MATLAB's simulation outputs when comparing the Symbolic Toolbox's Variable Precision Arithmetic (VPA) computation (25 digits) versus double precision floating point calculations.

All plots presented in this Appendix show the trend of the differences between the sample interval at transmission versus the interval between the corresponding samples, as noted at reception, for a simulation scenario. As explained in Chapter II, the spread in the samples is due to the spread in propagation time due to transmitter and target motions.

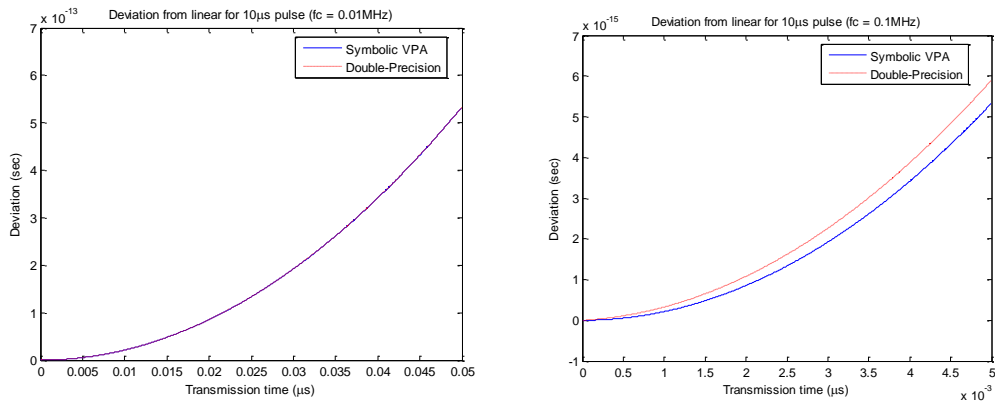
In these plots, a linear line formed by extrapolating from the first two samples is subtracted from actual difference (as compared to the transmitted sampling time) at reception to accentuate any non-linearity present in the trend (i.e., if the spread is linear), then the deviation from a linear line should be consistently *zero*, or *else the differences from the linear line will show up clearly*.

A good example of a sanity check would be a case where a clear 1-D Doppler shift effect can be predicted: The target starts from [0,0,0] km with velocity [0,50,0] m/s and the transmitter starts from [0,50,0] km with velocity [0,-200,0];

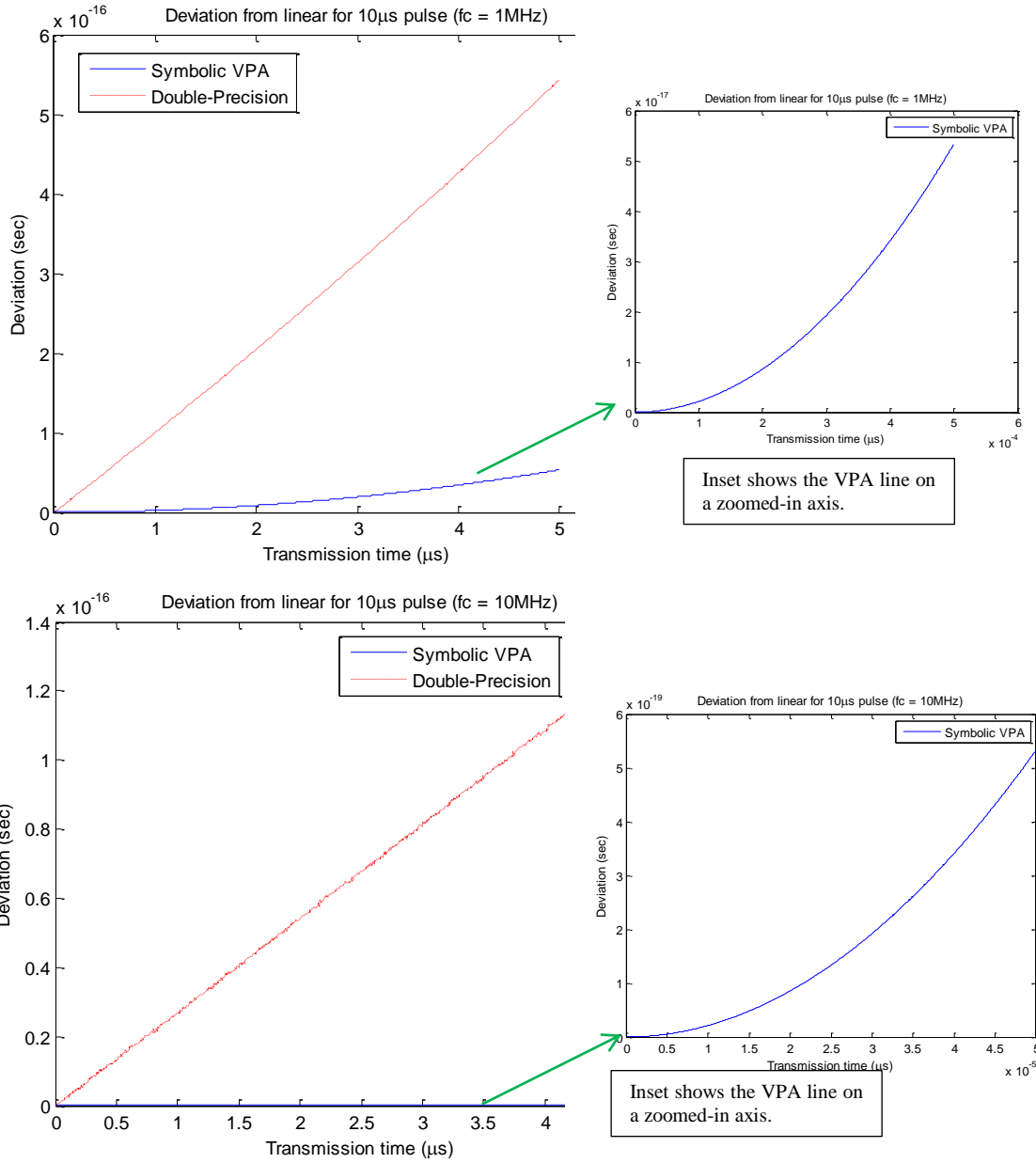


This gives a first hint that the limits of double precision have been reached, since the VPA result is around 10^{-40} (nearly zero) but the double precision results give around 10^{-17} .

In the next example, the target starts from $[0,0,0]$ km with velocity $[50,0,0]$ m/s and the transmitter starts from $[500,0,0]$ km with velocity $[100,-200,0]$. A sample size of 1000 samples is always assumed, with sampling frequency equal to $2f_c$ where the value of f_c is given in each graph. Here f_c acts as a scaling factor for the deviation from a linear line, since the amount of deviation from a linear line increases with decreased f_c (i.e., increased the time between samples).



The results clearly indicate that as frequency increases (i.e., interval between samples shrink), the double precision floating point calculations can no longer accurately present the results (due to insufficient dynamic range), whereas the VPA calculations continue to show the same trend. At f_c greater than 1 MHz in this example, it can be seen that the floating point calculations are unable to accurately depict the non-linearity at all, whereas calculations using VPA continue to faithfully reproduce the non-linear curve correctly.



While accuracy is improved, the tradeoff is that VPA calculations take up much more computation time, hence judicious design of the MATLAB model has to be undertaken to optimise simulation time if VPA is needed. In this thesis study, the use of VPA is avoided since the intent is to study fast moving targets and longer pulses, both of which do not require the precision of VPA to represent accurately.

THIS PAGE INTENTIONALLY LEFT BLANK

LIST OF REFERENCES

- [1] A. Bauer, "Christian Hülsmeyer and the early days of radar, sense and nonsense - a survey," *100 Years of RADAR*, Bonn, Germany: German Institute of Navigation (DGON), pp. 13–57, 2004.
- [2] P. Z. Peebles, *Radar Principles*. New York, NY: Wiley Inter-Science, 1998.
- [3] Center for Remote Imaging, Sensing and Processing, "Principles of remote sensing: interpreting SAR images," 2001.
http://www.crisp.nus.edu.sg/~research/tutorial/sar_int.htm.
- [4] A. Doerry, D. Dubbert, M. Thompson and V. Gutierrez, "A portfolio of fine resolution Ka band SAR imagery: Part 1," 2005.
<http://www.sandia.gov/radar/imageryka.html>.
- [5] D. L. Mensa, *High Resolution Radar Cross Range Imaging*. Boston, MA: Artech House, 1991.
- [6] D. K. Barton, *Modern Radar System Analysis*. Norwood, MA: Artech House, 1988.
- [7] S. Doughty, K. Woodbridge and C. Baker, "Improving resolution using multistatic radar," in *RADAR 2007: The Institution of Engineering and Technology International Conference on Radar Systems*, 2007, pp. 1-5
- [8] G. Franceschetti and R. Lanari, *Synthetic Aperture Radar Processing*. Boca Raton, FL: CRC Press, 1999.
- [9] M. Cheney and B. Borden, "Problems in synthetic aperture radar," *Inverse Problems*, vol. 25 no. 12, pp. 1–18, 2009.
- [10] C. L. Teo, "Bistatic radar system analysis and software development," M.S thesis, Naval Postgraduate School, Monterey, CA, USA, 2007.
- [11] B. Borden, *Radar imaging of airborne targets: A primer for Applied mathematicians and Physicists*. New York, NY: Taylor and Francis, 1999.
- [12] M. Cheney and B. Borden, "Imaging moving radar from scattered waves," *RPI Inverse Problems 24 (2008) 035005 (reprint)*, pp. 1–25, 2008.
- [13] M. Soumekh, *Synthetic Aperture Radar Signal Processing with MATLAB algorithms*. New York, NY: Wiley Interscience, 1999.
- [14] B. Borden and M. Cheney, "SAR imaging of dynamic scenes," 6–12 Feb. 2012.
<https://www.ipam.ucla.edu/schedule.aspx?pc=sar2012>.
- [15] M. Cheney and B. Borden, "Waveform Diverse Moving Target Spotlight SAR," in *Algorithms for Synthetic Aperture Radar XVIII*, 2011, vol. 8051 pp. 80510T1 - 80510T9
- [16] R. K. Raney, "Synthetic aperture radars and moving targets," *IEEE Transactions on Aerospace and Electronic Systems*, vol. AES-7, issue 3, pp. 499–505, 1971.
- [17] V. C. Chen and H. Ling, *Time-frequency transforms for radar imaging and signal analysis*. Boston, MA: Artech House, 2002.

- [18] S. Yi and S. D. Blostein, "Unknown motion compensation for spotlight mode synthetic aperture radar imagery," in *2000 International conference on Image Processing*, 2000, pp. 689-692
- [19] K. J. Jao, "Theory of synthetic aperture radar imaging for a moving target," *IEEE Transactions on Geoscience and Remote Sensing*, vol. 39, no. 9, pp. 1984-1992, 2001.
- [20] M. Kirscht, "Detection and imaging of moving targets in single channel SAR," *IEE Proceedings on Radar, Sonar and Navigation* vol. 150, issue 1, pp. 7-11, 2003.
- [21] B. Friedlander and B. Porat, "Velocity SAR - A conceptual radar system for ocean imaging," *IEEE Transactions on Aerospace Electronic Systems*, vol. 34, no. 3, pp. 755-776, 1998.
- [22] A. Farina and P. Lombardo, "STAP for SAR," in *Applications for Space-Time Adaptive Processing*. Stevenage, United Kingdom: The Institution of Electrical Engineers, 2004, pp. 73-120.
- [23] J. Wang, L. Gang, L. Yimin and W. Xiqin, "SAR imaging of moving targets via compressive sensing," in *2010 International Conference on Electrical and Control Engineering*, 2010, pp. 1855-1858
- [24] I. Stojanovic, W. C. Karl and M. Cetin, "Compressed sensing of mono-static and multi-static SAR," in *SPIE Defense and Security Symposium, Algorithms for Synthetic Aperture Radar Imagery XVI*, 2009, vol. 7337 pp.7337051-73370512
- [25] I. Stojanovic and W. C. Karl, "Imaging of moving target using SAR with an overcomplete dictionary," *IEEE Journal of selected topics on Signal Processing*, vol. 4 no. 1, pp. 164-176, 2010.
- [26] V. M. Patel, G. R. Easley, D. M. H. Jr and R. Chellapa, "Compressed sensing for synthetic aperture radar imaging," in *16th IEEE International Conference on Image Processing*, 2009, pp. 2141-2144
- [27] N. Levanon and E. Mozeson, *Radar Signals*. Hoboken, NJ: John Wiley & Sons, 2004.
- [28] G. L. Bretthorst, "Non-uniform sampling: bandwidth and aliasing," in *Bayesian Inference and maximum entropy methods in science and engineering: 19th International Workshop*, AIP Conference Proceedings, vol. 567, 2001, pp. 1-28
- [29] S. Maymon and A. V. Oppenheimer, "Sinc interpolation of non-uniform samples," *IEEE Transactions on Signal Processing*, vol. 59, issue 10, pp. 4745-4758, 2011.
- [30] F. Le Chevalier, *Principles of Radar and Sonar signal processing*. Norwood, MA: Artech House Inc, 2002.
- [31] Mathworks, "MATLAB - R2012a documentation, "Image processing toolbox - iradon,"" 2012. <http://www.mathworks.com/help/toolbox/images/ref/iradon.html>.

INITIAL DISTRIBUTION LIST

1. Defense Technical Information Center
Ft. Belvoir, Virginia
2. Dudley Knox Library
Naval Postgraduate School
Monterey, California
3. Professor Andres Larraza
Naval Postgraduate School
Monterey, California
4. Professor Brett H. Borden
Naval Postgraduate School
Monterey, California
5. Professor Roberto Cristi
Naval Postgraduate School
Monterey, California
6. Professor Yeo Tat Soon
Director, Temasek Defence Science Institute
National University of Singapore
7. Tan Lai Poh (Ms)
Assistant Manager, Temasek Defence Science Institute
National University of Singapore
8. Teo Tiat Leng
Deputy Director(Land Systems), Defence Science and Technology Agency
Singapore
9. Yan Siong Tng
Defence Science and Technology Agency
Singapore